Shape, thermodynamics and kinetics of nanoparticles

Laurence D Marks, Department of Materials Science and Engineering, Northwestern University, Evanston, IL, United States

Abstract

Nanoparticles can be beautiful, as in stained glass windows, or they can be ugly as in wear and corrosion debris from implants. Methods for synthesizing nanoparticles have exploded over the last decade, but our understanding of how and why they take their forms has not progressed as fast. This article looks at models and themes which are largely independent of the exact synthetic method whether it is deposition, gas-phase condensation, solution based or hydrothermal synthesis. Elements are old dating back to the beginning of the 20th century – some of the pioneering models developed then are still relevant today. Others are newer, a merging of older concepts such as kinetic-Wulff constructions with methods to understand minimum energy shapes for particles with twins. Overall the broad framework of understanding and predicting the structure of nanoparticles via diverse Wulff constructions, either thermodynamic, local minima or kinetic has been exceedingly successful.

Key Points

- Outlines the main thermodynamics for describing the bulk and surface energies of nanoparticles
- Describes thermodynamic Wulff constructions for both supported and unsupported nanoparticles
- Describes kinetic Wulff constructions
- Discuss thermodynamic energy balance of twinned particles versus size
- Provides some general comments about how growth populations will evolve

Introduction

Small is Beautiful

The stained-glass windows in medieval churches whose color is due to nanoparticles have awed worshippers for centuries.

Small is Ugly

Nanoparticulate debris from wear and corrosion of dental and orthopedic implants can lead to severe illness and pain, a major health issue.

Nanoparticles are everywhere. They play a critical role in modern society in areas from heterogeneous catalysis to produce chemicals, to enhancing the mechanical properties of advanced metals used in the aerospace industry. Sometimes their size, shape and structure are exceedingly well controlled, sometimes it is the luck of the draw. They will continue to play a critical role into the future, and there are large efforts around the world to exploit them for numerous applications from controlled drug delivery in nanomedicine to controlling light using nanoplasmonics.

Given the size of the existing literature a complete overview within a short article is not possible, rather the intent is to overview methods to predict nanoparticle shape by understanding the thermodynamic and kinetic driving forces independent of whether they are produced by evaporation onto substrates, gas-phase condensation, solution synthesis or hydrothermal methods. Some other reviews discussing different aspects can be found in references (Marks, 1994; Hofmeister, 1998; Gryaznov *et al.*, 1999; Winn and Doherty, 2000; Yacaman *et al.*, 2001; Astruc *et al.*, 2005; Baletto and Ferrando, 2005; Rosi and Mirkin, 2005; Hu *et al.*, 2006; Jun *et al.*, 2006; Fan *et al.*, 2007; Anker *et al.*, 2008; Grzelczak *et al.*, 2008; Hofmeister, 2009; Millstone *et al.*, 2009; Xia *et al.*, 2009; Mayoral *et al.*, 2010; Cao *et al.*, 2011; Henry *et al.*, 2011; Prabhu and Poulose, 2012; Li *et al.*, 2014b; Thanh *et al.*, 2014; Ringe, 2014; Alex and Tiwari, 2015; Haider and Kang, 2015; Rabenau, 1985; Adschiri *et al.*, 2000; Goh *et al.*, 2002; Suchanek and Riman, 2006; Modeshia and Walton, 2010; Zhu and Hang, 2013; Wales, 2015; Marks and Peng, 2016; Guisbiers, 2019; Elahi *et al.*, 2018; Jeevanandam *et al.*, 2018). It is important to recognize that the question of thermodynamic versus kinetic control of shapes has been a source of confusion in the literature. For instance, the seminal paper by Wulff (1901) is routinely cited as the origin of the thermodynamic Wulff construction, but the title is "*On the question of speed of growth and dissolution of crystal surfaces*". The paper really deals with growth experiments, i.e., kinetic control of the shape, although Wulff assumed a direct relationship between the surface energy and growth rate.

In many cases nanoparticles are simple, single crystals with well-defined faces and simple platonic shapes such as octahedra or cubes. A different class of nanoparticles have more complex shapes and internal structure. The most common of these are in fcc materials, and contain twins, either parallel in "Lamellar Twinned Particles" (LTPs) or either five or twenty different single crystal units separated by twin boundaries, the latter being called "Multiply-Twinned Particles" or MTPs. As discussed by Hofmeister (Hofmeister, 2009; Hofmeister, 2004) there are reports of MTPs in the 19th century, what were called "fivelings" with cyclic twinning, see **Fig. 1** taken from Goldschmidt's atlas (Goldschmidt, 1913a,b, 1916, 1918a,b, 1920, 1922a,b) and a number of reports in the 50's and 60's of five-fold particles in whiskers (e.g., Evans and Wilman, 1952; Melmed and Hayward, 1959; Ogburn *et al.*, 1964; Schwoebel, 1966). The first definitive work analyzing in particular the icosahedral particles was performed by Ino and Ogawa (Ino, 1966; Ino and Ogawa, 1967; Ino, 1969) who were able to piece together the two main types of MTPs, the icosahedral (Ic) as well as the decahedral (Dh) MTPs. I will use herein these abbreviations for these particles which have become common in the literature, and correlate to the point group symmetries Ic and D5h respectively (Marks, 1980). Almost concurrently the structure of these particles was confirmed by Allpress and Sanders (1967). In the early work MTPs were described as assemblies of tetrahedral subunits with an angular gap equivalent to one or more Volterra disclinations (Volterra, 1907) elastically strained by ~2% for the Dh and ~6% for the Ic to form space-filling structures. The presence of elastic strain was confirmed at the atomic scale first using lattice imaging (Komoda, 1968) then later by atomic resolution imaging (Marks and Smith, 1981; Smith and Marks, 1981). For completeness, there are many more complicated shapes such as what were called "polyparticles" (Smith and Marks, 1981) which are either poly-icosahedral structures similar to those first analyzed by Hoare and Pal (1972) or due to incomplete coalescence.

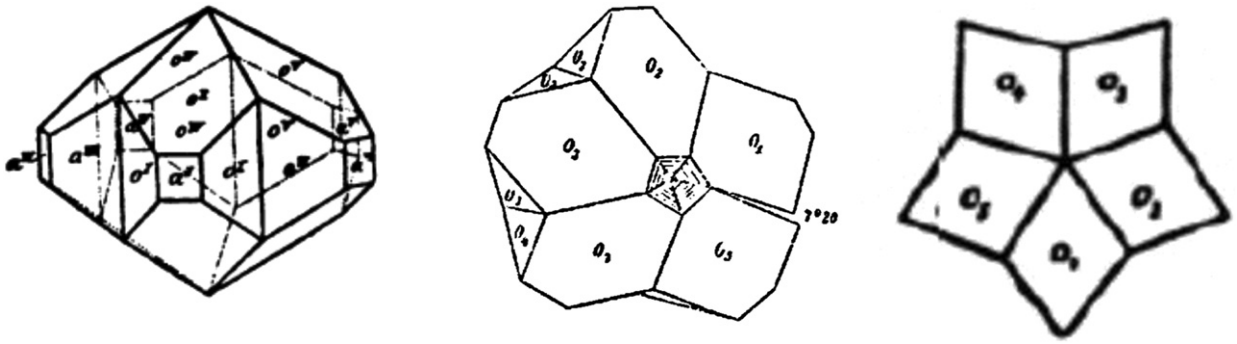

Fig. 1 Early drawings of five-fold crystals taken the Goldschmidt's Atlas, in a) for gold, b) for copper and c) for silver. All three shapes are different forms of modified Wulff constructions, probably kinetic.

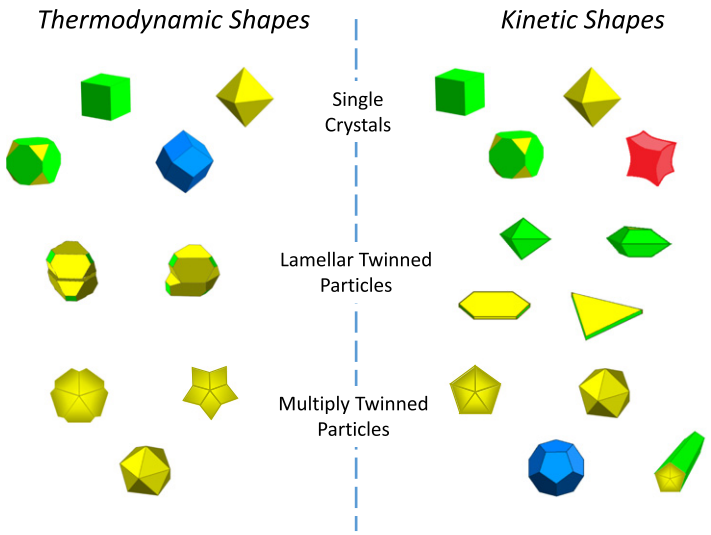

Fig. 2 Shapes discussed in the paper split into ones which can occur from thermodynamic control and ones which are only from kinetic control, split into the three broad categories of Single Crystals, Lamellar Twinned particles and Multiply Twinned Particles. Every thermodynamic shape can also arise from kinetics, but the converse is not true. The facets are color coded, yellow for {111}, green for {100} blue for {110} and red for higher index.

The focus of this article is the fundamentals that control the shape of nanoparticles, with a little more attention paid to the more complicated case of these multiply twinned particles. A schematic illustrating many of the shapes of interest is given in **Fig. 2**, split into cases where thermodynamic control determines the final shape and those where kinetics control. Several shapes appear on both sides, both single crystals as well as multiply-twinned particles. Every structure that is thermodynamically stable can also occur under kinetic control, but the converse is not true.

The structure of this article is as follows. First, some aspects of the thermodynamic fundamentals are described, particularly how one transitions from an atomistic approach to a continuum one. This is followed by a description of the large family of thermodynamic Wulff construction shapes for both supported and unsupported nanoparticles, as well as other variants such as when there is another degree of freedom in alloys at the nanoscale. I then turn from thermodynamic control to the kinetic Wulff constructions with the addition of enhancement terms for growth at twin boundaries or effects due to diffusion gradients. I next discuss some of the extended possibilities of kinetic shapes including why corners should be round and also symmetry breaking. Finally I turn to a brief discussion of the thermodynamic energy balance of MTPs versus size, pointing out the important ambiguities due to the role of chemisorbants in changing the surface stress, and provide a brief analysis of how structures of nanoparticle populations may evolve during growth, either *Survival of the Fittest; Survival of the Fastest* or *Survival of a Population*. A longer version of this article was published previously (Marks and Peng, 2016); this article includes a few more recent publications and newer work.

Thermodynamic Fundamentals

Fundamental to understanding nanoparticles is to consider the energy as a function of size, shape, stress and the external environment. This is not completely simple, and it is most important is to pay attention to what reference states are used and follow a specific set of conventions – different references yield wildly different results for some of the key parameters, particularly the surface stress tensor.

In a purely atomistic description, the total energy of an ordered, crystalline nanoparticle can be written as the infinite series:

$$E = \sum_{i,j,k} a_{ijk} n_i n_j n_k + \sum_{i,j} b_{ij} n_i n_j + \sum_i c_i n_i + d + \sum_i e_i / n_i + \sum_{ij} f_{ij} / n_i n_j \ldots \quad (1)$$

where the n_i are positive integers indicating the number of atoms along particular directions. To converge for an infinitely large crystal the series cannot contain any terms higher than third-order in n_i, and inverse powers may be needed to achieve the proper limits for a single atom.

Assuming convex shapes for all single crystal regions and replacing Eq. (1) with a vector of normal distances for each face from a common origin $h = (h_1, h_2 \ldots h_k)$ for k facets, with all h_i real but not necessarily positive numbers this leads to:

$$E = \sum_{i,j,k} A_{ijk} h_i h_j h_k + \sum_{i,j} B_{ij} h_i h_j + \sum_i C_i h_i + D + \sum_j F_i / h_i \ldots \quad (2)$$

As illustrated in **Fig. 3** each h_i is a combination of a geometric distance from the origin to the outermost plane of atoms plus what is called a "Gibbs distance" outside the surface, the latter is needed to properly transition from atomistic to continuum models (Cleveland and Landman, 1991; Hamilton, 2006). This decomposition corresponds to a Gibbs equimolar partition for the surface. For a bulk surface the relevant distance is half that to the first atomic plane removed to create the surface, effectively using a

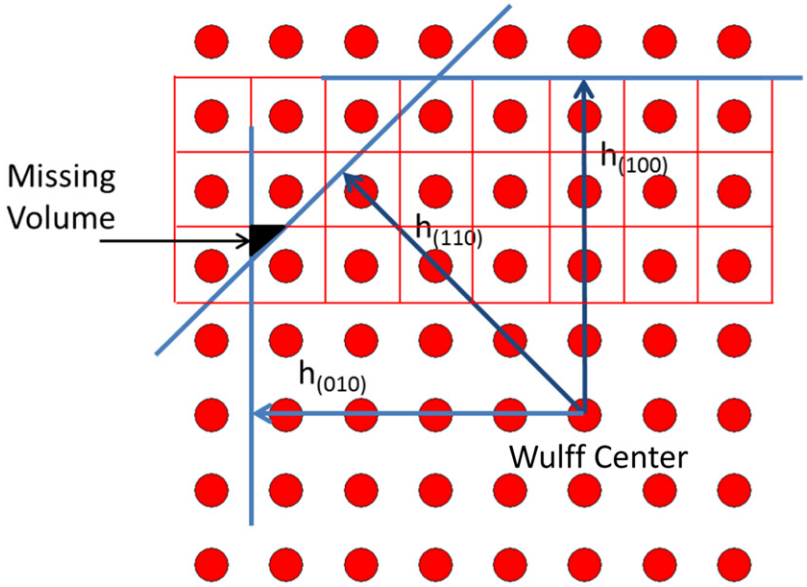

Fig. 3 Illustration of the equimolar cut for surfaces using the Wigner-Seitz unit cells. There may be a small discrepancy in the total volume as indicated, but this can generally be neglected.

Wigner-Seitz unit cell around each atom or basis of atoms in the unit cell. For very large sizes the first term on the right is then proportional to the volume and the number of atoms. When the size of the cluster is small there is a non-linear relationship between the h_i and the number of atoms along specific directions as discussed by Hamilton (2006). With the equimolar definition (s = (n-0.5)d) the effective edge energy terms are small and can be safely ignored, whereas with other definitions they are anomalously large.

The continuum shape is then defined by the set of planes normal to all h_i, and all continuum quantities are defined using the appropriate partial derivatives or integrals taking care to include non-linearity. For instance, the "Gibbs Volume" (V_G) would be the volume within this shape, whereas the "Gibbs Surface Area" (A_G) would be the external area, both in conventional units.

The energy terms $O(h^3)$ are the bulk cohesive energy and strain energy terms, those of $O(h^2)$, the total surface free energy and surface stress terms, those of $O(h)$, edge terms as well as counting corrections, and those of $O(h^0)$, corner as well as additional counting corrections (e.g., to ensure the correct limit for a single atom). As a general guide the relative importance of the different terms is:

Δ surface energy ≈ Δ strain energy > Δ surface stress energy > Δ twin boundary energy ≈ Δ lattice parameter ≈ Δ counting corrections.

Converting to a continuum model with the volume V_G (proportional to the number of atoms due to the definition) as the descriptor, then

$$\sum_{i,j,k} A_{ijk} h_i h_j h_k = V_G \left(\frac{\mu^B}{v_0} + W_D \right) \tag{3}$$

where μ^B is the bulk chemical potential per atom in the absence of any strain, v_0 the volume per atom and W_D the strain energy density. In principle the total strain energy of the nanoparticle can be size dependent. While energy models excluding the strain energy have been suggested, (Barnard *et al.*, 2009, 2010) these go to a physically incorrect limit at large sizes and are therefore incorrect. Additional terms can be added for pressure contributions, but these are small and cancel when different structures are compared. Including the temperature dependence will include entropy contributions, which can be important.

In a similar fashion the second term on the right of Eq. (2) can be written as

$$\sum_{i,j} B_{ij} h_i h_j = V^{\frac{2}{3}} \left(\gamma_{111} \varepsilon_W + < g_{ij} e_{ij} > \varepsilon_g \right) \tag{4}$$

which contains the surface free energy (γ) per unit area as well as that of any twin boundaries in $V^{\frac{2}{3}} \gamma_{111} \varepsilon_W$ and the coupling of strains and the surface free energy in $V^{\frac{2}{3}} < g_{ij} e_{ij} > \varepsilon_g$ (Marks, 1983a; Howie and Marks, 1984; Marks, 1984) where g_{ij} is the surface stress tensor and e_{ij} strains which will be discussed a little later in Eqs. (7) and (8). The constant ε_W is defined as

$$\varepsilon_W = \left(\frac{1}{\gamma_{111}} \right) \int \gamma dS / V^{2/3} \tag{5}$$

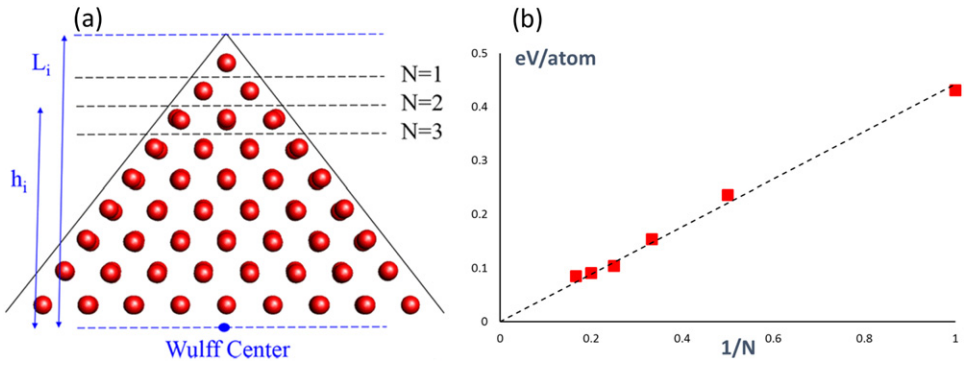

Fig. 4 Density functional theory results for the chemical potential (weighted mean curvature) in the limit of small sizes. In (a) the model used indicating truncations for N = 1, 2, 3 with the corresponding equimolar surfaces and facet length, and (b) the chemical potential as a function of truncation. The scaling matches very well to the continuum expectation.

and is a size independent constant which only depends upon the external surface of the nanoparticle and (weakly) upon the twin boundaries.

To obtain the total energy, the volume and surface terms Eqs. (3) and (4) are substituted into Eq. (2):

$$E = V\left(\frac{\mu^B}{v_0} + W_D\right) + V^{\frac{2}{3}}\left(\gamma_{111}\varepsilon_W + <g_{ij}e_{ij}>\varepsilon_g\right) + O(h) \tag{6}$$

where the rightmost term includes any residual corrections due to counting effects as well as edge and corner energies, and the inverse terms in Eqs. (1) and (2) have been ignored. For very small clusters these may be important; otherwise they can be neglected if the correct equimolar partition is used.

How a full conversion to a continuum formulation where the *final volume and area* (not the initial Gibbsian values) would be performed is worth indicating. The Gibbs volume and surface area are proportional to the number of atoms involved in each at some reference condition, for instance standard temperature and pressure (STP) and no strain. The classical volume and surface area are referenced to the *final* state of the nanoparticle, and as such vary with temperature, pressure and strain, and are not proportional to the number of atoms.

This distinction is important when it comes to how to describe the surface free energy in the presence of strain. Most liquids cannot be strained, so there is only one energy term of importance, typically called the surface tension. However, solids can be strained so there are two terms, the free energy per surface unit and the change in the total energy of the surface with strain. Referencing to the free energy E_S of a flat surface per surface atom (N_S) or the Gibbsian area A_G, then the total energy, surface free energy γ.and the surface stress tensor as g_{ij} are:

$$E_S = A_G\gamma; \gamma = \partial E_S/\partial A_G; g_{ij} = \partial\gamma/\partial e_{ij}. \tag{7}$$

with the surface free energy proportional to the surface chemical potential per atom, the surface stress the change with respect to some strain component e_{ij}. An alternative approach is to define the energy of the flat surface referenced to its final area A, where the later changes with the strain, in which case

$$E_S = A\gamma; \gamma = \partial E_S/\partial A; g_{ij} = \gamma\delta_{ij} + \partial\gamma/\partial e_{ij}. \tag{8}$$

since the final area changes with strain, with δ_{ij} the Kronicker delta function. The two are different, and the sign and magnitude of the surface stress tensor depends upon the definition use. This second definition is problematic for analyses of the elastic strain contributions, since this is normally considered in terms of a nominal strain-free volume. The first, atomistic or Gibbsian definition is more convenient when dealing with nanoparticles since it is also consistent with how the volume was defined earlier.

The minimum energy shape (discussed further in the next section) is then obtained by minimizing Eq. (6) at constant volume. If the strain and surface stress terms are ignored this is equivalent to minimizing the dimensionless parameter ε_W. An alternative is a Lagrangian approach and minimize

$$L = \int \gamma dS - \lambda \int dV \tag{9}$$

Setting the variation to zero for any and all facets (or curved regions) leads to an additional term called the "weighted mean curvature", the ratio of the change in surface energy (E_S) for a given facet (including surface stress contributions) and the change in volume V (Taylor, 1992):

$$wmc(h_i) = \lim_{\delta\to 0}\Delta E_s(h_i + \delta h_i)/\Delta V(h_i + \delta h_i) = \mu^s(h_i)/v_0 \tag{10}$$

where $\mu^s(h_i)$ is the chemical potential for facet i as a function of h_i and v_0 is the atomic volume. The variables in Eq. (10) can be either Gibbsian or fully classical. Where the weighted mean curvature differs from the surface free energy is that it can be used for

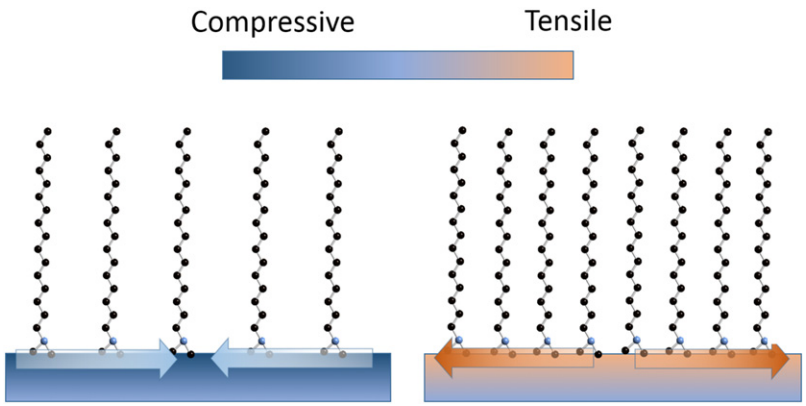

Fig. 5 Illustration of how chemisorption can affect the surface stress. On the left, when chemisorbed molecules are far apart attraction between them can lead to a compressive stress; on the right when they are too close the surface stress will be tensile. Changes in the surface stress with coverage will occur for large ligands, as drawn, or for smaller chemisorbed species such as water, oxygen or carbon monoxide.

shapes which are not flat, for instance rounded corners and edges. For instance, for faceted nanoparticles the weighted mean-curvature is piecewise continuous and will scale with h_i as shown in **Fig. 4** as

$$wmc(h_i) = \overline{\gamma}_i/(L_i - h_i) \tag{11}$$

where the facet disappears for $h_i \geq L_i$ and Eqs. (10) and (11) define a weighted mean surface energy $\overline{\gamma}_i$. The chemical potential goes towards infinity as the facet gets smaller, l as verified by density function calculations (Alpay *et al.*, 2015) shown in **Fig. 4**. This implicit singularity in the chemical potential for corners has been known for a long time, and is frequently handled in numerical models by adding a regularization term (e.g., Cahn and Hoffman, 1974; Voorhees *et al.*, 1984; Dicarlo *et al.*, 1992; Golovin *et al.*, 1998; Akaiwa *et al.*, 2001; Eggleston *et al.*, 2001; Wise *et al.*, 2007; Torabi *et al.*, 2009; Mastroberardino and Spencer, 2010) and references therein. Note that this indicates that sharp corners are energetically unreasonable, rationalizing the fact that most experimental particles show at least some rounding (Alpay *et al.*, 2015).

Since many nanoparticles also contain strains with the strain energy density implicitly a functional of the shape, a complete description includes a term

$$w(h_i) = \lim_{\delta \to 0} \Delta W_D(h_i + \delta h_i)/\Delta V(h_i + \delta h_i) = \mu^W(h_i)/v_0 \tag{12}$$

To date there is no evidence that this shape-dependent strain energy contribution to the chemical potential matters for solution growth, although it is known to be important in epitaxial growth (e.g., Drucker, 1993; Hammar *et al.*, 1996; Ross *et al.*, 1998), and there are special cases where minima of the strain energy for certain sizes are believed to be important in favoring specific sizes of precipitates (Hamilton *et al.*, 2007).

The bulk chemical potential will vary with temperature, pressure etc., but when comparing different shapes this cancels out. When nanoparticles are grown by solution methods exact numbers for the chemical potential are not known, but they have been measured in a number of cases on different substrates by the group of Campbell (Campbell and Sellers, 2013; Campbell and Mao, 2017; Hemmingson and Campbell, 2017). There will be a weak dependence of the strain energy upon temperature, but this can almost certainly be neglected. Both the surface free energy and the surface stress will depend upon temperature, and in particular the environment. There is now relatively good data on the surface free energy of most metals and they can be calculated fairly accurately with recent functional via density functional methods,. When the surface is clean surface free energies are of the order of one to few J/m^2, but can be reduced by a factor of 2–3 when other species are adsorbed onto the surface. For most metals the surface stress tensor is positive, i.e., the surface free energy is lower when the surfaces contract. However, with chemisorption this need not be true and the sign of the surface stress tensor changes depending upon whether there are attractive or repulsive interactions between molecules on the surface as illustrated in **Fig. 5**; that this can occur for small molecules on metals is very well established (e.g., Muller and Saul, 2004; Pimpinelli and Villain, 2010), less well known but also known to exist for larger molecules (Watari *et al.*, 2011).

For other materials such as oxides how the terms vary with chemisorption is much less clear, with relatively few measurements and only a few calculations, and there may well be rearrangements of the surface atoms to yield reconstructed surfaces. These are well known for many of the simple metals, and have been observed in a number of cases for nanoparticles (Marks, 1983b; Takeguchi *et al.*, 2001; Casillas *et al.*, 2012). It is only rather recently that they have also been observed on oxide nanoparticles (Lin *et al.*, 2013, 2014; Zhang and Zheng, 2015; Crosby *et al.*, 2016; Yuan *et al.*, 2016, 2017; Ek *et al.*, 2018; Liu *et al.*, 2020) and example being shown in **Fig. 6**, where the exact structure formed depended upon the synthesis conditions. For strontium titanate nanocuboids synthesized by a hydrothermal route using oleic acid, strong chemisorption of the acid on the surface favored a strontium oxide termination; synthesis using acetic acid which is highly water soluble, a titanium dioxide double-layer surface forms similar to what occurs for mesoscale (100) surfaces (Jiang and Zegenhagen, 1999; Castell, 2002a,b; Erdman *et al.*, 2002, 2003; Johnston *et al.*, 2004; Warschkow *et al.*, 2004; Silly and Castell, 2005; Silly *et al.*, 2006; Newell, 2007; Herger *et al.*, 2007; Kienzle *et al.*, 2011; Zhu *et al.*, 2012; Kienzle and Marks, 2012; Marshall *et al.*, 2015; Ciston *et al.*, 2015) due to dissolution of strontium from the near surface region.

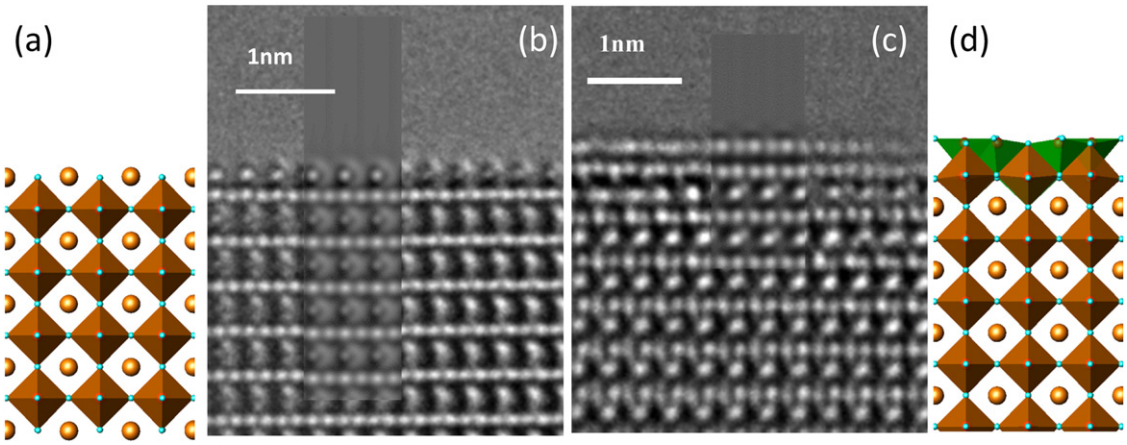

Fig. 6 Images of the surface of $SrTiO_3$ nanocuboids prepared using different approaches. On the left in (a) and (b) with oleic acid, which leads to a SrO termination and on the right in (c) and (d) in acetic acid, which leads to a TiO_2 double layer. The surface is shown with brown tetrahedra for TiO_6 units, green for TiO5[] and the Sr are gold.

Minimum Energy Solutions

I next turn to discuss the thermodynamic equilibrium shape of nanoparticles ranging from single crystals to those on supports or ones with twin boundaries. As will be seen there are common elements to the solutions, for which the general term of Wulff constructions will be used.

Wulff Construction for Single Crystals

In the absence of any strain terms the minimum energy shape at constant volume is the variational minimum of ε_W, equivalently, the total energy at constant volume, which is also equivalent to a constant weighted mean curvature (chemical potential) for all facets. For a single crystal this is the thermodynamic Wulff construction, the shape (set of points) S_w given by (Cahn and Hoffman, 1974; Hoffman and Cahn, 1972):

$$S_W = x : x.\hat{n} \leq \lambda\gamma(\hat{n}) \text{ for all unit vectors } \hat{n} \tag{13}$$

This is all the points x within $\hat{n} \leq \lambda\gamma(\hat{n})$, where $\hat{n}$ is a unit vector defined by the crystallographic orientation of a face (hkl), $\gamma(\hat{n})$ is the orientation-dependent surface free energy, and λ is a constant that accounts for the volume. An alternative form is through the envelope planes of the particle, as first proved by von Laue (1943) and Dinghas (1944)

$$\gamma_i = h_i/\lambda, \tag{14}$$

where h_i is the normal distance from the center of the particle to a crystallographic facet i as defined earlier and γ_i is the orientation-dependent surface free energy of the facet.

One can generate the Wulff shape by plotting the surface energy as a function of angle and then taking the inner envelope of points, as shown in **Fig. 7** for the simplified case when only {111} and {100} facets are relevant. In general nanoparticles are more complex with small additional regions of higher index facets. An alternative method which has some mathematical advantages is to use a vector definition instead of the scalar surface free energy (Cahn and Hoffman, 1974; Hoffman and Cahn, 1972). The Wulff shape is relatively easy to determine experimentally from electron microscopes images, and one example for strontium titanate is shown in **Fig. 8** (Crosby *et al.*, 2015) where there is good agreement between experimental results on the left and the Wulff shape on the right, here constructed using the Wulff Maker software (Zucker *et al.*, 2012); other available software can also be useful (Boukouvala and Ringe, 2019; Rahm and Erhart, 2020; Boukouvala *et al.*, 2021) particularly for twinned crystals as described later.

Winterbottom and SummerTop for Supported Nanoparticles

The Wulff construction applies to a free-floating particle in vacuum, a gas or a liquid; changing the environment will change the surface free energies but nothing else. A second type of shape occurs when the particle is supported on a flat substrate when the substrate is constrained to remain flat. If the surface free energy of the metal particle is γ_i, there is an additional free energy term γ_A for the adhesion (per nanoparticle atom at the interface) when the exposed surface of the nanoparticle is replaced by an interface, which leads to an effective interfacial term of $\gamma_{Int} = \gamma_i + \gamma_A$. This is used instead of γ_i when calculating the total surface energy. The interfacial free energy term can be either positive or negative depending upon the chemical bonding between the nanoparticle and the substrate. This will depend upon the chemical species, the misfit between the nanoparticle and the substrate as well as details

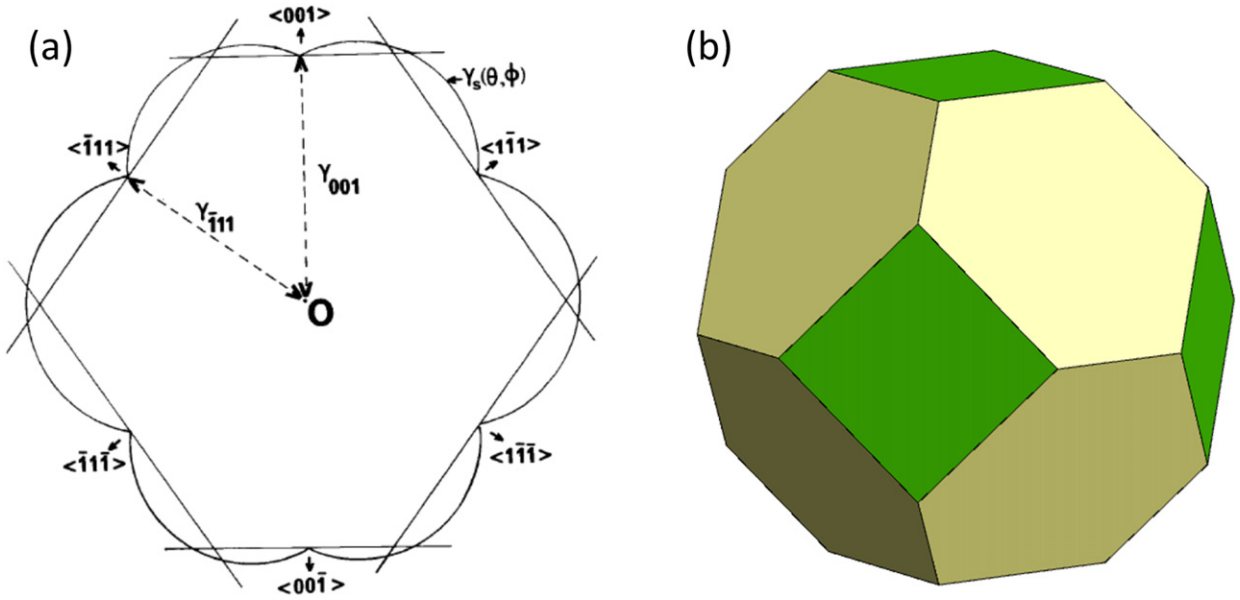

Fig. 7 Illustration of the Wulff construction for a fcc material where {111} and {100} surfaces dominate, drawn for a [110] projection on the left in (a), and the corresponding three-dimensional shape on the rightin (b), with green for {100} and yellow for [111].

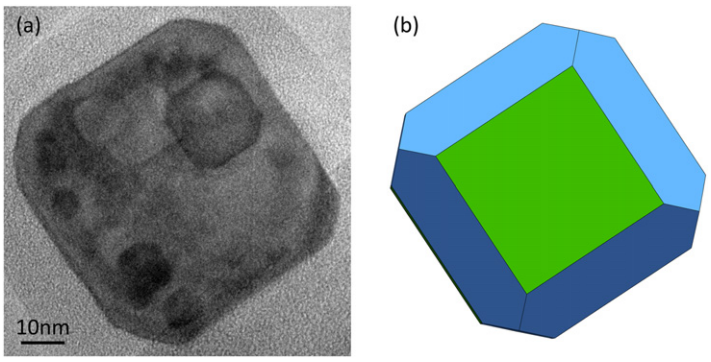

Fig. 8 Experimental results for the Wulff shape of annealed strontium titanate nanocuboids based upon both the external shape and that of internal Kirkendall voids, an image on the left in (a) and the three-dimensional Wulff shape on the right in (b) with {100} green and {110} blue. The ratio of the surface energies from twenty-nine measurements was $\gamma_{110}/\gamma_{100} = 1.139(55)$.

of the interfacial structure. The equilibrium shape, called the Winterbottom shape (Winterbottom, 1967) includes a facet to represent this interfacial energy in an otherwise standard Wulff construction. As illustrated in **Fig. 9**, if $\gamma_A$is greater than zero we have the equivalent of dewetting; if it is the negative of the surface free energy we have the equivalent of wetting with a full range in between. This can also be extended for two interfaces which yields the SummerTop construction (Zia *et al.*, 1988) although this is rare in real physical systems.

Fig. 10 shows experimental images of the Winterbottom case, in (a) and (b) showing how the interface can depend upon the chemical character of the substrate (Lin *et al.*, 2015) where in (b) the ceria has been slightly reduced due to testing for the water-gas shift reaction. As a caveat, as shown in **Fig. 10**(c) for gold on magnesium oxide, the substrate does not have to be flat and in this case the particle is partially embedded in the support (Ajayan and Marks, 1989a; Marks and Ajayan, 1990). This has been observed for metal nanoparticles (Ajayan and Marks, 1989a; Marks and Ajayan, 1990; Bernal *et al.*, 1996, 1999, 2003; Fu *et al.*, 2005; Zhang *et al.*, 2016) and more recently for oxide nanoparticles (Cheng *et al.*, 2019) and plays an important role in what is called "Strong Metal-Support Interactions" (Zhang *et al.*, 2016; Tauster, 1978; Tauster *et al.*, 1978, 1981; Tauster, 1987; Haller and Resasco, 1989; Liu, 2011; van Deelen *et al.*, 2019). Partial embedding of the particles may be quite common particularly with heterogeneous catalysts, and to date does not have any simple model although shapes can be predicted by numerical minimization of the total energy. Note that these shapes have also been observed in more complex cases where the mathematics is the same, for instance for nanoparticle superlattices (Lewis *et al.*, 2020).

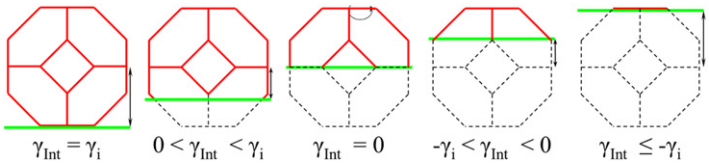

Fig. 9 Schematic of the variation in shape of a nanoparticle with a [100] epitaxy on the substrate, as a function of the interfacial free energy. From left to right is the solid analogue of going from dewetting to wetting.

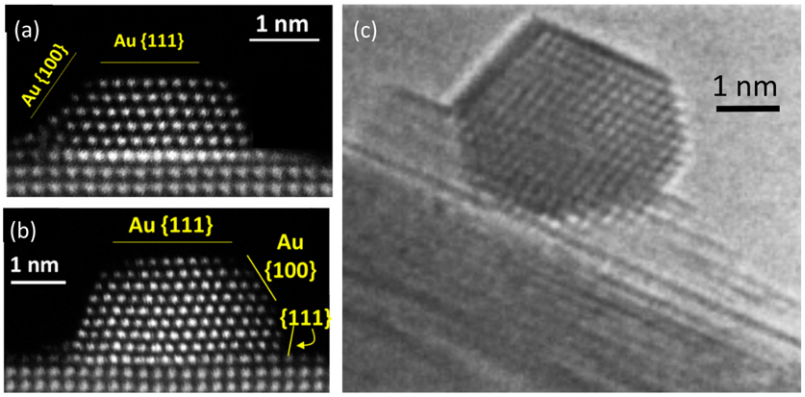

Fig. 10 Experimental images in (a) and (b) for gold on ceria supports where the sample in (b) has been used during catalytic testing. Due to reduction of the ceria the interface and Winterbottom shape changes. Shown in (c) is an example for gold on magnesium oxide where the interface is not flat.

Modified Wulff Construction for MTPs

Instead of a boundary to an external support, there can be internal boundaries, most frequently twin boundaries. The general approach is to find the minimum energy shape for each single crystal subunits including the twin boundaries, and then assemble the composite particle from these units, see **Fig. 11**. Similar to the Winterbottom construction we associate an additional free energy γ_T with each twin boundary, but different from it we partition this energy to the two sides and generate a variant of the Wulff construction for each single crystal subunit. Finally the subunits are assembled to create the full twinned nanoparticle. This approach was called the "modified Wulff construction" (Marks, 1983a, 1984) Each individual single crystal subunit will be convex, but the overall composite particle does not have to be.

In a set notation the modified Wulff construction can be written as the superset of Wulff shapes S_m for all the individual single-crystal subunits where

$$S_m = x : (x - o_m).\hat{n} \leq \lambda_m \gamma_m(\hat{n}) \text{for all unit vectors } \hat{n} \tag{15}$$

where the O_m are the origins for each single-crystal unit, $\gamma_m(\hat{n})$ the surface free-energy appropriately oriented in space which includes a "twin facet" energy for each segment "m" adjacent to a segment "n" of $\alpha_{mn}\gamma_t$, with the additional conditions

$$S^t_{mn} = S^t_{nm} \text{ and } \alpha_{mn} + \alpha_{nm} = 1 \tag{16}$$

with S^t_{mn} is the bounding twin surface of segment "m" where it joins to segment "n".

The simplest case is with $\alpha_{mn} = 1/2$ and all λ_m the same, a symmetric solution. One twin plane gives a singly twinned particle, while a sequence of parallel twin boundaries gives lamellar-twinned particles or LTPs, first observed for nanomaterials in the inert gas evaporation literature (Kimoto and Nishida, 1967; Yatsuya *et al.*, 1973; Kasukabe *et al.*, 1974; Ohno *et al.*, 1976; Granqvist, 1976; Hayashi *et al.*, 1977; Dmitrieva *et al.*, 2007) although they occur for many bulk crystals (e.g., the drawings in Goldschmidt's Atlas (Goldschmidt, 1913a,b, 1916, 1918a,b, 1920, 1922a,b)). **Fig. 12** shows the three-dimensional shape of the a single-twin LTP from the construction (Marks, 1983a) together with experimental results based upon an electron tomography experiment projected in three directions (Gontard *et al.*, 2009) Five segments each bounded by two non-parallel planes gives a Dh (see **Figs. 11** and **13**, the later from (Mariscal *et al.*, 2012; Yacaman, 2012; Ji *et al.*, 2014)), slightly different forms depending upon the surface free energies; twenty segments bounded by three non-parallel boundaries, an Ic (see **Fig. 14** from (Mariscal *et al.*, 2012; Yacaman, 2012; Hubert *et al.*, 1998)) with again a number of variants depending upon which facets have the lowest surface free energy.

From the properties of the Wulff construction, for specified values of α_{mn} and λ_m this is the global minimum total surface energy shape. With respect to variation in α_{mn} and λ_m it may be a local minimum in order to satisfy $S^t_{mn} = S^t_{nm}$ or alternatively a saddle point. Numerical calculations for a Dh yield a minimum for only {111} and {100} faceting (Dundurs *et al.*, 1988) although it is a saddle-point for an isotropic surface free energy (Marks, 1983a, 1984). There is to date no analytical theory describing what values of the surface-free energy anisotropy the construction leads to minima versus a saddle points, a topic that merits further attention. Asymmetric

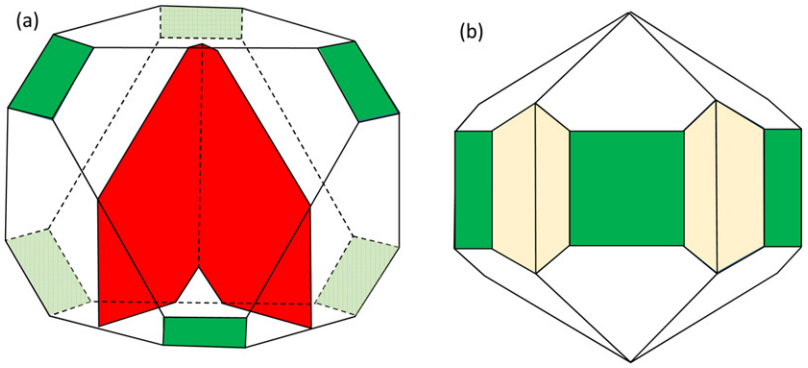

Fig. 11 Illustration of the modified Wulff construction. For the three-dimensional Wulff shape shown on the left in (a) the region between two twin planes (red) is extracted. Five of these joined at the twin boundaries leads to the Dh shape shown on the right in (b), with the re-entrant {111} surfaces in yellow. In both diagrams {100} faces are green.

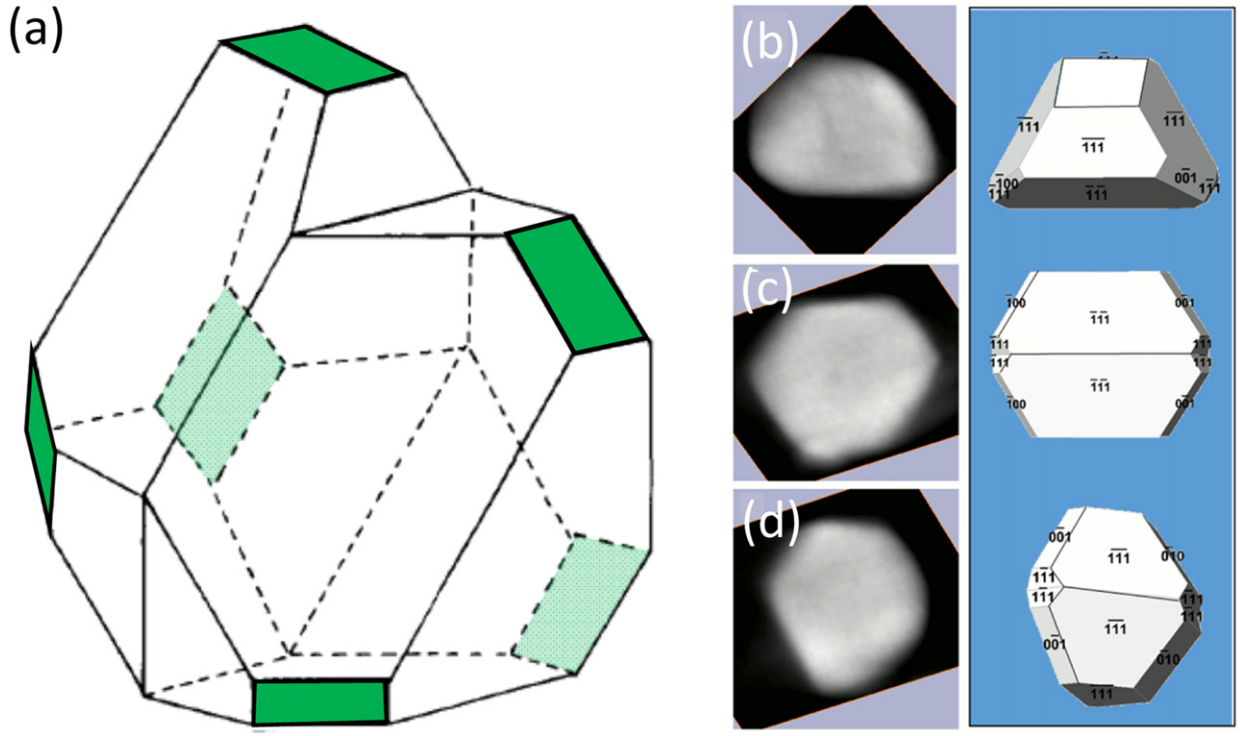

Fig. 12 Shape of an LTP on the left with one twin boundary for only {111} and {100} facets, the later green with experimental results based on a three-dimensional tomographic analysis projected onto three directions, in (b)-(d) which are is good agreement with the theoretical prediction. Parts (b)-(d) reprinted with permission from Gontard, L.C., Dunin-Borkowski, R.E., Gass, M.H., Bleloch, A.L., Ozkaya, D., 2009. Three-dimensional shapes and structures of lamellar-twinned fcc nanoparticles using ADF STEM. Journal of Electron Microscopy 58, 167–174. After a slight modification, with thanks to R. Dunin-Borkowski for supplying an original.

partitioning of the twin boundary is also possible ($\alpha_{mn} \neq 1/2$), in which case the scaling term λ_m for each segment is different. This leads to some of the asymmetric nanoparticle structures observed experimentally (Marks, 1983a) and described further below.

The most common example of the modified Wulff construction for face-centered cubic (fcc) Dh occurs when only the {111} and {100} surfaces are low energy, yielding the shape shown in **Figs. 11** and **13**(a). One feature which makes this different from most shapes is the presence of a re-entrant surface at the twin boundaries, different from single crystals which are always convex. In their early atomistic work Cleveland and Landman coined the term "Marks Decahedron" for this, which has now become a generic term frequently appearing without citation.

The term Marks decahedra has become common in the literature, but is only one example and the construction is general, and yields all of the shapes in **Fig. 13**. If the free energy of the {100} facets is decreased such that $\gamma_{111}/\gamma_{100} > 2/\sqrt{3}$, these notches disappear and the particle elongates to a rod-like shape similar to that first investigated by Ino (Ino, 1966; Ino and Ogawa, 1967; Ino, 1969) (see

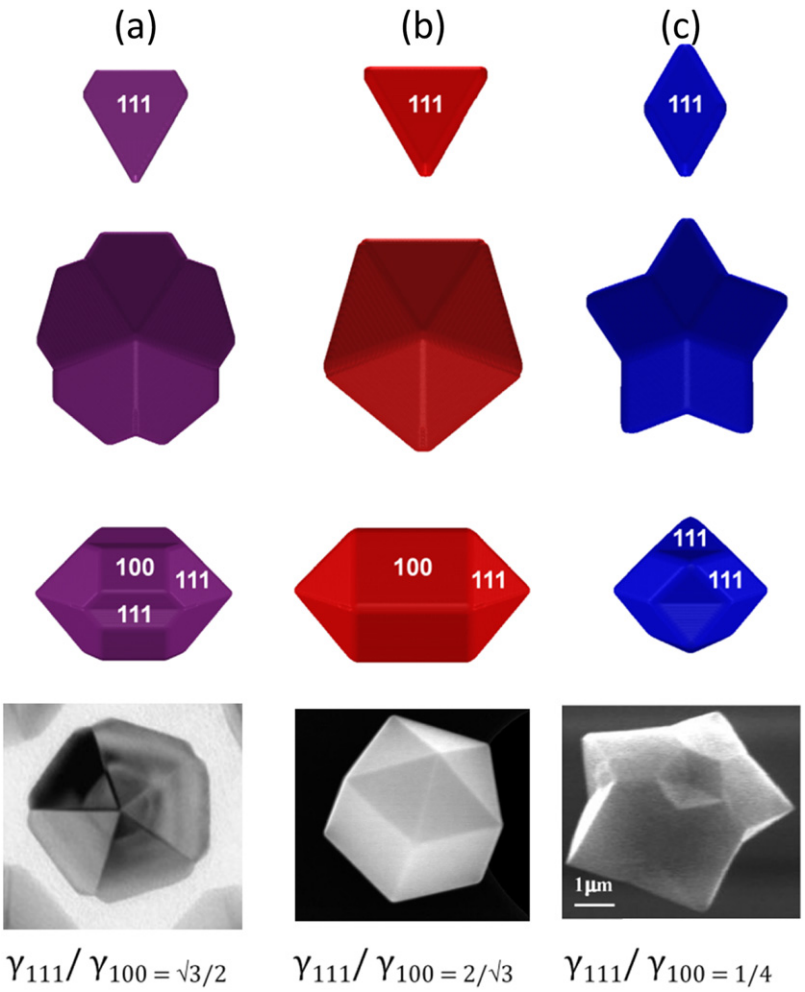

Fig. 13 Different cases for Dh in three columns (a)-(c) with different ratios of the {111} and {100} surface energies. Shown at the top is the single segment, below the particle down the common [011] direction and below from the side. Experimental images are shown below. on the lower left reproduced with permission from Ji, W.H., Qi, W.H., Tang, S.S., *et al.*, 2014. Synthesis of marks-decahedral Pd nanoparticles in aqueous solutions. Particle & Particle Systems Characterization 31, 851–856. In the lower middle reproduced with permission from Mariscal, M.M., Velazquez-Salazar, J.J., Yacaman, M.J., 2012. Growth mechanism of nanoparticles: Theoretical calculations and experimental results. Crystengcomm 14, 544–549. and on the lower right from Yacaman, M.J., 2012. Private Communication.

Fig. 13(b)). This is a constrained thermodynamic structure, not a global minimum. If instead the {100} energy is increased and is much larger than the {111} energy ($\gamma_{111}/\gamma_{100} < < 1$), the {100} faces no longer appear in the minimal energy shape, and the result is a star decahedron (Fig. 13(c)), similar to those found in several cases (Lim *et al.*, 2009a). This is a plausible global thermodynamic structure. Addition of {110} facets will lead to more rounded structures, as will inclusion of other higher-index surface facets if these are of low enough surface free energy although these are always higher in energy than single crystals. Sadly the generalization of the modified-Wulff construction is rarely used, and often these are considered as different cases when in fact they are not.

For the icosahedral particles the possibilities are more limited. If {111} surfaces dominate one has the conventional icosahedron as shown in Fig. 14(a). There will be marginal stability if {110} surfaces dominate which yields a regular dodecahedron as shown in Fig. 14(b), and there can be intermediate cases as also shown in Fig. 14(c). Similar to the Dh, these are not different nanoparticles, they are all understandable and are solely due to slight differences in the surface energies or growth kinetics.

With clean surfaces the twin-boundary energy is small compared to the surface free-energies and can be neglected to first order, in which case the origins O_m are common. This approximation is accurate to second-order in the energy (Marks, 1983a, 1984) and the difference in the shape will be below experimental error for vacuum or inert gas evaporation experiments. For solvent-based growth the surface free energies may be substantially lower and this leads to re-entrant surfaces at the disclination line for both Dh and Ic, as sometimes observed experimentally (Yacaman, 2012) and outlined in previous publications (Marks, 1983a, 1984); for experimental examples see Fig. 13(c) and 14(d).

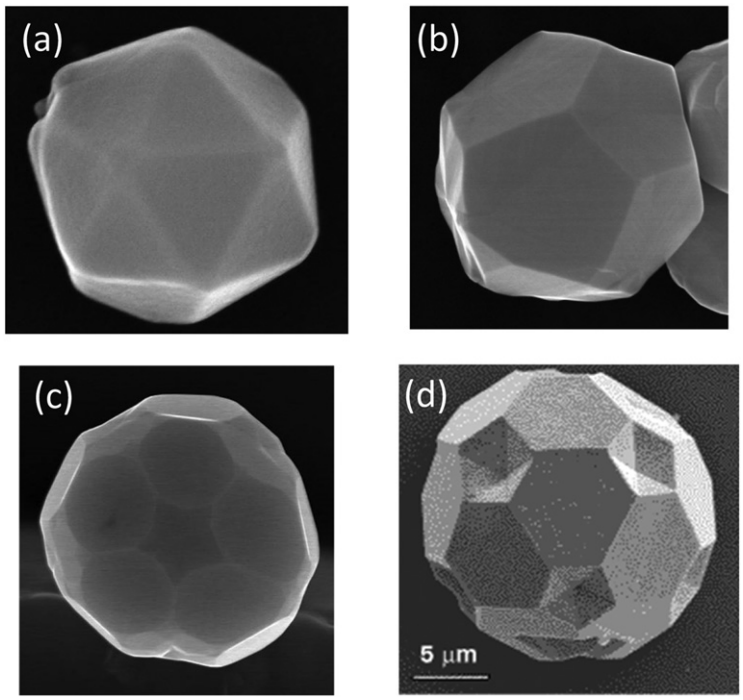

Fig. 14 SEM images, in (a)-(c) and d) in B_6O, showing different types of Ic, a regular icosahedron with {111} facets in a), a dodecahedron with {110} in b) and a combination of {111} and {110} in c). In d) the re-entrant surfaces at the twins are evident, indicating that the twin boundary energy is relatively large. Figures reproduced with permission from (a)-(b) Yacaman, M.J., 2012. Private Communication. (c) Mariscal, M.M., Velazquez-Salazar, J.J., Yacaman, M.J., 2012. Growth mechanism of nanoparticles: Theoretical calculations and experimental results. Crystengcomm 14, 544–549. (d) Hubert, H., Devouard, B., Garvie, L.A.J., *et al.*, 1998. Icosahedral packing of B-12 icosahedra in boron suboxide (B6O). Nature 391, 376–378.

To illustrate the magnitude of the variations, values of ε_W for a few different particles with only {111} and {100} facets are given in **Table 1** (Marks, 1980; Marks, 1983a; Marks, 1984) with the term β parameterizing the relative surface free energies given by

$$\beta = 1 - \gamma_{100}/\sqrt{3}\gamma_{111} \tag{17}$$

For clean fcc metals the surface free energy of {100} is larger than that of {111}, so based just upon the surface energies, the Ic is lowest followed by the Marks decahedron then single crystals. The difference between single crystals and LTPs is so small that they can coexist and it is unlikely that LTPs will transform to the (lower energy) single crystals in finite time. Some other shapes such as a Dh with just a single (100) truncation (Ino Dh) as well as a pentagonal bipyramid with only {111} facets ((111) only Dh) are included in the table – these are always energetically unfavorable for typical values of the {100} and {111} surface free energies. If the {100} surface energy is low a rod-shaped Dh will be a constrained thermodynamic shape, never a global minimum.

A few more complex shapes are included in the table with are sometimes observed experimentally. One set of structures included are asymmetric particles as illustrated in **Fig. 15**; the portioning of the twin boundary energy does not have to be equal. Asymmetric Dh have been known for more than fifty years dating back to at least the early work of Yagi (Yagi *et al.*, 1975) the work by the author in the first modified-Wulff paper (Marks, 1983a) they play an important role in quasi-melting (Dundurs *et al.*, 1988; Marks *et al.*, 1986; Ajayan and Marks, 1988; Ajayan and Marks, 1989b) have been analyzed many times (Uppenbrink *et al.*, 1992; Walsh *et al.*, 2015) up to more recent work such as analysis of disclination migration (Song *et al.*, 2019). Unfortunately the eye is drawn more to the symmetric variants, so they probably are much more common that they have been reported to date. They have intermediate surface energies, as shown in **Table 1**.

There are also many more complex particles which were originally termed polyparticles. Assuming a constraint that the twin boundaries cannot be eliminated there are many more ways to assemble structures which are local minima, not necessarily global minima. One of these is a Bi-Ic where five segments are shared between two Ic, see **Fig. 16**. These more complex particles were first described by Komoda (Komoda, 1968) and then analyzed in some detail by Smith and Marks (1981) They can be described as larger scale analogs of the polytetrahedral structures first considered by Hoare and Pal (1972,1971,1975). They have been rediscovered in the literature many times.

We can generalize for when Ic and Dh are lower in surface energy than single crystals. From solid geometry the total surface energy can be written, (ignoring the twin boundary contribution) in terms of the parameter ε_W as:

$$\varepsilon_W = \left[\frac{9}{\gamma_{111}}/N_1S_1 + N_2S_2\}\right]^{1/3} \tag{18}$$

Table 1 Values of ε_W for a few different particles with only {111} and {100} facets in terms of the parameterization of the {100} and {111} surface energies

Particle		$\beta = 1/3$	$\beta = 5/12$
(111) Tetrahedron		7.206	7.206
(111) Octahedron		5.719	5.719
(100) Cube		6.928	6.062
Single Crystal		5.499	5.271
LTP with m twins	m = 1	5.500	5.272
	m = 2	5.500	5.273
	m = 3	5.501	5.274
	m = 4	5.502	5.275
Marks Dh		5.436	5.243
Ino Dh		5.593	5.281
(111) only Dh		6.192	6.192
Ic		4.899	4.899
Bi-Ic		5.051	5.051
Asymmetric Twin		N/A	5.272
Asymmetric Dh		N/A	5.256

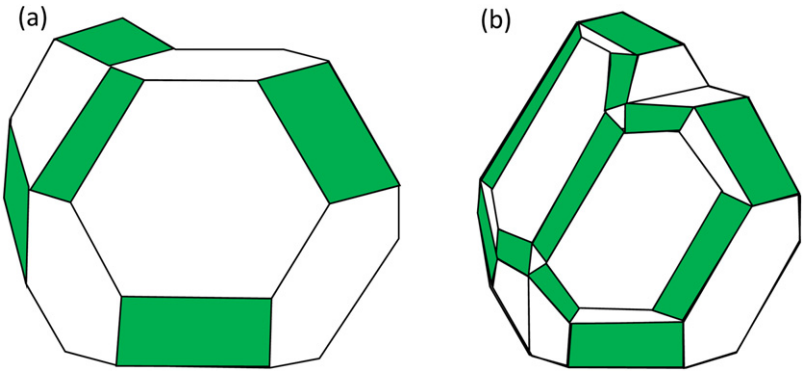

Fig. 15 Asymmetric solutions, on the left in (a) for an LTP and on the right in (b) for a Dh. Asymmetric solutions are common, but the eye is drawn to symmetry.

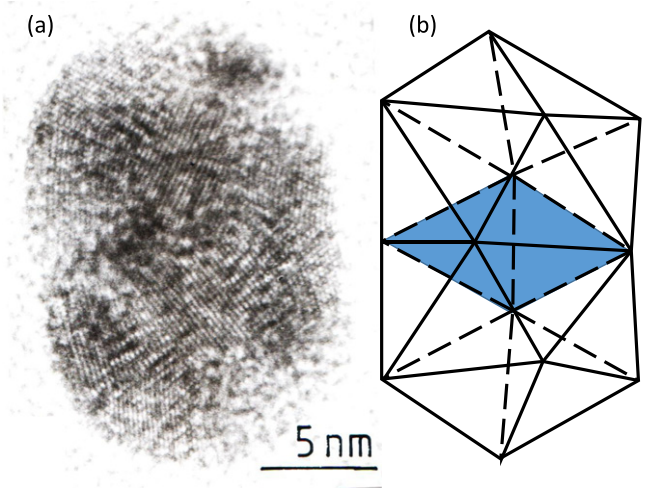

Fig. 16 Old HREM images of a bi-icosahedron on the left in (a), with a model of the structure showing the shared decahedral unit in blue on the right in (b).

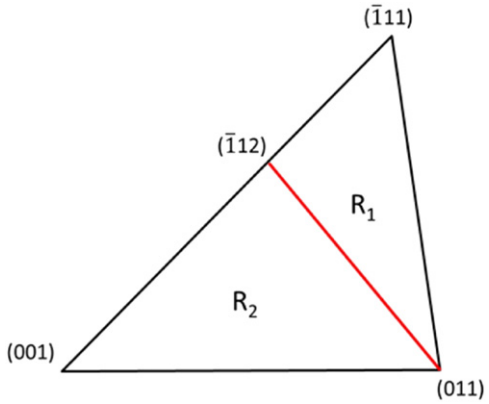

Fig. 17 Stereographic triangle split into the two regions R_1 and R_2. MTPs have more of region R_1.

where S_1 and S_2 are the integrated surface free energies of the two regions R_1 and R_2 of the stereographic triangle in **Fig. 17**, and N_1 and N_2 the numbers of each of these regions in the different types of particles. For a single crystal and LTPs $N_1 = N_2 = 48$; for a Dh $N_1 = 60$, $N_2 = 40$ and for an Ic $N_1 = 120$, $N_2 = 0$. So long as the average surface energy of region 1 is less than that of region 2, MTPs will have lower total surface energies. That MTPs are only stable when the {111} surface energy is small is an urban myth – this is a sufficient but not necessary condition. For instance, if only {110} faces are present the values of ε_W are almost the same for a single crystal (rhombic dodecahedron) and icosahedron (dodecahedron) at 5.345 and 5.312 respectively times the ratio $\gamma_{110}/\gamma_{111}$.

While the modified Wulff construction has proved to be successful in rationalizing some observations, most notably for the Dh with re-entrant surface in the thermodynamically lowest-energy shape, it does not explain everything. The simplest shortcoming is a pentagonal biprism with only {111} facet, described in the original papers on MTPs (Ino, 1966; Ino and Ogawa, 1967; Ino, 1969). Other shapes cannot be explained, such as sharp bipyramids, which have been synthesized using various protocols (Wiley *et al.*, 2006; McEachran and Kitaev, 2008; Zhang *et al.*, 2009) as well as truncated bitetrahedra, triangular platelets, and Dh rods, see for instance **Fig. 2**. In many papers these have been loosely attributed to "kinetics"; I will return to this.

For reference, the software packages, Crystal Creator (Boukouvala and Ringe, 2019) at see https://www.on.msm.cam.ac.uk/code.html and WulffPack (Rahm and Erhart, 2020) at see https://wulffpack.materialsmodeling.org/ can be used for these as well as for single crystals and (in WulffPack) Winterbottom constructions; see Boukouvala et al for a recent overview (Boukouvala *et al.*, 2021).

Other Variants

While the Wulff, Winterbottom and modified-Wulff are the three most common cases, there are others which will be briefly described in this section.

Alloy nanoparticles and segregation

The addition of a second element makes the structures of bimetallic nanoparticles more complex than their monometallic counterparts. The two elements can be phase separated as in core-shell structures, (Serpell *et al.*, 2011; Chen *et al.*, 2011; Lu *et al.*, 2014; Ellaby *et al.*, 2020; Eom *et al.*, 2021) chemically ordered (Stappert *et al.*, 2003; Wang *et al.*, 2013; Li *et al.*, 2014a) have Janus (Langlois *et al.*, 2012; Song *et al.*, 2012) structures, or the two species can be randomly mixed with complex segregation (Herzing *et al.*, 2008; Chen *et al.*, 2007; Cui *et al.*, 2013; Nelli and Ferrando, 2019; Deng *et al.*, 2019) For large sizes segregation of one species to the surface to reduce the surface free energy is straightforward, and has been extensively studied for flat surfaces. However, in a nanoparticle there is an additional contribution as removing atoms from the bulk to the surface changes the total energy contribution of the bulk. This cannot be ignored, especially when the number of bulk and surface atoms are comparable. This is also a constraint upon the composition, an additional Lagrangian variable in the formulation for the minimum energy of the nanoparticle.

This leads to a slightly different form of the solution, namely

$$\frac{\gamma_{\left(n,C_1^S,C_1^V,C_2^S,C_2^V,\ldots\right)}}{\{\Lambda-\Delta G\}}=h_{(n)} \tag{19}$$

Where an additional term has been introduced to account for the bulk dealloying terms. This form is described in more detail in (Ringe *et al.*, 2011) and leads to a size dependence of both the segregation and the shape, see **Fig. 18** where the ratio of the distances to {111} and {100} facets is plotted as a function of the overall gold concentration for three different particle sizes. While there is relatively little experimental and computational data as yet, overall it appears to be quite consistent with the predictions of this model (Peng *et al.*, 2015)

It worth mentioning that the entropy of mixing plays a role in bimetallic/alloy systems – the free energy has contributions from both enthalpy and entropy. At low temperature, the contribution from entropy of mixing is minimal, so the enthalpy term dominates. However at high temperature, the entropy of mixing will dominate and will drive the particle towards homogeneity. Therefore, surface

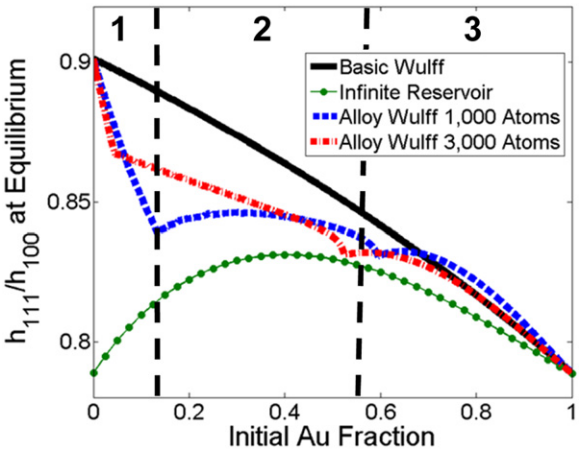

Fig. 18 Variation in the relative distance to a {111} versus a {100} facet for CuAu alloy nanoparticles, as a function of their size as well as with different approximations for the surface segregation. In region 1 there is not enough gold for full segregation to the surface, in 3 there is more than enough and in region 2 surface segregation and bulk desegregation compete.

segregation is temperature dependent and is more significant at lower temperature. One caveat is that experimental results often represent quenched structures and surface ligands are known to have effects on surface segregation (Suntivich *et al.*, 2013).

Polycrystalline particles on a substrate

An important case is polycrystalline particles on a substrate, where the isolated particles can be handled by variants of the modified Wulff construction, but how the substrate adheres needs an extension. For these cases one cannot describe the interface by a single energy terms as in the Winterbottom construction, but it can be described (Mansley and Marks, 2020) by introducing an effective interface free energy given by an integral of the different interfaces divided by the total interface area, that is

$$\gamma_{Int}^{Eff} = \int_{Int} \gamma_{Int} dS / \int_{Int} dS \tag{20}$$

This is then included in modified-Wulff constructions where for all segments this effective interface term is included. This requires a simultaneous numerical solution for the interface term so is a little more complex. An example is shown in **Fig. 19** for a Dh on a substrate; it can be generalized for other cases without complications.

The effect of size dependent strain

When the size of the nanoparticles is small the additional terms neglected earlier have to be included, which will lead to deviations from the Wulff construction (e.g., Marks, 1985). Exactly where this takes place has been debated for many years, and probably depends upon the material and the calculation method. As a caveat, in some cases the rigorous Gibbs equimolar partitioning of the nanoparticle has not been performed outside the surface, and this is needed to properly achieve the transition from atomistic to continuum models (Cleveland and Landman, 1991; Hamilton, 2006) so the magnitude of the deviations may be exaggerated.

One example of a size effect is the lattice contraction of small particles driven by the surface stress. Assuming a homogeneous strain and an isotropic surface stress (a good approximation for a cubic material), there is a fractional change in lattice parameter $\frac{\Delta a}{a}$ for a spherical particle given by

$$\frac{\Delta a}{a} = -\frac{4gK}{3R} \tag{21}$$

where K is the compressibility and R is the radius. This has been analyzed in the literature (e.g., Finch and Fordham, 1936; Boswell, 1951; Berry, 1952; Cimino *et al.*, 1966; Vermaak *et al.*, 1968; Mays *et al.*, 1968; Wasserma and Vermaak, 1970; Wasserman and Vermaak, 1972; Khanna *et al.*, 1983; Solliard and Flueli, 1985; Borel and Chatelain, 1985; Scamarcio *et al.*, 1992; Cammarata and Sieradzki, 1994; Lamber *et al.*, 1995; Reimann and Wurschum, 1997; Jiang *et al.*, 2001; Qi *et al.*, 2002; Li *et al.*, 2004; Shreiber and Jesser, 2006; Ahmad and Bhattacharya, 2009; Diehm *et al.*, 2012; Oehl *et al.*, 2015), and is typically a few percent for particles of 5 nm radius and normally (but not always) a contraction. Shown in **Fig. 20** is data for Ag_3Sn which shows a contraction (Oehl *et al.*, 2015) whereas anatase TiO_2 shows an expansion (Ahmad and Bhattacharya, 2009)

A second case is epitaxial nanoparticles on a substrate. For the growth of semiconductors at a slightly larger scale (typically 50–500 nm particles) the literature is large and there is generally good agreement between models where the elastic deformation of the nanoparticles, the surface stresses and the misfit stresses at the interface are all included; see for instance (Ross *et al.*, 1998; Muller and Saul, 2004; Spencer *et al.*, 1991; Spencer *et al.*, 1993; Tersoff and Tromp, 1993; Guyer and Voorhees, 1995; Spencer and Tersoff, 1997; Medeiros-Ribeiro *et al.*, 1998; Daruka *et al.*, 1999; Shchukin and Bimberg, 1999; Spencer, 1999; Li *et al.*, 2000; Cristini and Lowengrub, 2002; Aqua *et al.*, 2013; Feng *et al.*, 2015) and references therein. The thermodynamic minimum energy shape minimizes not only the external surface energy but also the interface strain energy so will deviate from the Winterbottom shape (Muller and

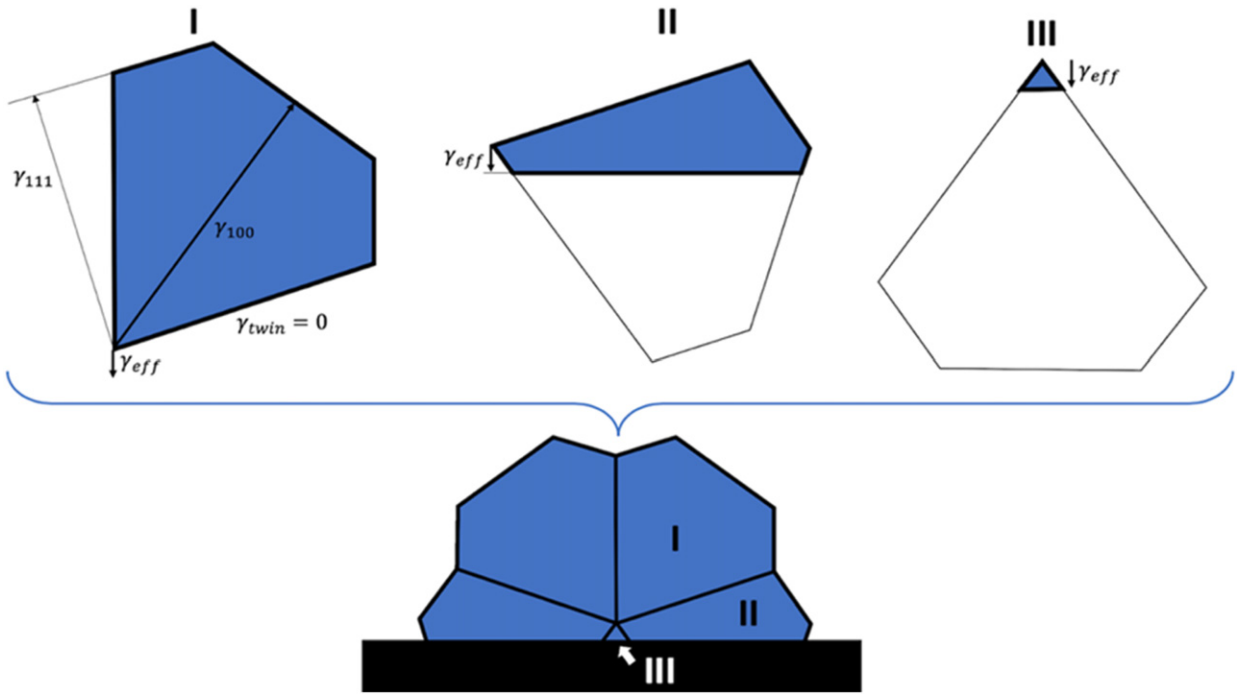

Fig. 19 Modified Wulff construction including an interface for a Dh. The structure involves two segments I which are standard modified Wulff, and three total segments II and III where the effective interface is included.

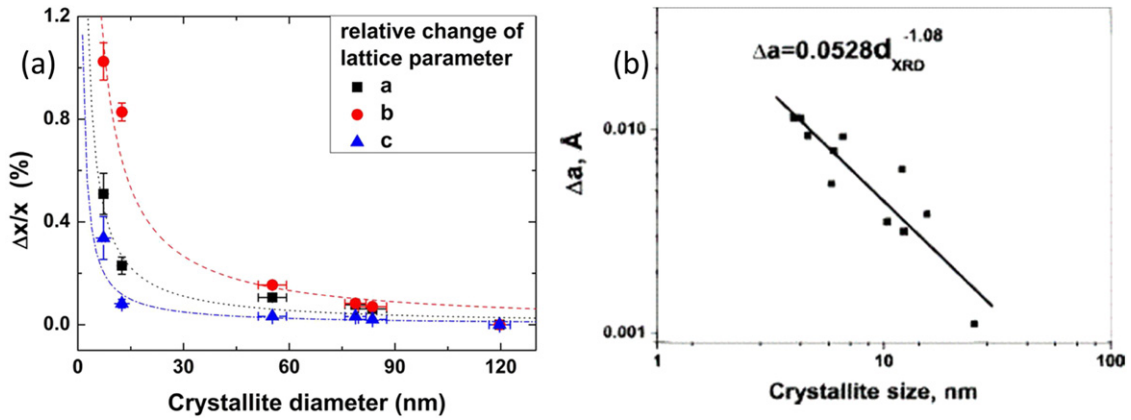

Fig. 20 Variation in lattice parameter with size, in (a) showing the relative decrease in lattice parameter at small size in Ag_3Sn. reproduced with permission from Oehl *et al.*, 2015 copyright (2015) American Chemical Society (sign reversed compared to common usage) and in (b) for anatase TiO_2 showing an expansion, reproduced with permission from Ahmad, M.I., Bhattacharya S.S., 2009. Size effect on the lattice parameters of nanocrystalline anatase, Applied Physics Letters 95, 191906.

Kern, 1998; Muller and Kern, 2000; Lazzari and Jupille, 2012) and it may also be important to include line energy terms for the vacuum/substrate/nanoparticle three-phase interface (e.g., Sivaramakrishnan *et al.*, 2010; Bettge *et al.*, 2011; Cosandey, 2013). An example of this is shown in **Fig. 21** (Sivaramakrishnan *et al.*, 2010) where the results indicate a size-dependent Wulff shape.

Kinetic Shapes

The various Wulff constructions yield the equilibrium shape. However many experimental nanoparticles are synthesized and examined or used before they reach equilibrium. In these cases the shape is a consequence of kinetic growth. While there are similarities, and the two are frequently confused, they are fundamentally different. The fact that kinetics matter for solution growth has been known for a long time, for instance in the early work of Berg (1938) and the detailed review and analysis of different terms by Bircumshaw (Bircumshaw and Riddiford, 1952) both of which cite even earlier literature. There is also an extensive early

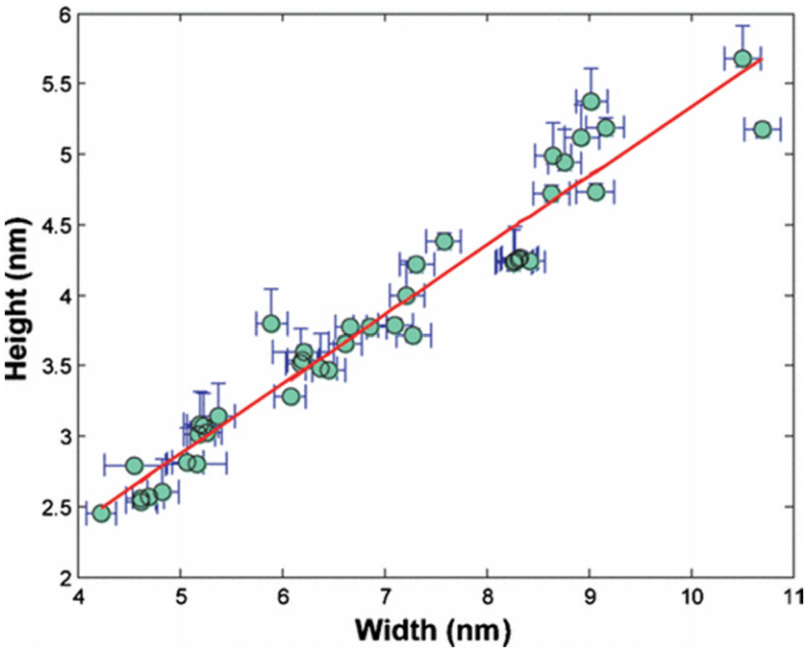

Fig. 21 Plot of the height versus width for gold nanoparticles on rutile TiO_2 (110). For a Wulff shape the intercept should go through the origin, but it does not. Reproduced with permission from Sivaramakrishnan, S., Wen, J.G., Scarpelli, M.E., Pierce, B.J., Zuo, J.M., 2010. Equilibrium shapes and triple line energy of epitaxial gold nanocrystals supported on TiO_2(110). Physical Review B 82, 195421.

literature for flat crystal growth, for instance the work of Volmer (1939) and Burton *et al.* (1951) The kinetic models in the following sections are excellent for predicting nanoparticle shapes qualitatively and in principle quantitatively, although the necessary parameters for the later are often unknown.

To aid in the analysis, it is useful to break down the processes taking place by considering three regions as illustrated in **Fig. 22**. Far from the particle one has Region I with some concentration of the relevant materials, dictated by the environment. Around the particle is Region II which includes atoms that interact with the growing nanoparticle, both via being chemisorbed onto the surface and as part of complexes. Lastly there is Region III composed of terraces on the surface of the nanoparticle which grow by the attachment of atoms from Region II. There will be a net flux of atoms from Region I → Region II → Region III.

Diffusion limited growth occurs when the controlling term is diffusion in Region I to Region II, with atoms attaching very rapidly to Region III as they arrive. This limit typically leads to complex patterns such as snowflakes with dendritic or similar structures; the topic has been well described in the literature and will not be discussed further here.

Interface limited growth is more important for shape-controlled nanoparticles, and is when atoms moving from Region II to Region III is rate limiting. If the size is small enough, as atoms are added the cluster will be flexible and the atomic arrangement can change. Above some size this will not be energetically possible, and the particle then acts as a seed for further growth. While there may still be some changes of the internal structure, this will be the exception.

The controlling terms are the nucleation of a small monatomic terrace on an existing flat facet, and the growth of this terrace across the facet, Region III. If nucleation is fast relative to the growth across this leads to rough surfaces. Flat surfaces occur when the nucleation is relatively slow. Making the simple approximation of a circular single atomic high terrace of radius R and introducing an edge energy γ_e per atom the total energy of the terrace can be written as

$$E = \pi R^2 \Delta\mu N_S + 2\pi R \gamma_e N_E \tag{22}$$

Where $\Delta\mu$ is the chemical potential change per atom (negative for growth) for addition to the nanoparticle versus being in Region II, N_S is the number of atoms per unit area of the terrace and N_E the number of atoms per unit length of step. This has the classic form of a nucleation barrier whose magnitude depends upon the step energy and the chemical potential relative to the external media. From classical nucleation theory the rate of formation of a terrace above the critical size R_C is given by

$$Rate = f_0 exp\left(\frac{-\Delta E}{k_B T}\right) \tag{23}$$

where f_0 is the attempt frequency of an atom to add to the terrace and ΔE is the nucleation barrier which gives a critical nucleus size for a two-dimensional terrace of

$$R = -\gamma_e N_E / \Delta\mu N_S \tag{24}$$

and an activation energy barrier of

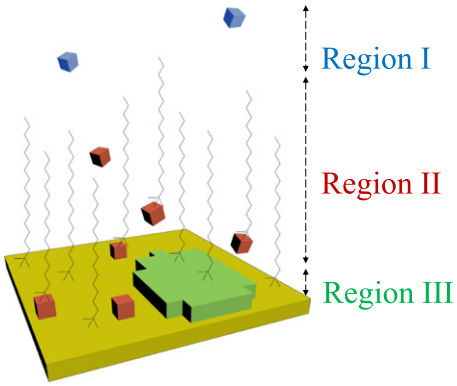

Fig. 22 Schematic of the relevant regions for kinetic growth. Region III contains a nucleating terrace, Region II atoms that can diffuse to the terrace and Region I external atoms. Atoms are represented by cubes which are color coded by region, with the substrate yellow, and ligands near the surface are illustrated.

$$\Delta E = -\pi(N_E\gamma_e)^2/N_S\Delta\mu \sim -\pi(\gamma_e)^2/\Delta\mu \tag{25}$$

As an estimate, using a broken bond model and taking the bulk cohesive energy as 4 eV per atom, for a {111} surface $\gamma_e \sim 2/3$eV. For gas phase deposition the chemical potential of an adatom will be around (in eV)

$$\Delta\mu = -3 + k_B T ln[c] \tag{26}$$

with [c] the concentration of atoms in Region II that can add to the terrace. If the deposition rate is fast then the critical nucleus may be only 2–3 atoms, in which case there can be multiple terraces on any given facet and the growth will tend to lead to relatively rough surfaces. With slow deposition the concentration in Region II will be small, via the concentration, and the critical nucleus could be 1 nm in radius, in which case it is unlikely that multiple terraces will be present on any surface and the growth will be layer by layer.

The transition between rough growth and flat growth will often occur during a synthesis from solution as the active chemicals deplete. An example of this is shown in **Fig. 23** for hydrothermal growth of $KTaO_3$ (Ly *et al.*, 2018) Changes of the chemical potential by chemisorption also have a significant effect on the competition between the nucleation of new terraces and the growth of existing ones (Ly *et al.*, 2020a; Ly *et al.*, 2020b).

For solution growth, the concentration in Region I is relatively high, typical solutions are in the mM regime. The concentration in Region II will depend upon surfactants as well as other factors such as chelation of neutral metal species. In quasi steady-state, the chemical potential change driving force of the metal in solution, Region I (which will be the same as that in Region II) will be small because only weak reductants such as citric acid are used. Note that for many solvent syntheses of nanoparticles the typical size of three-dimensional nuclei in the initial stage of the reaction is 1–2 nm (e.g., results from in-situ scattering experiments and kinetic modeling (Thanh *et al.*, 2014; Kumar *et al.*, 2007; Rodriguez-Gonzalez *et al.*, 2007; Soni *et al.*, 2007; Finney and Finke, 2008; Harada and Katagiri, 2010; Polte *et al.*, 2010a; Polte *et al.*, 2010b; Yao *et al.*, 2010; Harada *et al.*, 2011; Hudgens *et al.*, 2011; Harada and Kamigaito, 2012; Ojea-Jimenez and Campanera, 2012; Streszewski *et al.*, 2012; Wojnicki *et al.*, 2012; Wuithschick *et al.*, 2013; Perala and Kumar, 2014; Wuithschick *et al.*, 2015); it is straightforward to show that this has to be about the same size as that of the critical radius for a terrace. For completeness, as the reaction proceeds the concentration of the metal in solution drops so the chemical potential driving force will become even smaller.

Once nucleated, this layer will grow laterally with a rate which will also be influenced by the concentration in Region II. The net result is a velocity for the growth of any given facet v_i which is essentially independent of the particle size (except, perhaps, for very large particles). Fast growing facets will not appear in the final shape, only the slowest growing ones will be present.

This leads to a steady-state solution for a single crystal as the shape S_K given by:

$$S_K = \{x : x.\hat{n} \leq \lambda(t)v(\hat{n}) \text{ for all unit vectors } \hat{n}\} \tag{27}$$

i.e., the shape corresponds to the inner envelope of planes normal to

$$h_i(t) = \lambda(t)v_i \tag{28}$$

This is the "kinetic Wulff construction", and is confusingly similar to the Wulff shape with the difference that growth velocities (v) rather than the surface free-energies (γ) determine the shape.

Every different thermodynamic Wulff construction mentioned in the previous section has a corresponding kinetic Wulff shape. However, before proceeding further one other term needs to be included.

Kinetic Enhancement at Certain Sites

Many particles contain twins and the thermodynamic shape has re-entrant surfaces. This leads to an important additional term with enhanced growth at the twin, a well-established effect (e.g., Hamilton and Seidensticker, 1960; Wagner, 1960; Marks and

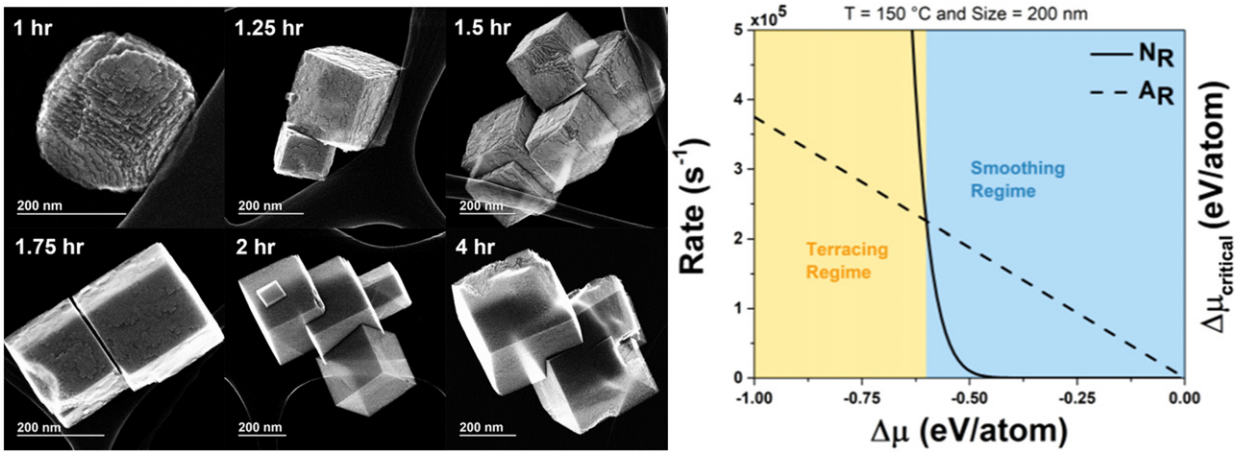

Fig. 23 On the left, secondary electron images of $KTaO_3$ nanoparticles at different growth times showing how the rough surface at 1 hr. changes to smooth surfaces after 1.75 hr. On the right is a plot of the terrace nucleation rate (NR) and annihilation rate (AR) versus chemical potential which leads to regions in yellow where terracing dominates and the surfaces are rough, versus smooth surfaces.

Howie, 1979; vandeWaal, 1996; Kirkland *et al.*, 1993; Lofton and Sigmund, 2005). From density functional calculations it is easy to show that the edge energy for a line of atoms at a twin is essentially zero (Alpay *et al.*, 2015) Reformulating the nucleation problem of Eq. (19) for a semicircle similar to Gamalski et al (Gamalski *et al.*, 2014) yields

$$E = \frac{1}{2}\pi R^2 \Delta\mu N_S + \pi R \gamma_e N_E \tag{29}$$

which has the same critical radius and half the nucleation barrier. This leads to an effective enhancement factor for the growth of facets which are re-entrant in the thermodynamic shape, so in general they will not appear. The importance of twins in the growth of shape controlled nanoparticles was discussed in some depth by Lofton and Sigmung (Lofton and Sigmund, 2005) although it appears that they were unaware of some of the earlier work on the thermodynamic shapes and the disclination strain field.

For the specific case of MTPs, there is also a disclination along the five-fold axis. It is well established that there can be faster growth at a screw dislocation; it is possible that the same occurs at the disclination. An alternative has recently been suggested by Qi *et al.* (2019) namely that the reentrant surfaces at the twin boundary can enhance one-dimensional surface diffusion encouraging the formation of rods.

Every thermodynamic variant of the Wulff construction discussed earlier has a kinetic equivalent, including those for twinned particles. Both the thermodynamic and kinetic Wulff shapes as well as the Winterbottom kinetic form have been extensively studied in the literature for single crystals, e.g., (Winn and Doherty, 2000; Taylor, 1992; Cahn and Hoffman, 1974; Hoffman and Cahn, 1972; Herring, 1951; Coriell and Sekerka, 1976; Cahn and Taylor, 1984; Villain, 1991; Taylor *et al.*, 1992; Almgren *et al.*, 1993; Cahn and Taylor, 1994; Carter *et al.*, 1995; Cahn and Carter, 1996; Ambrosio and Soner, 1996; Uehara and Sekerka, 2003; Sekerka, 2005; Du *et al.*, 2005a; Sun *et al.*, 2008; Sun *et al.*, 2011; Leung *et al.*, 2012) In some cases software is available to calculate these shapes, for instance for an isolated nanoparticle or with a support (Zucker *et al.*, 2012) Combining the kinetic enhancement with the modified Wulff construction for twins (Buhler and Prior, 2000; Ringe *et al.*, 2013) leads to a large family of shapes as a function of where the growth is enhanced which are illustrated for just {111} and {100} facets in **Fig. 24** for an LTP with one twin boundary. In **Fig. 24**(a) just twin enhancement will lead to hexagonal platelets; in (b) growth at the re-entrant surface triangular bipyramids and in (c) faster growth at both triangular platelets. Additional shapes are the regular icosahedron as well as the pentagonal bipyramid. While the icosahedron is also the thermodynamically stable shape, as first pointed out by Ino almost fifty years ago the pentagonal bipyramid is not. One of the major successes of this model is that it can correctly predict the formation of these commonly observed particles.

Note that the freely available software packages, Crystal Creator (Boukouvala and Ringe, 2019) at https://www.on.msm.cam.ac.uk/code.html can be used for these.

Similar to the thermodynamic constructions, these kinetic solutions are completely general. The growth rate of different types of particles will be determined by the relative growth rate of surfaces in the different angular regions of the stereographic triangle. A population of nanoparticles may be dominated by those which grow fastest, rather than by any thermodynamics. There is nothing that says that one type of particle should suddenly stop growing while others do – this would require exchange of atoms between the particles. The only way a particle is likely to change shape is if there is an injection of sufficient energy by some means such as heating or coalescence to provide the activation energy for a transformation. Without this very large MTPs are possible, and occur in practice well beyond any size when they are lower in energy than single crystals.

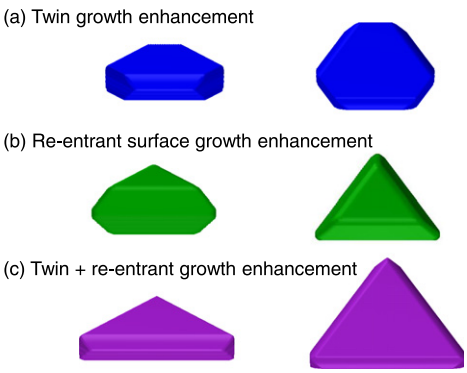

Fig. 24 Kinetic shapes for an LTP. In (a) with just enhanced growth at the twin producing hexagonal platelets, in (b) with faster growth at the re-entrant surface truncated triangular bipyramids and in (c) with both triangular platelets. In all cases on the left is a side view, on the right a view down [111].

Other Cases: Corner Rounding

As mentioned earlier, the chemical potential can be nominally singular at edges and corners. Experimental measurements indicate that corners are not necessarily sharp, and can be rounded with a local radius of curvature which is independent of the size of the nanoparticles except at very small sizes (Alpay *et al.*, 2015) see **Fig. 25** as well as many of the other figures in this review and the literature. This size independence was originally unexpected, but is an important clue as to the source. For very sharp corners the local chemical potential would be greater than that of the atoms in the solution used to grow the nanoparticles, so they cannot occur. In theoretical models sometimes regularization is used to avoid this (Mastroberardino and Spencer, 2010) Going further, at very small sizes it will not be possible to nucleate a new ledge on a small facet as there is insufficient area. Instead a steady-state solution will only be possible for a shape which already has steps where atoms can add, i.e., a locally rounded corner or edge with a radius of curvature which is about the same as that of a three-dimensional critical nucleus. Towards the end of an aqueous synthesis the critical radius for a terrace and a three-dimensional nucleus will be somewhat large, hence the rounding can be quite large as shown in **Fig. 25**. Recent theoretical work by Qi et al agree with this interpretation (Qi *et al.*, 2019) and the local chemical potential can experimentally lead to segregation (Peng *et al.*, 2016) Corner rounding is general and almost certainly should not be dismissed.

Strain in MTPs

As illustrated in **Fig. 26**, MTPs are not space filling but have a two-dimensional angular gap for the Dh and ten of these for the Ic. They have to be deformed by $\sim 2\%$ for the Dh and $\sim 6\%$ for the Ic to form space-filling structures. In the original paper by Ino it was proposed that this was an inhomogeneous strain although for simplicity a simple homogeneous strain was used in the first energy calculations (Ino, 1969) Apparently unaware of this work, de Wit pointed out that the Dh was an example of a disclination (DeWit, 1972) He assumed that the Dh was cylindrical, then described the deformation in cylindrical polar co-ordinates ρ, ϕ, z using a rotation $\omega_z(r)$ and a radial normal strain $e_{\rho\rho}(r)$. This leads to the displacements

$$u_r(r) = \left[\frac{1-2\upsilon}{2(1-\nu)}\right]\epsilon_D \rho \ln(\rho/R) - \epsilon_D \rho/2 \tag{30}$$

$$u_\phi(r) = \rho\epsilon_D \tag{31}$$

and a cubic dilatation, the local volume change of

$$\Delta(r) = \left[\frac{1-2\upsilon}{2(1-\nu)}\right]\epsilon_D(2\ln(\rho/R)+1) \tag{32}$$

with stresses

$$\sigma_{rr} = 2G\epsilon_D \ln(\rho/R) \tag{33}$$

$$\sigma_{\phi\phi} = \frac{G\epsilon_D}{(1-\nu)}[\ln(\rho/R)+1] \tag{34}$$

and G the shear modulus, R the particle radius and ν Poisson's ratio. At the outermost surface there is an expansion ($\Delta(r) > 0$), in the center a compression with no overall change in the volume. Compared to a homogeneous strain approach, the energy to close the angular gaps is about a factor of two smaller.

The same approach was extended to three dimensions by Yoffe (described in (Howie and Marks, 1984)) for an Ic. More complex analytical solutions have also been given by the group of Romanov and co-workers (Gryaznov *et al.*, 1999; Gryaznov *et al.*, 1991; Romanov, 2002; Romanov, 2003; Polonsky *et al.*, 2006; Romanov and Kolesnikova, 2009; Kolesnikova and Romanov,

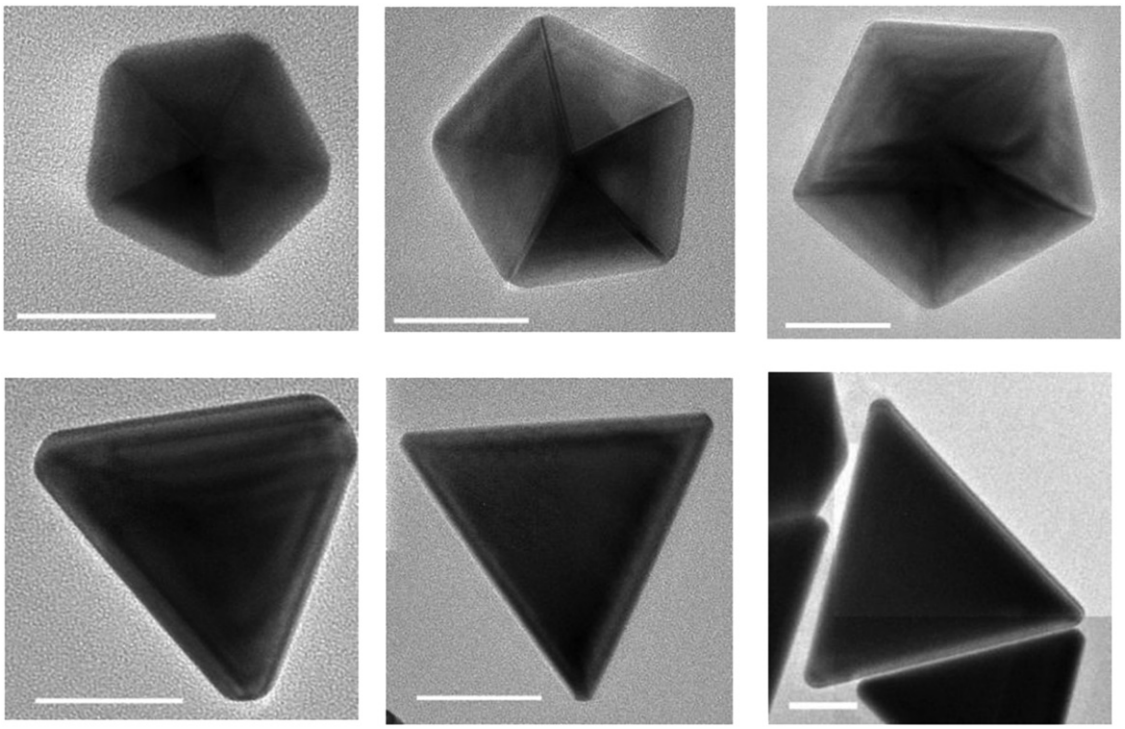

Fig. 25 Top row, Dh with rounded corners and bottom, truncated row bipyramids. In all cases the scale bars are 50 nm. The radius of curvature is approximately independent of the nanoparticle size. Other images in this manuscripts and the literature also show rounding.

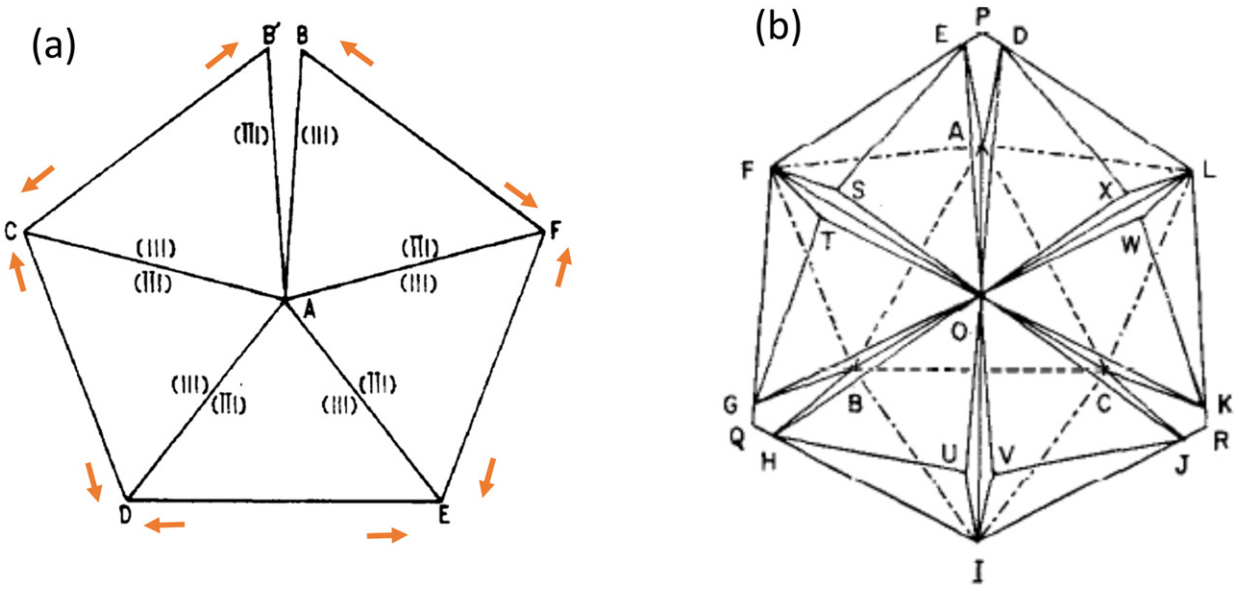

Fig. 26 Illustration of the angular gaps in a Dh (a) and an Ic(b), adapted from the original work of Ino and Ogawa. Reproduced with permission from Ino, S., Ogawa, S., 1967. Multiply twinned particles at earlier stages of gold film formation on alkalihalide crystals. Journal of the Physical Society of Japan 22, 1365–1374. Copyright (1967).

2010; Dorogin *et al.*, 2010a; Dorogin *et al.*, 2010b; Gutkin, 2011; Romanov *et al.*, 2012; Vikarchuk *et al.*, 2020) including recent gradient elasticity approaches (Tsagrakis *et al.*, 2018) and numerical solutions using finite element methods have also appeared (Johnson *et al.*, 2008; Patala *et al.*, 2013a; Patala *et al.*, 2013b) as well as comparable inhomogeneous strains in larger scale molecular dynamics calculations The same general conclusions apply to the Ic which can be considered as a number of disclinations, one for each five-fold axis, leading to a total strain energy which is about twenty times that of the Dh.

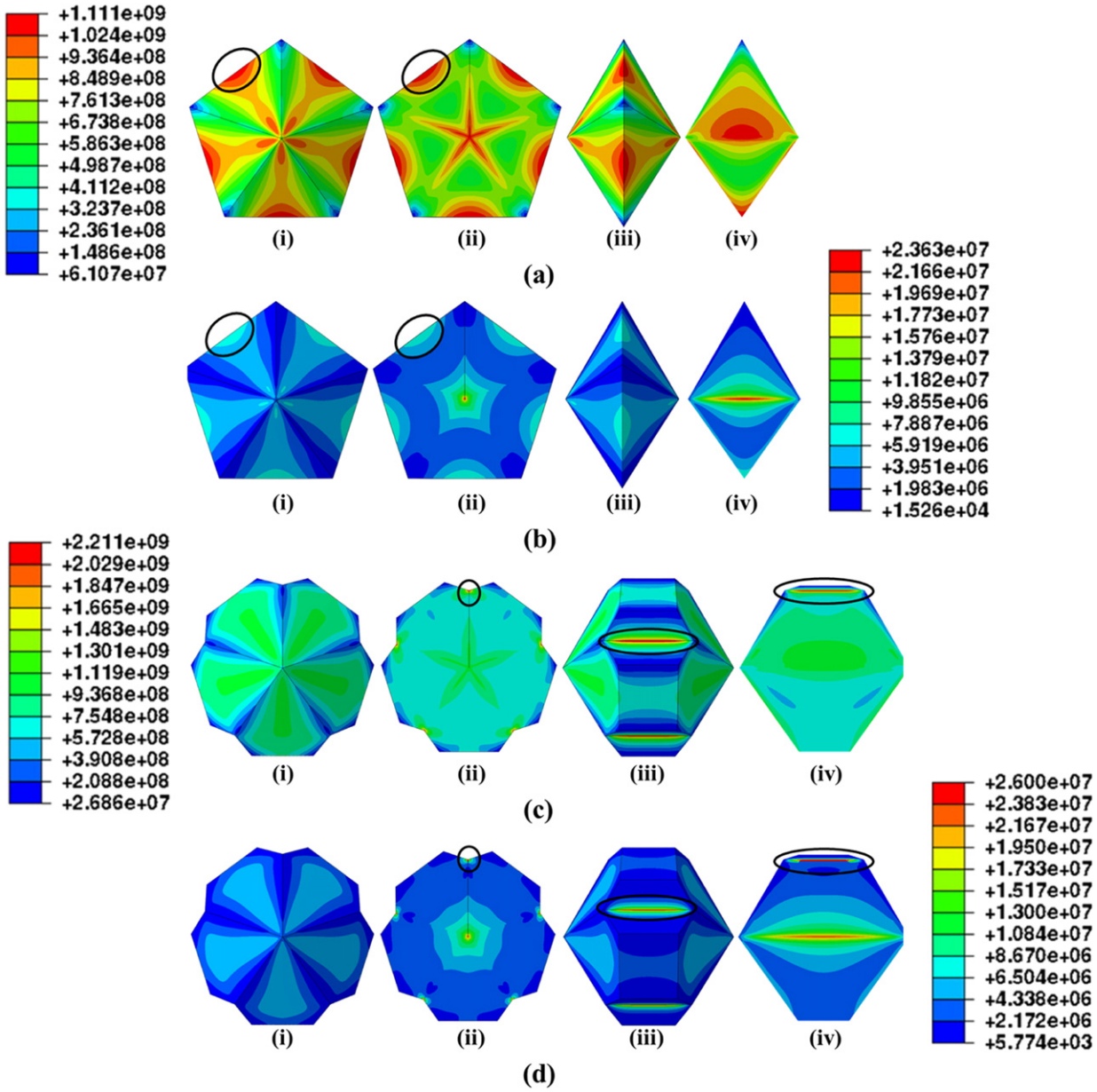

Fig. 27 In (a) and (c) the Von Mises stresses and in (b) and (d) the strain energy density. In (a) and (b) with a pentagonal bipyramid is used, in (c) and (d) the thermodynamic shape. Regions of high stress and strain energy density are indicated, and change with the three-dimensional shape of the particles.

An example of numerical results for the stresses (Patala *et al.*, 2013a) is shown in **Fig. 27**, with more accurate models for the external shape. The figure shows both the Von Mises stress, an indicator of how likely it is for dislocations to form as well as the strain energy density for a sharp Dh and one with {111} notches, with regions where these are large indicated. For the sharper Dh there are higher stress and energy densities in the center of the segments whereas they are both much closer to constant when notches are introduced as this leads to a shape closer to a circle in projection and the de Wit disclination result. For the Ic with the simplest perfect icosahedron shape there are also noticeable local variations with stress concentration in the center of the segments as shown in **Fig. 28**.

A number of recent papers have explored measuring the strains for the Dh using high-resolution electron microscope images (e.g., Johnson *et al.*, 2008; Walsh *et al.*, 2012; Pohl *et al.*, 2014; Ji *et al.*, 2015; Yu *et al.*, 2017; Wu *et al.*, 2021) It is possible that there could be some accommodation of the strain at the twin boundaries. In some recent experimental work (Johnson *et al.*, 2008) there was evidence that the net rotational component of the strain field did not add up to the required 7.35 degrees, but was substantially less. Other measurements with a Marks decahedron gave different results (Ji *et al.*, 2015) with the rotation larger than expected. Confusing this, all experiments to date are two-dimensional averages along the beam direction and as such will not give

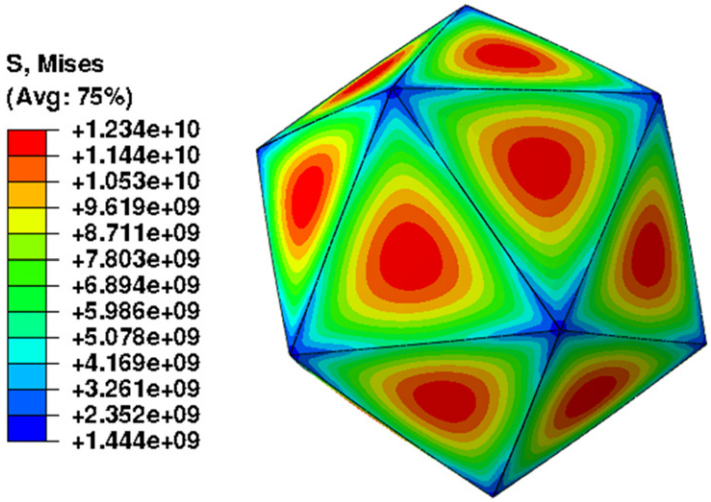

Fig. 28 Plot of the Von Mises stresses at the surface of an Ic.

a complete description; they have also ignored potential complications due to dynamical diffraction which is dangerous to do. Hopefully in the not too distant future full three-dimensional maps of the strains will be generated experimentally.

Energy Versus Size

The total energy of MTPs, as well as that of other nanoparticles can be written from earlier as

$$E = V\left(\frac{\mu^B}{\nu_0} + W_D\right) + V^{\frac{2}{3}}\left(\gamma_{111}\varepsilon_W + <g_{ij}e_{ij}>\varepsilon_g\right) + O(h) \tag{35}$$

Comparing nanoparticles with the same number of atoms the bulk chemical potential cancels out, as do small terms such as those due to changes in the lattice parameter via the surface stress. For simplicity all terms which scale linearly with the size will also be ignored, appropriate except at very small size provided Gibbsian definitions are used. It is then simplest to plot $E/V^{2/3}$ as illustrated in **Fig. 29** versus $V^{1/3}$ for two different values of the surface stress. Note the large changes with the surface stress, which has recently been indirectly detected using diamond-anvil experiments where high pressures promote the transition from MTPs to single crystals (Parakh *et al.*, 2020).

This energy balance yields the lowest enthalpy structures, but by itself is not a complete description of the system. For this one needs to use a statistical mechanics approach, writing the relative fraction of each type of particle in some form for a specific number of atoms such as

$$n_i = \frac{\exp\left(-\frac{\Delta G_i}{kT}\right)}{\sum \exp\left(-\frac{\Delta G_i}{kT}\right)} \tag{36}$$

This problem has been well studied (e.g., Baletto and Ferrando, 2005; Berry *et al.*, 1984; Berry, 1990; Uppenbrink and Wales, 1992; Ball *et al.*, 1996; Doye *et al.*, 1998; Wales *et al.*, 2000; Baletto *et al.*, 2000; Doye and Wales, 2001; Cox *et al.*, 2006; Berry and Smirnov, 2009; Berry and Smirnov, 2013; Cheng and Ngan, 2013; Goloven'ko *et al.*, 2013; Wells *et al.*, 2015; Chen *et al.*, 2017; Schebarchov *et al.*, 2018; Baletto, 2019; Fichthorn and Yan, 2021), and while the specific results can vary strongly with potential parameters (Baletto and Ferrando, 2005) the general results are quite clear. At reasonable temperatures and when the size is small enough, there is no single shape rather a diverse population of shapes. The transitions between the different shapes can occur on the millisecond time scale or faster. Even at larger sizes it is possible for particles to transition between one structure and another, either as a consequence of heating, exposure to the electron beam or during growth (Yagi *et al.*, 1975; Cheng and Ngan, 2013; Iijima and Ichihashi, 1986; Chen *et al.*, 1999; Buffat, 2003; Koga *et al.*, 2004; Du *et al.*, 2005b; Silly and Castell, 2009; van Huis *et al.*, 2009; Young *et al.*, 2010; Wang and Palmer, 2012) see for instance **Fig. 30** from (Young *et al.*, 2010) for an example of a single crystal changing to an Ic and then later to a Dh during an in-situ heating experiment. While shape transitions were mainly observed for larger particles, increases in microscope performance has made this possible at much smaller sizes, for instance reversable isomerization between clusters with 144 gold atoms (Takahata *et al.*, 2020) More recent work has started to look at the effects a statistical distribution can have, for instance, in heterogeneous catalysis (Cheula *et al.*, 2020; Rossi *et al.*, 2020).

Beyond some size transitions between shapes will become improbably under most experimental conditions, so one has a frozen seed from which a larger particle will grow without changes in structure in most cases. Hence it is not uncommon to find MTPs in the micron size range (Wei *et al.*, 2002) or in a few cases millimeter sized – see **Fig. 1**. One myth should be mentioned here, namely the idea that MTPs occur through the assembly of individual tetrahedral units. This concept was discussed early by, for instance, Gillet (1977)

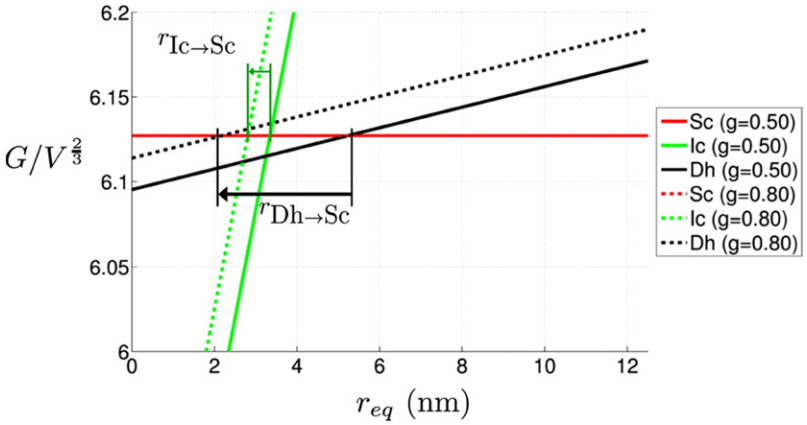

Fig. 29 Plot of the free energy divided by the volume to the two-third power, versus the equivalent radius for the volume for two different values of an isotropic surface stress (g). In all cases Ic are stable at smaller sizes, but whether the Dh have an intermediate stability range or not depends upon the surface stress, both its magnitude and sign.

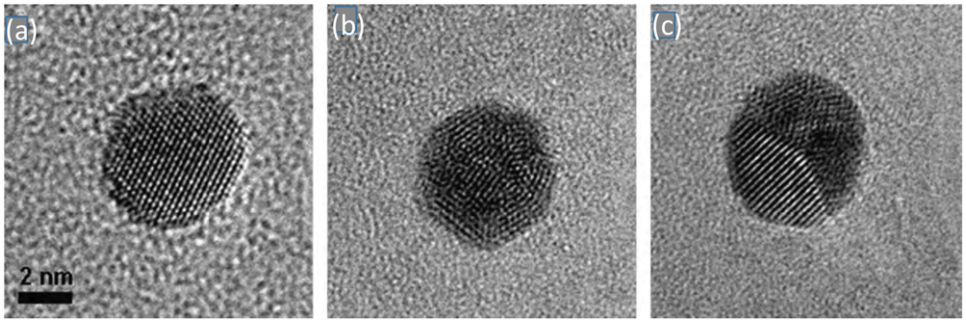

Fig. 30 Controlled heating of a 5.5 nm gold particle. (a) The original single crystalline fcc structure, near to a [110] orientation observed at room temperature. (b) At 300°C, the particle structure transforms to an icosahedral structure, oriented near to the [112] projection. (c) Finally a decahedral structure close to [110] is observed at 400°C. Reproduced with permission from Young, N.P., van Huis, M.A., Zandbergen, H.W., Xu, H., Kirkland, A.I., 2010. Transformations of gold nanoparticles investigated using variable temperature high-resolution transmission electron microscopy. Ultramicroscopy 110, 506–516.

who pointed out that it was not reasonable and that layer-by-layer growth as discussed earlier was by far the most reasonable explanation. While there are papers where it has been argued that the experimental evidence supports this concept of sequential assembly of MTPs, a closer examination of all the published images indicates that they are all highly asymmetric Dh particles which have been incorrectly interpreted. Asymmetric Dh have been known for more than fifty years dating back to at least the early work of Yagi (Yagi *et al.*, 1975) the work by the author in the first modified-Wulff paper (Marks, 1983a) they play an important role in quasi-melting (Dundurs *et al.*, 1988; Marks *et al.*, 1986; Ajayan and Marks, 1988; Ajayan and Marks, 1989b) have been analyzed many times (Uppenbrink *et al.*, 1992; Walsh *et al.*, 2015) up to more recent work such as analysis of disclination migration (Song *et al.*, 2019).

Because the strain energy of the Ic is about twenty times that of the Dh, these particles only occur at very small sizes; observation of them at larger sizes is common and can only be because kinetics not thermodynamics are controlling. Specific ligands can stabilize particular structures, and precise details of the atomic structures of a number of very small clusters have been recently determined by x-ray diffraction (e.g., Jadzinsky *et al.*, 2007; Akola *et al.*, 2008; Heaven *et al.*, 2008; Lopez-Acevedo *et al.*, 2009; Qian *et al.*, 2010; Zeng *et al.*, 2013; Crasto *et al.*, 2014a; Crasto *et al.*, 2014b; Das *et al.*, 2015; Dass *et al.*, 2015; Jin, 2015; Xu and Gao, 2015; Sakthivel *et al.*, 2020; Higaki *et al.*, 2019; Song *et al.*, 2020) and electron microscopy (Takahata *et al.*, 2020) As a function of size and temperature there will be a phase diagram for the thermodynamically most stable shapes as originally hypothesized by Ajayan and Marks (Ajayan and Marks, 1990) The number of theoretical calculations where aspects of this have been studied is immense; overall the literature (Barnard *et al.*, 2009; Ajayan and Marks, 1988; Ajayan and Marks, 1989b; Koga *et al.*, 2004; Silly and Castell, 2009; Young *et al.*, 2010; Reinhard *et al.*, 1997; Reinhard *et al.*, 1998; Dai *et al.*, 2002; Koga and Sugawara, 2003; MacArthur *et al.*, 2012; Volk *et al.*, 2013; Niekiel *et al.*, 2014) are consistent with this general model.

A complication is the surface stress energy term, which has a large environmental dependence and is comparable in magnitude to the differences in the total surface free energies of different shapes. One strategy is to analyze the stability ranges and the cross-over between the different types of MTPs and single crystals with the surface stress and surface free energies allowed to vary as a

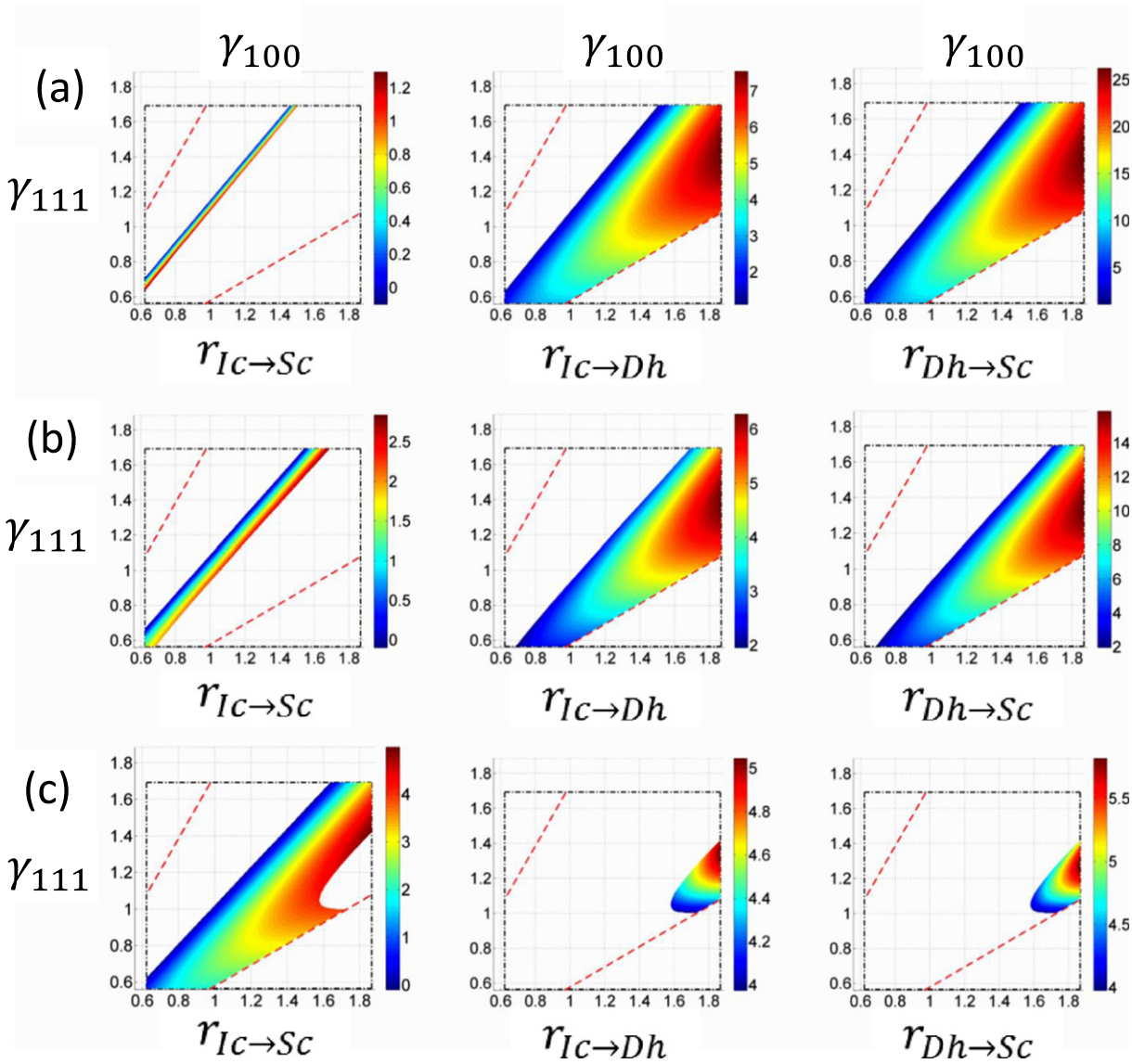

Fig. 31 Plots of the transition radii for different values of the surface energies and also different values of the surface stress, in (a) − 0.25, in (b) 0.50 and in (c) 1.25.

parameter. This leads to the results shown in **Fig. 31** (Patala *et al.*, 2013b) This behavior has very elegantly been verified recently by Parakh et al (Parakh *et al.*, 2020) who demonstrated that compressive stresses in a diamond anvil destabilizes MTPs.

Shape and Structure Versus Growth

As a final section, it is appropriate to link the different shapes and the different classes of structure to how they will evolve during growth. While the largest number of current papers deal with solution based growth, there are many other methods such as inert gas evaporation (e.g., Kimoto and Nishida, 1967; Yatsuya *et al.*, 1973; Kasukabe *et al.*, 1974; Ohno *et al.*, 1976; Granqvist, 1976; Hayashi *et al.*, 1977; Dmitrieva *et al.*, 2007), atomic layer deposition (e.g., Keranen *et al.*, 2002; Aaltonen *et al.*, 2003; Knez *et al.*, 2007; Christensen *et al.*, 2009; George, 2010; Enterkin *et al.*, 2011; Ray *et al.*, 2012; Christensen *et al.*, 2010; Cho *et al.*, 2012; Erkens *et al.*, 2013; Miikkulainen *et al.*, 2013; Masango *et al.*, 2014), evaporation or sputtering (e.g., Ino, 1966; Ino and Ogawa, 1967; Allpress and Sanders, 1967; Yagi *et al.*, 1975; Pashley and Stowell, 1963; Fukaya *et al.*, 1978; Shah and Gavrin, 2006; Penuelas *et al.*, 2009; Wender *et al.*, 2010)) and hydrothermal methods (e.g., Rabenau, 1985; Adschiri *et al.*, 2000; Goh *et al.*, 2002; Suchanek and Riman, 2006; Modeshia and Walton, 2010; Zhu and Hang, 2013; Crosby *et al.*, 2015; Ji *et al.*, 2015; Cordeiro *et al.*, 2013). In this short section the intent is to look at some of the commonalities rather than a detailed literature review.

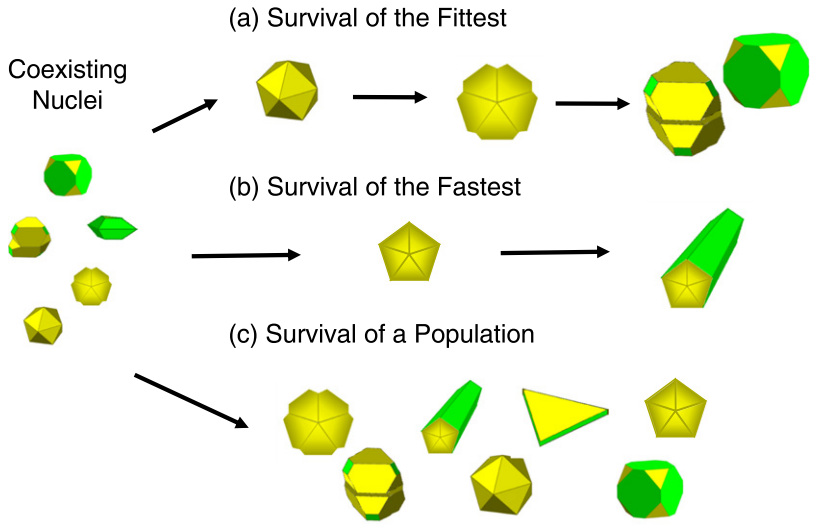

Fig. 32 Three general routes for nanoparticle shape and structure as a function of growth. Starting from a diverse population of nuclei illustrated on the left, in (a) is shown Survival of the Fittest, i.e., the thermodynamic route from Ic → Dh → Single crystals and LTP; in (b) Survival of the Fastest, here illustrated by rapidly growing Dh rods, and in (c) Survival of a Population where the initial nuclei all grow under kinetic control.

The initial step will always be nucleation, often after some incubation period. The nucleation may be homogeneous, for instance small groups of atoms in the gas phase or in a solution with ligands around them, or it can be heterogeneous at steps on a substrate, the side walls of the container or at contaminants. Some nuclei will disperse back to single atoms, some will grow, it is a statistical process. Depending upon the chemical potential the critical nucleus can be only two atoms or it can be 1–2 nm, as mentioned earlier. Experimentally detecting very small nuclei is not that easy, and often they can only be inferred from forensic data. The shape and structure of the nuclei will be system dependent, both the material as well as the external environment including any trace impurities such as oxygen leaks in a vacuum system or impurities in chemicals used in a solution-based synthesis.

After nucleation there will be growth. Around each nanoparticle there will be a population of monomers and perhaps dimers and trimers, on the substrate and diffusing across for deposition experiments; in the fluid phase for solution or argon-smoke based methods. Depending upon the rate of growth as well as the temperature the structures may change during growth (or not). Assuming that the structural transformations involve some form of vibration (phonon) the activation energy will scale as the particle volume; if it is via migration of an internal boundary it will scale as the volume to the two-third power. In both cases, as the size increases transformations will become slower and eventually cease to be relevant.

Depending upon conditions, the growth may involve local equilibration of the external surfaces via surface diffusion or not. In many cases chemisorbants, both small molecules and large surfactant molecules can play a large role in either accelerating or decelerating this. If surface diffusion is fast enough the shapes will tend to be the thermodynamic ones, either the global minima or the constrained minima; if it is slow then the kinetic routes will dominate (Carter *et al.*, 1995; Xia *et al.*, 2013).

The surrounding cloud of monomers may slowly drop as the growth proceeds, for instance as chemicals are depleted in solution growth. There will always be some equilibrium concentration, as monomers can leave the nanoparticle and return to the surrounding medium. At high enough temperatures the concentration of these monomers can be high enough that there will be exchange between nanoparticles, Ostwald ripening where small particles shrink and larger ones grow (e.g., Ostwald, 1900; Greenwood, 1956; Voorhees, 1985; Voorhees, 1992; Zinke-Allmang *et al.*, 1992; Zhang and Lagally, 1997; Brune, 1998). More rigorously, it will be those with higher chemical potentials that shrink, either because of their internal structure or other contributions such as interfacial stresses.

There can also be growth via coalescence. In a fluid there is random Brownian motion of nanoparticles whereas on a substrate there can be net translation due to local fluctuations in the concentrations of monomers. With solution growth chemisorbed ligands can play an important role to prevent coalescence by acting as buffers. When two particle coalesce there will be a substantial release of energy due to reduction of exposed surfaces, which may be large enough to lead to a full restructuring. They may rotate relative to each other to form low-angle boundaries or adopt the same orientation (e.g., Chan and Balluffi, 1985; Chan and Balluffi, 1986; Bonevich and Marks, 1992; Yeadon *et al.*, 1998; Cahn and Taylor, 2004; Jose-Yacaman *et al.*, 2005; Niederberger and Colfen, 2006; Theissmann *et al.*, 2008), be frozen leading to polyparticles or other complex structures (Smith and Marks, 1981; Yin *et al.*, 2014) or transform to MTPs (Yagi *et al.*, 1975); the general process will involve neck formation and is referred to as sintering (e.g., Nichols, 1966; Rankin and Sheldon, 1995; Shao *et al.*, 2007; Lim *et al.*, 2009b; Holland *et al.*, 2010; Klinger and Rabkin, 2010; Ingham *et al.*, 2011; Niu *et al.*, 2014).

Of course the kinetic shapes will eventually revert back to thermodynamic ones – as Homer Simpson knows you cannot beat thermodynamics. This is particularly important for heterogeneous catalysis where catalysts used in any commercial system will almost always contain nanoparticles with the thermodynamic structures for the particular set of conditions of gas and temperature

used. However, this shape conversion does not have to be that fast. Just as there is an activation energy barrier to the formation of a new terrace during growth, there is an activation energy barrier to the formation of new regions on a nanoparticle during equilibration of the shape via surface diffusion. This has been fairly well discussed in the literature (e.g., Combe *et al.*, 2000; Combe and Larralde, 2000; Mullins and Rohrer, 2000; Rohrer *et al.*, 2002; Sheldon and Rankin, 2002; Hendy *et al.*, 2003; Thurmer *et al.*, 2003; Degawa and Williams, 2005; Degawa *et al.*, 2006) and references therein).

In a very general sense the final result will tend to fall into one of three classes as illustrated in **Fig. 32**:

Survival of the Fittest

Thermodynamic equilibria dominate, either global or constrained local minima with the nanoparticles tending to be close to spherical with facets and in some cases surface steps, small terraces and at higher temperatures roughened regions.

Survival of the Fastest

Kinetics dominate, those which grow fastest will tend to dominate the population and the nanoparticles will tend to have sharp facets with rounded corners and edges, the rounding depending upon the chemical potentials during growth.

Survival of a Population

The stochastics of the evolution of the combination of different nanoparticles and different local concentrations of monomers will dominate, and there will be many slightly asymmetric shapes including polyparticles as well as the symmetric ones.

Conclusion

Nanoparticles stretch back at least to the 4th-century Lycargus Cup, perhaps much further to nanosheets of blue pigments in Nefertiti's crown from about 3000 BCE. They are everywhere, sometimes intentionally, often not; sometimes safely, but not always. They are pivotal in many existing industries, particularly heterogeneous catalysts, and may be transformative for 21st century medicine – or not.

Over the last hundred years our understanding has advanced considerably. We can now combine continuum models of shape, stress, internal structure and chemical composition to model the shape nanoparticles take, often competitive with how well these can be experimentally determined. This is both for thermodynamic shapes of Wulff, modified-Wulff and similar constructions, as well as the comparable shapes when kinetic growth controls. We are not limited to simple single crystals, but can handle without problems complicated polycrystals both in fluids or on supports, including how their shapes will change with the environment. Ab-initio methods are now well enough advanced that most of the relevant numbers can be calculated without assumptions to quite high accuracy.

Unfortunately science is not always linear; sometimes for every five steps forward one is taken backwards, and known science is forgotten or reinvented. As we move further into the 21st century, continuing to improve our control and synthesis of nanoparticles for enhanced properties, we must always remember to build science, not just publish papers.

References

Aaltonen, T., Ritala, M., Sajavaara, T., Keinonen, J., Leskela, M., 2003. Atomic layer deposition of platinum thin films. Chemistry of Materials 15, 1924–1928.
Adschiri, T., Hakuta, Y., Arai, K., 2000. Hydrothermal synthesis of metal oxide fine particles at supercritical conditions. Industrial & Engineering Chemistry Research 39, 4901–4907.
Ahmad, M.I., Bhattacharya, S.S., 2009. Size effect on the lattice parameters of nanocrystalline anatase. Applied Physics Letters 95. 191906.
Ajayan, P.M., Marks, L.D., 1988. Quasimelting and phases of small particles. Physical Review Letters 60, 585–587.
Ajayan, P.M., Marks, L.D., 1989a. Evidence for sinking of small particles into substrates and implications for heterogeneous catalysis. Nature 338, 139–141.
Ajayan, P.M., Marks, L.D., 1989b. Experimental evidence for quasimelting in small particles. Physical Review Letters 63, 279–282.
Ajayan, P.M., Marks, L.D., 1990. Phase instabilities in small particles. Phase Transitions 24–6, 229–258.
Akaiwa, N., Thornton, K., Voorhees, P.W., 2001. Large-scale simulations of microstructural evolution in elastically stressed solids. Journal of Computational Physics 173, 61–86.
Akola, J., Walter, M., Whetten, R.L., Hakkinen, H., Gronbeck, H., 2008. On the structure of thiolate-protected Au25. Journal of the American Chemical Society 130, 3756–3757.
Alex, S., Tiwari, A., 2015. Functionalized gold nanoparticles: Synthesis, properties and applications-a review. Journal of Nanoscience and Nanotechnology 15, 1869–1894.
Allpress, J.G., Sanders, J.V., 1967. Structure and orientation of crystals in deposits of metals on mica. Surface Science 7, 1–25.
Almgren, F., Taylor, J.E., Wang, L., 1993. Curvature-driven flows - a variational approach. Siam Journal on Control and Optimization 31, 387–437.
Alpay, D., Peng, L., Marks, L.D., 2015. Are nanoparticle corners round? The Journal of Physical Chemistry C 119, 21018–21023.
Ambrosio, L., Soner, H.M., 1996. Level set approach to mean curvature flow in arbitrary codimension. Journal of Differential Geometry 43, 693–737.
Anker, J.N., Hall, W.P., Lyandres, O., *et al.*, 2008. Biosensing with plasmonic nanosensors. Nature Materials 7, 442–453.
Aqua, J.N., Berbezier, I., Favre, L., Frisch, T., Ronda, A., 2013. Growth and self-organization of SiGe nanostructures. Physics Reports-Review Section of Physics Letters 522, 59–189.
Astruc, D., Lu, F., Aranzaes, J.R., 2005. Nanoparticles as recyclable catalysts: the frontier between homogeneous and heterogeneous catalysis. Angewandte Chemie International Edition 44, 7852–7872.
Baletto, F., 2019. Structural properties of sub-nanometer metallic clusters. Journal of physics. Condensed matter : An Institute of Physics Journal 31. 113001.
Baletto, F., Ferrando, R., 2005. Structural properties of nanoclusters: Energetic, thermodynamic, and kinetic effects. Reviews of Modern Physics 77, 371–423.
Baletto, F., Mottet, C., Ferrando, R., 2000. Reentrant morphology transition in the growth of free silver nanoclusters. Physical Review Letters 84, 5544–5547.
Ball, K.D., Berry, R.S., Kunz, R.E., *et al.*, 1996. From topographies to dynamics on multidimensional potential energy surfaces of atomic clusters. Science 271, 963–966.

Barnard, A.S., 2010. Modelling of nanoparticles: Approaches to morphology and evolution. Reports on Progress in Physics 73. 086502.
Barnard, A.S., Young, N.P., Kirkland, A.I., van Huis, M.A., Xu, H.F., 2009. Nanogold: A quantitative phase map. Acs Nano 3, 1431–1436.
Berg, W.F., 1938. Crystal growth from solutions. Proceedings of the Royal Society of London Series a-Mathematical and Physical Sciences 164, 0079–0095.
Bernal, S., Botana, F.J., Calvino, J.J., *et al.*, 1996. High-resolution electron microscopy investigation of metal-support interactions in Rh/TiO_2. Journal of the Chemical Society-Faraday Transactions 92, 2799–2809.
Bernal, S., Calvino, J.J., Cauqui, M.A., *et al.*, 1999. Some recent results on metal/support interaction effects in NM/CeO2 (NM: noble metal) catalysts. Catalysis Today 50, 175–206.
Bernal, S., Calvino, J.J., Cauqui, M.A., *et al.*, 2003. Some contributions of electron microscopy to the characterisation of the strong metal-support interaction effect. Catalysis Today 77, 385–406.
Berry, C.R., 1952. Electron diffraction from small crystals. Physical Review 88, 596–599.
Berry, R.S., 1990. Clusters, melting, freezing and phase-transitions - introductory lecture. Journal of the Chemical Society-Faraday Transactions 86, 2343–2349.
Berry, R.S., Smirnov, B.M., 2009. Phase transitions in various kinds of clusters. Physics 52, 137–164.
Berry, R.S., Smirnov, B.M., 2013. Configurational transitions in processes involving metal clusters. Physics Reports-Review Section of Physics Letters 527, 205–250.
Berry, R.S., Jellinek, J., Natanson, G., 1984. Melting of clusters and melting. Physical Review A 30, 919–931.
Bettge, M., MacLaren, S., Burdin, S., *et al.*, 2011. Importance of line and interfacial energies during VLS growth of finely stranded silica nanowires. Journal of Materials Research 26, 2247–2253.
Bircumshaw, L.L., Riddiford, A.C., 1952. Transport control in heterogeneous reactions. Quarterly Reviews 6, 157–185.
Bonevich, J.E., Marks, L.D., 1992. The sintering behavior of ultrafine alumina particles. Journal of Materials Research 7, 1489–1500.
Borel, J.P., Chatelain, A., 1985. Surface stress and surface-tension - equilibrium and pressure in small particles. Surface Science 156, 572–579.
Boswell, F.W.C., 1951. Precise determination of lattice constants by electron diffraction and variations in the lattice constants of very small crystallites. Proceedings of the Physical Society of London A 64, 465–476.
Boukouvala, C., Ringe, E., 2019. Wulff-based approach to modeling the plasmonic response of single crystal, twinned, and core-shell nanoparticles. Journal of Physical Chemistry C 123, 25501–25508.
Boukouvala, C., Daniel, J., Ringe, E., 2021. Approaches to modelling the shape of nanocrystals. Nano Convergence 8, 26.
Brune, H., 1998. Microscopic view of epitaxial metal growth: Nucleation and aggregation. Surface Science Reports 31, 121–229.
Buffat, P.A., 2003. Dynamical behaviour of nanocrystals in transmission electron microscopy: Size, temperature or irradiation effects. Philosophical Transactions of the Royal Society A 361, 291–295.
Buhler, J., Prior, Y., 2000. Study of morphological behavior of single diamond crystals. Journal of Crystal Growth 209, 779–788.
Burton, W.K., Cabrera, N., Frank, F.C., 1951. The growth of crystals and the equilibrium structure of their surfaces. Philosophical Transactions of the Royal Society of London Series a-Mathematical and Physical Sciences 243, 299–358.
Cahn, J.W., Hoffman, D.W., 1974. Vector thermodynamics for anisotropic surfaces .2. Curved and faceted surfaces. Acta Metallurgica 22, 1205–1214.
Cahn, J.W., Taylor, J.E., 1984. A contribution to the theory of surface-energy minimizing shapes. Scripta Metallurgica 18, 1117–1120.
Cahn, J.W., Taylor, J.E., 1994. Overview No-113 - Surface motion by surface-diffusion. Acta Metallurgica Et Materialia 42, 1045–1063.
Cahn, J.W., Carter, W.C., 1996. Crystal shapes and phase equilibria: A common mathematical basis. Metallurgical and Materials Transactions A 27, 1431–1440.
Cahn, J.W., Taylor, J.E., 2004. A unified approach to motion of grain boundaries, relative tangential translation along grain boundaries, and grain rotation. Acta Materialia 52, 4887–4898.
Cammarata, R.C., Sieradzki, K., 1994. Surface and interface stresses. Annual Review of Materials Science 24, 215–234.
Campbell, C.T., Sellers, J.R.V., 2013. Anchored metal nanoparticles: Effects of support and size on their energy, sintering resistance and reactivity. Faraday Discussions 162, 9.
Campbell, C.T., Mao, Z., 2017. Chemical potential of metal atoms in supported nanoparticles: Dependence upon particle size and support. ACS Catalysis 7, 8460–8466.
Cao, Y.L., Ding, X.L., Li, H.C., *et al.*, 2011. Morphology-controllable noble metal nanoparticles: synthesis, optical property and growth mechanism. Acta Physico-Chimica Sinica 27, 1273–1286.
Carter, W.C., Roosen, A.R., Cahn, J.W., Taylor, J.E., 1995. Shape evolution by surface-diffusion end surface attachment limited kinetics on completely faceted surfaces. Acta Metallurgica Et Materialia 43, 4309–4323.
Casillas, G., Velazquez-Salazar, J.J., Jose-Yacaman, M., New, A., 2012. Mechanism of stabilization of large decahedral nanoparticles. Journal of Physical Chemistry C 116, 8844–8848.
Castell, M.R., 2002a. Nanostructures on the SrTiO3(001) surface studied by STM. Surface Science 516, 33–42.
Castell, M.R., 2002b. Scanning tunneling microscopy of reconstructions on the SrTiO3(001) surface. Surface Science 505, 1–13.
Chan, S.-W., Balluffi, R.W., 1985. Study of energy vs misorientation for grain boundaries in gold by crystallite rotation method—I. [001] Twist boundaries. Acta Metallurgica 33, 1113–1119.
Chan, S.-W., Balluffi, R.W., 1986. Study of energy vs misorientation for grain boundaries in gold by crystallite rotation method—II. Tilt boundaries and mixed boundaries. Acta Metallurgica 34, 2191–2199.
Chen, H.Y., Li, Y., Zhang, F.B., Zhang, G.L., Fan, X.B., 2011. Graphene supported Au-Pd bimetallic nanoparticles with core-shell structures and superior peroxidase-like activities. Journal of Materials Chemistry 21, 17658–17661.
Chen, Q., Tanaka, M., Furuya, K., 1999. Unusual crystallographic structure and its fluctuation of indium nanoparticles as-deposited and observed with HRTEM using the UHV-DC-TEM system. Surface Science 440, 398–406.
Chen, S., Ferreira, P.J., Shao-Horn, Y., 2007. Surface segregation in Pt_3Co nanoparticles characterized by scanning transmission electron microscopy. Microscopy and Microanalysis 13, 604–605.
Chen, Z., Li, J., Li, S., Wang, L.-W., 2017. Glass-like energy and property landscape of Pt nanoclusters. Nano Research 10, 2721–2731.
Cheng, B., Ngan, A.H., 2013. Thermally induced solid-solid structural transition of copper nanoparticles through direct geometrical conversion. The Journal of Chemical Physics 138. 164314.
Cheng, X., Wong, J.C., Weyland, M., Valanoor, N., 2019. Encapsulation of metal oxide nanoparticles by oxide supports during epitaxial growth. ACS Applied Electronic Materials 1, 1482–1488.
Cheula, R., Maestri, M., Mpourmpakis, G., 2020. Modeling morphology and catalytic activity of nanoparticle ensembles under reaction conditions. Acs Catalysis 10, 6149–6158.
Cho, S., Kim, D.-H., Lee, B.-S., *et al.*, 2012. Ethanol sensors based on ZnO nanotubes with controllable wall thickness via atomic layer deposition, an O2 plasma process and an annealing process. Sensors & Actuators, B: Chemical 162, 300–306.
Christensen, S.T., Feng, H., Libera, J.L., *et al.*, 2010. Supported ru-pt bimetallic nanoparticle catalysts prepared by atomic layer deposition. Nano Letters 10, 3047–3051.
Christensen, S.T., Elam, J.W., Rabuffetti, F.A., *et al.*, 2009. Controlled growth of platinum nanoparticles on strontium titanate nanocubes by atomic layer deposition. Small 5, 750–757.
Cimino, A., Porta, P., Valigi, M., 1966. Dependence of lattice parameter of magnesium oxide on crystallite size. Journal of the American Ceramic Society 49, 152–156.
Ciston, J., Brown, H.G., D'Alfonso, A.J., *et al.*, 2015. Surface determination through atomically resolved secondary-electron imaging. Nature Communications 6, 7358.
Cleveland, C.L., Landman, U., 1991. The energetics and structure of nickel clusters - size dependence. Journal of Chemical Physics 94, 7376–7396.
Combe, N., Larralde, H., 2000. Low-temperature shape relaxation of two-dimensional islands by edge diffusion. Physical Review B 62, 16074–16084.
Combe, N., Jensen, P., Pimpinelli, A., 2000. Changing shapes in the nanoworld. Physical Review Letters 85, 110–113.

Cordeiro, M.A.L., Weng, W.H., Stroppa, D.G., Kiely, C.J., Leite, E.R., 2013. High Resolution Electron Microscopy Study of Nanocubes and Polyhedral Nanocrystals of Cerium (IV) Oxide. Chemistry of Materials 25, 2028–2034.
Coriell, S.R., Sekerka, R.F., 1976. Effect Of Anisotropy Of Surface-Tension And Interface Kinetics On Morphological Stability. Journal of Crystal Growth 34, 157–163.
Cosandey, F., 2013. Epitaxy, interfacial energy and atomic structure of Au/TiO2 interfaces. Philosophical Magazine 93, 1197–1218.
Cox, G., Berry, R.S., Johnston, R.L., 2006. Characterizing potential surface topographies through the distribution of saddles and minima. The Journal of Physical Chemistry A 110, 11543–11550.
Crasto, D., Barcaro, G., Stener, M., *et al*., 2014a. Au(2)(4)(SAdm)(1)(6) nanomolecules: X-ray crystal structure, theoretical analysis, adaptability of adamantane ligands to form Au(2)(3)(SAdm)(1)(6) and Au(2)(5)(SAdm)(1)(6), and its relation to Au(2)(5)(SR)(1)(8). Journal of the American Chemical Society 136, 14933–14940.
Crasto, D., Malola, S., Brosofsky, G., Dass, A., Hakkinen, H., 2014b. Single crystal XRD structure and theoretical analysis of the chiral Au30S(S-t-Bu)18 cluster. Journal of the American Chemical Society 136, 5000–5005.
Cristini, V., Lowengrub, J., 2002. Three-dimensional crystal growth - I: linear analysis and self-similar evolution. Journal of Crystal Growth 240, 267–276.
Crosby, L., Enterkin, J., Rabuffetti, F., Poeppelmeier, K., Marks, L.D., 2015. Wulff shape of strontium titanate nanocuboids. Surface Science 632, L22–L25.
Crosby, L.A., Kennedy, R.M., Chen, B.R., *et al*., 2016. Complex surface structure of (110) terminated strontium titanate nanododecahedra. Nanoscale 8, 16606–16611.
Cui, C.H., Gan, L., Heggen, M., Rudi, S., Strasser, P., 2013. Compositional segregation in shaped Pt alloy nanoparticles and their structural behaviour during electrocatalysis. Nature Materials 12, 765–771.
Dai, Z.R., Sun, S.H., Wang, Z.L., 2002. Shapes, multiple twins and surface structures of monodisperse FePt magnetic nanocrystals. Surface Science 505, 325–335.
Daruka, I., Tersoff, J., Barabasi, A.L., 1999. Shape transition in growth of strained islands. Physical Review Letters 82, 2753–2756.
Das, A., Liu, C., Byun, H.Y., *et al*., 2015. Structure determination of [Au18(SR)14]. Angewandte Chemie International Edition England 54, 3140–3144.
Dass, A., Theivendran, S., Nimmala, P.R., *et al*., 2015. Au133(SPh-tBu)52 nanomolecules: X-ray crystallography, optical, electrochemical, and theoretical analysis. Journal of the American Chemical Society 137, 4610–4613.
Degawa, M., Williams, E.D., 2005. Barriers to shape evolution of supported nano-crystallites. Surface Science 595, 87–96.
Degawa, M., Thurmer, K., Williams, E.D., 2006. Constrained evolution of nanocrystallites. Physical Review B 74. 155432.
Deng, L., Liu, X., Zhang, X., *et al*., 2019. Intrinsic strain-induced segregation in multiply twinned Cu-Pt icosahedra. Physical Chemistry Chemical Physics 21, 4802–4809.
DeWit, R., 1972. Partial disclinations. Journal of Physics Part C Solid 5, 529.
Dicarlo, A., Gurtin, M.E., Podioguidugli, P., 1992. A regularized equation for anisotropic motion-by-curvature. SIAM Journal of Applied Mathematics 52, 1111–1119.
Diehm, P.M., Agoston, P., Albe, K., 2012. Size-dependent lattice expansion in nanoparticles: Reality or anomaly? Chemphyschem 13, 2443–2454.
Dinghas, A., 1944. Uber einen geometrischen sat von Wulff fur die gleichgewitchtsform von kristallen. Z. Kristallogr 105, 304–314.
Dmitrieva, O., Rellinghaus, B., Kästner, J., Dumpich, G., 2007. Quantitative structure analysis of L10-ordered FePt nanoparticles by HRTEM. Journal of Crystal Growth 303, 645–650.
Dorogin, L.M., Vlassov, S., Kolesnikova, A.L., *et al*., 2010a. Crystal mismatched layers in pentagonal nanorods and nanoparticles. Physica Status Solidi B 247, 288–298.
Dorogin, L.M., Vlassov, S., Kolesnikova, A.L., *et al*., 2010b. Pentagonal nanorods and nanoparticles with mismatched shell layers. Journal of Nanoscience and Nanotechnology 10, 6136–6143.
Doye, J.P., Wales, D.J., 2001. Polytetrahedral clusters. Physical Review Letters 86, 5719–5722.
Doye, J.P.K., Wales, D.J., Miller, M.A., 1998. Thermodynamics and the global optimization of Lennard-Jones clusters. Journal of Chemical Physics 109, 8143–8153.
Drucker, J., 1993. Coherent islands and microstructural evolution. Physical Review. B, Condensed Matter 48, 18203–18206.
Du, D., Srolovitz, D.J., Coltrin, M.E., Mitchell, C.C., 2005a. Systematic prediction of kinetically limited crystal growth morphologies. Physical Review Letters 95. 155503.
Du, X.W., Wang, B., Zhao, N.Q., Furuya, K., 2005b. Structure evolution of silicon nanocrystals under electron irradiation. Scripta Materialia 53, 899–903.
Dundurs, J., Marks, L.D., Ajayan, P.M., 1988. Structural fluctuations in small particles. Philosophical Magazine A: Physics of Condensed Matter, Structure, Defects and Mechanical Properties 57, 605–620.
Eggleston, J.J., McFadden, G.B., Voorhees, P.W., 2001. A phase-field model for highly anisotropic interfacial energy. Physica D 150, 91–103.
Ek, M., Beinik, I., Bruix, A., *et al*., 2018. Step edge structures on the anatase TiO2 (001) surface studied by atomic-resolution TEM and STM. Faraday Discussions 208, 325–338.
Elahi, N., Kamali, M., Baghersad, M.H., 2018. Recent biomedical applications of gold nanoparticles: A review. Talanta 184, 537–556.
Ellaby, T., Varambhia, A., Luo, X.N., *et al*., 2020. Strain effects in core-shell PtCo nanoparticles: a comparison of experimental observations and computational modelling. Physical Chemistry Chemical Physics 22, 24784–24795.
Enterkin, J.A., Poeppelmeier, K.R., Marks, L.D., 2011. Oriented catalytic platinum nanoparticles on high surface area strontium titanate nanocuboids. Nano Letters 11, 993–997.
Eom, N., Messing, M.E., Johansson, J., Deppert, K., 2021. General trends in core-shell preferences for bimetallic nanoparticles. ACS Nano 15, 8883–8895.
Erdman, N., Poeppelmeier, K.R., Asta, M., *et al*., 2002. The structure and chemistry of the TiO(2)-rich surface of SrTiO(3) (001). Nature 419, 55–58.
Erdman, N., Warschkow, O., Asta, M., *et al*., 2003. Surface structures of $SrTiO_3$ (001): A TiO_2-rich reconstruction with a c(4 x 2) unit cell. Journal of the American Chemical Society 125, 10050–10056.
Erkens, I., Blauw, M., Verheijen, M., Roozeboom, F., Kessels, W.M.M., 2013. Room temperature sensing of O_2 and CO by atomic layer deposition prepared ZnO films coated with Pt nanoparticles. ECS Transactions 58, 203–214.
Evans, D.M., Wilman, H., 1952. Crystal growth and orientation in deposits condensed from the vapour. Acta Crystallographica 5, 731–738.
Fan, H.J., Gosele, U., Zacharias, M., 2007. Formation of nanotubes and hollow nanoparticles based on Kirkendall and diffusion processes: A review. Small 3, 1660–1671.
Feng, L., Wang, J., Wang, S.B., *et al*., 2015. Understanding the effects of strain on morphological instabilities of a nanoscale island during heteroepitaxial growth. Journal of Applied Physics 118. 035304.
Fichthorn, K.A., Yan, T., 2021. Shapes and shape transformations of solution-phase metal particles in the sub-nanometer to nanometer size range: progress and challenges. Journal of Physical Chemistry C 125, 3668–3679.
Finch, G.I., Fordham, S., 1936. The effect of crystal-size on lattice-dimensions. Proceedings of the Physical Society 48, 85–94.
Finney, E.E., Finke, R.G., 2008. Nanocluster nucleation and growth kinetic and mechanistic studies: A review emphasizing transition-metal nanoclusters. Journal of Colloid and Interface Science 317, 351–374.
Fu, Q., Wagner, T., Olliges, S., Carstanjen, H.D., 2005. Metal-oxide interfacial reactions: encapsulation of Pd on TiO2 (110). The Journal of Physical Chemistry B 109, 944–951.
Fukaya, K., Ino, S., Ogawa, S., 1978. Orientation and structure of palladium particles formed by evaporation on alkali-halide crystals. Transactions of the Japan Institute of Metals 19, 445–453.
Gamalski, A.D., Voorhees, P.W., Ducati, C., Sharma, R., Hofmann, S., 2014. Twin plane re-entrant mechanism for catalytic nanowire growth. Nano Letters 14, 1288–1292.
George, S.M., 2010. Atomic layer deposition: An overview. Chemical Reviews 110, 111–131.
Gillet, M., 1977. Structure of small metallic particles. Surface Science 67, 139–157.
Goh, G.K.L., Haile, S.M., Levi, C.G., Lange, F.F., 2002. Hydrothermal synthesis of perovskite and pyrochlore powders of potassium tantalate. Journal of Materials Research 17, 3168–3176.
Goloven'ko, Z.V., Gafner, Y.Y., Gafner, S.L., Redel, L.V., 2013. Thermal stability of structure in small gold clusters. Physics of Metals and Metallography 114, 1038–1044.
Golovin, A.A., Davis, S.H., Nepomnyashchy, A.A., 1998. A convective Cahn-Hilliard model for the formation of facets and corners in crystal growth. Physica D 122, 202–230.
Goldschmidt, V., 1913a. Atlas der Kristallformen, V1, Plates, Carl Winters Universitätsbuchhandlung, Heidelberg.

Goldschmidt, V., 1913b. Atlas der Kristallformen, V2, Plates, Carl Winters Universitätsbuchhandlung, Heidelberg.
Goldschmidt, V., 1916. Atlas der Kristallformen, V3, Plates, Carl Winters Universitätsbuchhandlung, Heidelberg.
Goldschmidt, V., 1918a. Atlas der Kristallformen, V4, Plates, Carl Winters Universitätsbuchhandlung, Heidelberg.
Goldschmidt, V., 1918b. Atlas der Kristallformen, V5, Plates, Carl Winters Universitätsbuchhandlung, Heidelberg.
Goldschmidt, V., 1920. Atlas der Kristallformen, V6, Plates, Carl Winters Universitätsbuchhandlung, Heidelberg.
Goldschmidt, V., 1922a. Atlas der Kristallformen, V7, Plates, Carl Winters Universitätsbuchhandlung, Heidelberg.
Goldschmidt, V., 1922b. Atlas der Kristallformen, V8, Plates, Carl Winters Universitätsbuchhandlung, Heidelberg.
Gontard, L.C., Dunin-Borkowski, R.E., Gass, M.H., Bleloch, A.L., Ozkaya, D., 2009. Three-dimensional shapes and structures of lamellar-twinned fcc nanoparticles using ADF STEM. Journal of Electron Microscopy 58, 167–174.
Granqvist, C.G., 1976. Ultrafine metal particles. Journal of Applied Physics 47, 2200.
Greenwood, G.W., 1956. The growth of dispersed precipitates in solutions. Acta Metallurgica 4, 243–248.
Gryaznov, V.G., Kaprelov, A.M., Romanov, A.E., Polonskii, I.A., 1991. Channels of relaxation of elastic stresses in pentagonal nanoparticles. Physica Status Solidi B-Basic Research 167, 441–450.
Gryaznov, V.G., Heydenreich, J., Kaprelov, A.M., *et al.*, 1999. Pentagonal symmetry and disclinations in small particles. Crystal Research and Technology 34, 1091–1119.
Grzelczak, M., Perez-Juste, J., Mulvaney, P., Liz-Marzan, L.M., 2008. Shape control in gold nanoparticle synthesis. Chemical Society Reviews 37, 1783–1791.
Guisbiers, G., 2019. Advances in thermodynamic modelling of nanoparticles. Advances in Physics-X 4. 1668299.
Gutkin, M.Y., 2011. Elastic and plastic deformation in nanocrystalline metals. In: Whang, S.H. (Ed.), Nanostructured Metals and Alloys: Processing, Microstructure, Mechanical Properties and Applications. Elsevier.
Guyer, J.E., Voorhees, P.W., 1995. Morphological stability of alloy thin films. Physical Review Letters 74, 4031–4034.
Hofmeister, H., 2004. Fivefold twinned nanoparticles. In: Nalwa, H.S. (Ed.), Encyclopedia of Nanoscience and Nanotechnology. Elsevier.
Haider, A., Kang, I.K., 2015. Preparation of silver nanoparticles and their industrial and biomedical applications: A comprehensive review. Advances in Materials Science and Engineering 2015. 165257.
Haller, G.L., Resasco, D.E., 1989. Metal support interaction - Group-Viii metals and reducible oxides. Advances in Catalysis 36, 173–235.
Hamilton, D.R., Seidensticker, R.G., 1960. Propagation mechanism of germanium dendrites. Journal of Applied Physics 31, 1165–1168.
Hamilton, J.C., 2006. Edge energies: Atomistic calculations of a continuum quantity. Physical Review B 73. 125447.
Hamilton, J.C., Léonard, F., Johnson, E., Dahmen, U., 2007. Pb nanoprecipitates in Al: Magic-shape effects due to elastic strain. Physical Review Letters 98. 236102.
Hammar, M., LeGoues, F.K., Tersoff, J., Reuter, M.C., Tromp, R.M., 1996. In situ ultrahigh vacuum transmission electron microscopy studies of hetero-epitaxial growth I. Surface Science 349, 129–144.
Harada, M., Katagiri, E., 2010. Mechanism of silver particle formation during photoreduction using in situ time-resolved SAXS analysis. Langmuir 26, 17896–17905.
Harada, M., Kamigaito, Y., 2012. Nucleation and aggregative growth process of platinum nanoparticles studied by in situ quick XAFS spectroscopy. Langmuir 28, 2415–2428.
Harada, M., Tamura, N., Takenaka, M., 2011. Nucleation and growth of metal nanoparticles during photoreduction using in situ time-resolved SAXS analysis. Journal of Physical Chemistry C 115, 14081–14092.
Hayashi, T., Ohno, T., Yatsuya, S., Uyeda, R., 1977. Formation of ultrafine metal particles by gas-evaporation technique .4. crystal habits of iron and fcc metals, Al, Co, Ni, Cu, Pd, Ag, In, Au And Pb. Japanese Journal of Applied Physics 16, 705–717.
Heaven, M.W., Dass, A., White, P.S., Holt, K.M., Murray, R.W., 2008. Crystal structure of the gold nanoparticle [N(C8H17)4][Au25(SCH2CH2Ph)18]. Journal of the American Chemical Society 130, 3754–3755.
Hemmingson, S.L., Campbell, C.T., 2017. Trends in adhesion energies of metal nanoparticles on oxide surfaces: Understanding support effects in catalysis and nanotechnology. ACS Nano 11, 1196–1203.
Hendy, S., Brown, S.A., Hyslop, M., 2003. Coalescence of nanoscale metal clusters: Molecular-dynamics study. Physical Review B 68. 241403.
Henry, A.I., Bingham, J.M., Ringe, E., *et al.*, 2011. Correlated structure and optical property studies of plasmonic nanoparticles. Journal of Physical Chemistry C 115, 9291–9305.
Herger, R., Willmott, P.R., Bunk, O., *et al.*, 2007. Surface of strontium titanate. Physical Review Letters 98. 076102.
Herring, C., 1951. Some theorems on the free energies of crystal surfaces. Physical Review 82, 87–93.
Herzing, A.A., Watanabe, M., Edwards, J.K., *et al.*, 2008. Energy dispersive X-ray spectroscopy of bimetallic nanoparticles in an aberration corrected scanning transmission electron microscope. Faraday Discussions 138, 337–351. discussion 421-334.
Higaki, T., Liu, C., Morris, D.J., *et al.*, 2019. $Au_{130-x}Ag_x$ nanoclusters with non-metallicity: A drum of silver-rich sites enclosed in a marks-decahedral cage of gold-rich sites. Angewandte Chemie-International Edition 58, 18798–18802.
Hoare, M.R., Pal, P., 1971. Physical cluster mechanics - statics and energy surfaces for monatomic systems. Advances in Physics 20, 161.
Hoare, M.R., Pal, P., 1972. Statistics and stability of small assemblies of atoms. Journal of Crystal Growth 17, 77–96.
Hoare, M.R., Pal, P., 1975. Physical cluster mechanics - statistical thermodynamics and nucleation theory for monatomic systems. Advances in Physics 24, 645–678.
Hoffman, D.W., Cahn, J.W., 1972. Vector thermodynamics for anisotropic surfaces .1. Fundamentals and application to plane surface junctions. Surface Science 31, 368–388.
Hofmeister, H., 1998. Forty years study of fivefold twinned structures in small particles and thin films. Crystal Research and Technology 33, 3–25.
Hofmeister, H., 2009. Shape variations and anisotropic growth of multiply twinned nanoparticles. Z Kristallogr 224, 528–538.
Holland, T.B., Thron, A.M., Bonifacio, C.S., Mukherjee, A.K., van Benthem, K., 2010. Field assisted sintering of nickel nanoparticles during in situ transmission electron microscopy. Applied Physics Letters 96. 243106.
Howie, A., Marks, L.D., 1984. Elastic strains and the energy-balance for multiply twinned particles. Philosophical Magazine A: Physics of Condensed Matter, Structure, Defects and Mechanical Properties 49, 95–109.
Hu, M., Chen, J., Li, Z.Y., *et al.*, 2006. Gold nanostructures: Engineering their plasmonic properties for biomedical applications. Chemical Society Reviews 35, 1084–1094.
Hubert, H., Devouard, B., Garvie, L.A.J., *et al.*, 1998. Icosahedral packing of B-12 icosahedra in boron suboxide (B6O). Nature 391, 376–378.
Hudgens, J.W., Pettibone, J.M., Senftle, T.P., Bratton, R.N., 2011. Reaction mechanism governing formation of 1,3-bis(diphenylphosphino)propane-protected gold nanoclusters. Inorganic Chemistry 50, 10178–10189.
Iijima, S., Ichihashi, T., 1986. Structural instability of ultrafine particles of metals. Physical Review Letters 56, 616–619.
Ingham, B., Lim, T.H., Dotzler, C.J., *et al.*, 2011. How nanoparticles coalesce: An in situ study of au nanoparticle aggregation and grain growth. Chemistry of Materials 23, 3312–3317.
Ino, S., 1966. Epitaxial growth of metals on rocksalt faces cleaved in vacuum .2. Orientation and structure of gold particles formed in ultrahigh vacuum. Journal of the Physical Society of Japan 21, 346–362.
Ino, S., 1969. Stability of multiply-twinned particles. Journal of the Physical Society of Japan 27, 941–953.
Ino, S., Ogawa, S., 1967. Multiply twinned particles at earlier stages of gold film formation on alkalihalide crystals. Journal of the Physical Society of Japan 22, 1365.
Jadzinsky, P.D., Calero, G., Ackerson, C.J., Bushnell, D.A., Kornberg, R.D., 2007. Structure of a thiol monolayer-protected gold nanoparticle at 1.1 A resolution. Science 318, 430–433.
Jeevanandam, J., Barhoum, A., Chan, Y.S., Dufresne, A., Danquah, M.K., 2018. Review on nanoparticles and nanostructured materials: History, sources, toxicity and regulations. Beilstein Journal of Nanotechnology 9, 1050–1074.
Ji, W.H., Qi, W.H., Li, X., *et al.*, 2015. Investigation of disclinations in Marks decahedral Pd nanoparticles by aberration-corrected HRTEM. Materials Letters 152, 283–286.

Ji, W.H., Qi, W.H., Tang, S.S., *et al*., 2014. Synthesis of marks-decahedral Pd nanoparticles in aqueous solutions. Particle & Particle Systems Characterization 31, 851–856.
Jiang, Q., Liang, L.H., Zhao, D.S., 2001. Lattice contraction and surface stress of fcc nanocrystals. Journal of Physical Chemistry B 105, 6275–6277.
Jiang, Q.D., Zegenhagen, J., 1999. c(6 × 2) and c(4 × 2) reconstruction of SrTiO3(001). Surface Science 425, 343–354.
Jin, R., 2015. Atomically precise metal nanoclusters: Stable sizes and optical properties. Nanoscale 7, 1549–1565.
Johnson, C.L., Snoeck, E., Ezcurdia, M., *et al*., 2008. Effects of elastic anisotropy on strain distributions in decahedral gold nanoparticles. Nature Materials 7, 120–124.
Johnston, K., Castell, M.R., Paxton, A.T., Finnis, M.W., 2004. $SrTiO_3(001)(2 \times 1)$ reconstructions: First-principles calculations of surface energy and atomic structure compared with scanning tunneling microscopy images. Physical Review B 70. 085415.
Jose-Yacaman, M., Gutierrez-Wing, C., Miki, M., *et al*., 2005. Surface diffusion and coalescence of mobile metal nanoparticles. The Journal of Physical Chemistry B 109, 9703–9711.
Jun, Y.-W., Choi, J.-S., Cheon, J., 2006. Shape control of semiconductor and metal oxide nanocrystals through nonhydrolytic colloidal routes. Angewandte Chemie International Edition 45, 3414–3439.
Kasukabe, S., Yatsuya, S., Uyeda, R., 1974. Ultrafine metal particles formed by gas-evaporation technique .2. Crystal habits of magnesium, manganese, beryllium and tellurium. Japanese Journal of Applied Physics 13, 1714–1721.
Keranen, J., Auroux, A., Ek, S., Niinisto, L., 2002. Preparation, characterization and activity testing of vanadia catalysts deposited onto silica and alumina supports by atomic layer deposition. Applied Catalysis a-General 228, 213–225.
Khanna, S.N., Bucher, J.P., Buttet, J., Cyrotlackmann, F., 1983. Stability and lattice contraction of small platinum particles. Surface Science 127, 165–174.
Kienzle, D.M., Marks, L.D., 2012. Surface transmission electron diffraction for $SrTiO_3$ surfaces. Crystengcomm 14, 7833–7839.
Kienzle, D.M., Becerra-Toledo, A.E., Marks, L.D., 2011. Vacant-site octahedral tilings on SrTiO(3) (001), the (sqrt[13]xsqrt[13])R33.7 degrees surface, and related structures. Physical Review Letters 106. 176102.
Kimoto, K., Nishida, I., 1967. An electron microscope and electron diffraction study of fine smoke particles prepared by evaporation in argon gas at low pressures (II), Jpn. Journal of Applied Physics 6, 1047.
Kirkland, A.I., Jefferson, D.A., Duff, D.G., *et al*., 1993. Structural studies of trigonal lamellar particles of gold and silver. Proceedings of the Royal Society of London Series a-Mathematical Physical and Engineering Sciences 440, 589–609.
Klinger, L., Rabkin, E., 2010. Sintering of fully faceted crystalline particles. International Journal of Materials Research 101, 75–83.
Knez, M., Niesch, K., Niinisto, L., 2007. Synthesis and surface engineering of complex nanostructures by atomic layer deposition. Advanced Materials 19, 3425–3438.
Koga, K., Sugawara, K., 2003. Population statistics of gold nanoparticle morphologies: direct determination by HREM observations. Surface Science 529, 23–35.
Koga, K., Ikeshoji, T., Sugawara, K., 2004. Size- and temperature-dependent structural transitions in gold nanoparticles. Physical Review Letters 92. 115507.
Kolesnikova, A.L., Romanov, A.E., 2010. Representations of elastic fields of circular dislocation and disclination loops in terms of spherical harmonics and their application to various problems of the theory of defects. International Journal of Solids and Structures 47, 58–70.
Komoda, T., 1968. Study on structure of evaporated gold particles by means of a high resolution electron microscope. Japanese Journal of Applied Physics 7, 27–30.
Kumar, S., Gandhi, K.S., Kumar, R., 2007. Modeling of formation of gold nanoparticles by citrate method. Industrial & Engineering Chemistry Research 46, 3128–3136.
Lamber, R., Wetjen, S., Jaeger, N.I., 1995. Size dependence of the lattice parameter of small palladium particles. Physical Review B Condensed Matter 51, 10968–10971.
Langlois, C., Li, Z.L., Yuan, J., *et al*., 2012. Transition from core-shell to Janus chemical configuration for bimetallic nanoparticles. Nanoscale 4, 3381–3388.
Lazzari, R., Jupille, J., 2012. Growth kinetics and size-dependent wetting of Ag/alpha-Al(2)O(3)(0001) nanoparticles studied via the plasmonic response. Nanotechnology 23. 135707.
Leung, B., Sun, Q., Yerino, C.D., Han, J., Coltrin, M.E., 2012. Using the kinetic Wulff plot to design and control nonpolar and semipolar GaN heteroepitaxy. Semiconductor Science and Technology 27. 024005.
Lewis, D.J., Zornberg, L.Z., Carter, D.J.D., Macfarlane, R.J., 2020. Single-crystal Winterbottom constructions of nanoparticle superlattices. Nature Materials 19, 719. (- +).
Li, A., Liu, F., Lagally, M.G., 2000. Equilibrium shape of two-dimensional islands under stress. Physical Review Letters 85, 1922–1925.
Li, B., Wen, X., Li, R., *et al*., 2014a. Stress-induced phase transformation and optical coupling of silver nanoparticle superlattices into mechanically stable nanowires. Nature Communications 5, 4179.
Li, N., Zhao, P., Astruc, D., 2014b. Anisotropic gold nanoparticles: Synthesis, properties, applications, and toxicity. Angewandte Chemie International Edition 53, 1756–1789.
Li, G.S., Boerio-Goates, J., Woodfield, B.F., Li, L.P., 2004. Evidence of linear lattice expansion and covalency enhancement in rutile TiO2 nanocrystals. Applied Physics Letters 85, 2059–2061.
Lim, B., Wang, J.G., Camargo, P.H.C., *et al*., 2009a. Twin-induced growth of palladium-platinum alloy nanocrystals. Angewandte Chemie-International Edition 48, 6304–6308.
Lim, T.H., McCarthy, D., Hendy, S.C., *et al*., 2009b. Real-time TEM and kinetic Monte Carlo studies of the coalescence of decahedral gold nanoparticles. ACS Nano 3, 3809–3813.
Lin, Y., Wu, Z., Wen, J., Poeppelmeier, K.R., Marks, L.D., 2014. Imaging the atomic surface structures of CeO2 nanoparticles. Nano Letters 14, 191–196.
Lin, Y., Wen, J., Hu, L., *et al*., 2013. Synthesis-dependent atomic surface structures of oxide nanoparticles. Physical Review Letters 111, 156101.
Lin, Y., Wu, Z., Wen, J., *et al*., 2015. Adhesion and atomic structures of gold on ceria nanostructures: The role of surface structure and oxidation state of ceria supports. Nano Letters 15, 5375–5381.
Liu, J.Y., 2011. Advanced electron microscopy of metal-support interactions in supported metal catalysts. Chemcatchem 3, 934–948.
Liu, L.H., Cheng, Z.Y., Zhu, J., Yu, R., 2020. Flexible cation distribution for stabilizing a spinel surface. Journal of Physical Chemistry C 124, 16431–16438.
Lofton, C., Sigmund, W., 2005. Mechanisms controlling crystal habits of gold and silver colloids. Advanced Functional Materials 15, 1197–1208.
Lopez-Acevedo, O., Akola, J., Whetten, R.L., Gronbeck, H., Hakkinen, H., 2009. Structure and bonding in the ubiquitous icosahedral metallic gold cluster Au-144(SR)(60). Journal of Physical Chemistry C 113, 5035–5038.
Lu, J., Low, K.B., Lei, Y., *et al*., 2014. Toward atomically-precise synthesis of supported bimetallic nanoparticles using atomic layer deposition. Nature Communications 5, 3264.
Ly, T., Wen, J., Marks, L.D., 2018. Kinetic growth regimes of hydrothermally synthesized potassium tantalate nanoparticles. Nano Letters 18, 5186–5191.
Ly, T., Wen, J., Marks, L.D., 2020a. Chemisorption-driven roughening of hydrothermally grown KTa1–xNbxO3 Nanoparticles. The Journal of Physical Chemistry C 124, 7988–7993.
Ly, T., Wen, J., Marks, L.D., 2020b. Complex fluorine chemical potential effects on the shape and compositional heterogeneity of KTa1–xNbxO3 nanoparticles. The Journal of Physical Chemistry C 124, 26012–26017.
MacArthur, K.E., Young, N.P., Critchell, J.W., Kirkland, A.I., 2012. 'Ex-Situ' annealing and structural transformations in gold nanoparticles. In: Proceedings of the Electron Microscopy and Analysis Group Conference 2011 (Emag 2011), p. 371, 012068.
Mansley, Z.R., Marks, L.D., 2020. Modified winterbottom construction including boundaries. The Journal of Physical Chemistry C 124, 28038–28043.
Mariscal, M.M., Velazquez-Salazar, J.J., Yacaman, M.J., 2012. Growth mechanism of nanoparticles: Theoretical calculations and experimental results. Crystengcomm 14, 544–549.
Marks, L.D., 1980. The Structure of Small Silver Particles. University of Cambridge.
Marks, L.D., 1983a. Modified wulff constructions for twinned particles. Journal of Crystal Growth 61, 556–566.
Marks, L.D., 1983b. Direct imaging of carbon-covered and clean gold (110) surfaces. Physical Review Letters 51, 1000–1002.
Marks, L.D., 1984. Surface-structure and energetics of multiply twinned particles. Philosophical Magazine A: Physics of Condensed Matter, Structure, Defects and Mechanical Properties 49, 81–93.

Marks, L.D., 1985. Particle-size effects on wulff constructions. Surface Science 150, 358–366.
Marks, L.D., 1994. Experimental studies of small-particle structures. Reports on Progress in Physics 57, 603–649.
Marks, L.D., Howie, A., 1979. Multiply-twinned particles in silver catalysts. Nature 282, 196–198.
Marks, L.D., Smith, D.J., 1981. High-resolution studies of small particles of gold and silver .1. Multiply-twinned particles. Journal of Crystal Growth 54, 425–432.
Marks, L.D., Ajayan, P.M., 1990. Equilibrium shape of a buoyant particle. Journal of Materials Research 5, 1496–1501.
Marks, L.D., Peng, L., 2016. Nanoparticle shape, thermodynamics and kinetics. Journal of Physics Condensed Matter : An Institute of Physics Journal 28. 053001.
Marks, L.D., Ajayan, P.M., Dundurs, J., 1986. Quasi-melting of small particles. Ultramicroscopy 20, 77–82.
Marshall, M.S.J., Becerra-Toledo, A.E., Marks, L.D., Castell, M.R., 2015. Defects on strontium titanate. In: Jupille, J., Thornton, G. (Eds.), Defects at Oxide Surfaces. Springer International Publishing, pp. 327–349.
Masango, S.S., Peng, L.X., Marks, L.D., Van Duyne, R.P., Stair, P.C., 2014. Nucleation and growth of silver nanoparticles by AB and ABC-type atomic layer deposition. Journal of Physical Chemistry C 118, 17655–17661.
Mastroberardino, A., Spencer, B.J., 2010. Three-dimensional equilibrium crystal shapes with corner energy regularization. IMA Journal of Applied Mathematics 75, 190–205.
Mayoral, A., Barron, H., Estrada-Salas, R., Vazquez-Duran, A., Jose-Yacaman, M., 2010. Nanoparticle stability from the nano to the meso interval. Nanoscale 2, 335–342.
Mays, C.W., Vermaak, J.S., Kuhlmann-Wilsdorf, D., 1968. On surface stress and surface tension. Surface Science 12, 134–140.
McEachran, M., Kitaev, V., 2008. Direct structural transformation of silver platelets into right bipyramids and twinned cube nanoparticles: Morphology governed by defects. Chemical Communications. 5737–5739.
Medeiros-Ribeiro, G., Bratkovski, A.M., Kamins, T.I., Ohlberg, D.A.A., Williams, R.S., 1998. Shape transition of germanium nanocrystals on a silicon (001) surface from pyramids to domes. Science 279, 353–355.
Melmed, A.J., Hayward, D.O., 1959. Occurrence of fivefold rotational symmetry in metal whiskers. Journal of Chemical Physics 31, 545–546.
Miikkulainen, V., Nilsen, O., Laitinen, M., Sajavaara, T., Fjellvåg, H., 2013. Atomic layer deposition of LixTiyOz thin films. RSC Advances 3, 7537–7542.
Millstone, J.E., Hurst, S.J., Metraux, G.S., Cutler, J.I., Mirkin, C.A., 2009. Colloidal gold and silver triangular nanoprisms. Small 5, 646–664.
Modeshia, D.R., Walton, R.I., 2010. Solvothermal synthesis of perovskites and pyrochlores: Crystallisation of functional oxides under mild conditions. Chemical Society Reviews 39, 4303–4325.
Muller, P., Kern, R., 1998. Equilibrium shape of epitaxially strained crystals (Volmer-Weber case). Journal of Crystal Growth 193, 257–270.
Muller, P., Kern, R., 2000. Equilibrium nano-shape changes induced by epitaxial stress (generalised Wulf-Kaishew theorem). Surface Science 457, 229–253.
Muller, P., Saul, A., 2004. Elastic effects on surface physics. Surface Science Reports 54, 157–258.
Mullins, W.W., Rohrer, G.S., 2000. Nucleation barrier for volume-conserving shape changes of faceted crystals. Journal of the American Ceramic Society 83, 214–216.
Nelli, D., Ferrando, R., 2019. Core–shell vs. multi-shell formation in nanoalloy evolution from disordered configurations. Nanoscale 11, 13040–13050.
Newell, D.T., 2007. The surface structure and reconstructions of $SrTiO_3$(001). In Materials. Oxford: Oxford, p. 168.
Nichols, F.A., 1966. Coalescence of 2 spheres by surface diffusion. Journal of Applied Physics 37, 2805–2808.
Niederberger, M., Colfen, H., 2006. Oriented attachment and mesocrystals: Non-classical crystallization mechanisms based on nanoparticle assembly. Physical Chemistry Chemical Physics 8, 3271–3287.
Niekiel, F., Bitzek, E., Spiecker, E., 2014. Combining atomistic simulation and X-ray diffraction for the characterization of nanostructures: A case study on fivefold twinned nanowires. ACS Nano 8, 1629–1638.
Niu, K.Y., Liao, H.G., Zheng, H., 2014. Visualization of the coalescence of bismuth nanoparticles. Microscopy and Microanalysis: The Official Journal of Microscopy Society of America, Microbeam Analysis Society, Microscopical Society of Canada 20, 416–424.
Oehl, N., Knipper, M., Parisi, J., Plaggenborg, T., Kolny-Olesiak, J., 2015. Size-dependent lattice distortion in epsilon-Ag3Sn alloy nanoparticles. Journal of Physical Chemistry C 119, 14450–14454.
Ogburn, F., Peiser, H.S., Paretzkin, B., 1964. Pseudopentagonal twins in electrodeposited copper dendrites. Acta Crystallographica 17, 774.
Ohno, T., Yatsuya, S., Uyeda, R., 1976. Formation of ultrafine metal particles by gas-evaporation technique .3. Al in He, Ar and Xe, and Mg in mixtures of inactive gas and air. Japanese Journal of Applied Physics 15, 1213–1217.
Ojea-Jimenez, I., Campanera, J.M., 2012. Molecular modeling of the reduction mechanism in the citrate mediated synthesis of gold nanoparticles. Journal of Physical Chemistry C 116, 23682–23691.
Ostwald, W., 1900. On the assumed isomerism of red and yellow mercury oxide and the surface-tension of solid bodies. Zeitschrift Fur Physikalische Chemie–Stochiometrie Und Verwandtschaftslehre 34, 495–503.
Parakh, A., Lee, S., Kiani, M.T., *et al.*, 2020. Stress-induced structural transformations in Au nanocrystals. Nano Letters 20, 7767–7773.
Pashley, D.W., Stowell, M.J., 1963. Electron microscopy and diffraction of twinned structures in evaporated films of gold. Philosophical Magazine 8, 1605.
Patala, S., Marks, L.D., de la Cruz, M.O., 2013a. Elastic strain energy effects in faceted decahedral nanoparticles. Journal of Physical Chemistry C 117, 1485–1494.
Patala, S., Marks, L.D., de la Cruz, M.O., 2013b. Thermodynamic analysis of multiply twinned particles: Surface stress effects. The Journal of Physical Chemistry Letters 4, 3089–3094.
Peng, L., Ringe, E., Van Duyne, R.P., Marks, L.D., 2015. Segregation in bimetallic nanoparticles. Physical Chemistry Chemical Physics 17, 27940–27951.
Peng, L.X., Van Duyne, R.P., Marks, L.D., 2016. Compositional inhomogeneity and corner enrichment of Pt in Pt/Pd bimetallic nanoparticles. Journal of Physical Chemistry C 120, 21069–21075.
Penuelas, J., Andreazza, P., Andreazza-Vignolle, C., *et al.*, 2009. Real-time icosahedral to fcc structure transition during CoPt nanoparticles formation. European Physical Journal-Special Topics 167, 19–25.
Perala, S.R., Kumar, S., 2014. On the two-step mechanism for synthesis of transition-metal nanoparticles. Langmuir 30, 12703–12711.
Pimpinelli, A., Villain, J., 2010. Physics of Crystal Growth. Cambridge: Cambridge University Press.
Pohl, D., Wiesenhutter, U., Mohn, E., Schultz, L., Rellinghaus, B., 2014. Near-surface strain in icosahedra of binary metallic alloys: Segregational versus intrinsic effects. Nano Letters 14, 1776–1784.
Polonsky, I.A., Romanov, A.E., Gryaznov, V.G., Kaprelov, A.M., 2006. Disclination in an elastic sphere. Philosophical Magazine A 64, 281–287.
Polte, J., Ahner, T.T., Delissen, F., *et al.*, 2010a. Mechanism of gold nanoparticle formation in the classical citrate synthesis method derived from coupled in situ XANES and SAXS evaluation. Journal of the American Chemical Society 132, 1296–1301.
Polte, J., Erler, R., Thunemann, A.F., *et al.*, 2010b. Nucleation and growth of gold nanoparticles studied via in situ small angle X-ray scattering at millisecond time resolution. ACS Nano 4, 1076–1082.
Prabhu, S., Poulose, E.K., 2012. Silver nanoparticles: mechanism of antimicrobial action, synthesis, medical applications, and toxicity effects. International Nano Letters 2, 32.
Qi, W.H., Wang, M.P., Su, Y.C., 2002. Size effect on the lattice parameters of nanoparticles. Journal of Materials Science Letters 21, 877–878.
Qi, X., Chen, Z., Yan, T., Fichthorn, K.A., 2019. Growth mechanism of five-fold twinned Ag nanowires from multiscale theory and simulations. ACS Nano 13, 4647–4656.
Qian, H., Eckenhoff, W.T., Zhu, Y., Pintauer, T., Jin, R., 2010. Total structure determination of thiolate-protected Au38 nanoparticles. Journal of the American Chemical Society 132, 8280–8281.
Rabenau, A., 1985. The role of hydrothermal synthesis in preparative chemistry. Angewandte Chemie International Edition 24, 1026–1040.
Rahm, J., Erhart, P., 2020. WulffPack: A Python package for Wulff constructions. Journal of Open Source Software 5, 1944.
Rankin, J., Sheldon, B.W., 1995. In situ TEM sintering of nano-sized ZrO2 particles. Materials Science and Engineering a-Structure 204, 48–53.
Ray, N.A., Van Duyne, R.P., Stair, P.C., 2012. Synthesis strategy for protected metal nanoparticles. Journal of Physical Chemistry C 116, 7748–7756.

Reimann, K., Wurschum, R., 1997. Distribution of internal strains in nanocrystalline Pd studied by x-ray diffraction. Journal of Applied Physics 81, 7186–7192.
Reinhard, D., Hall, B.D., Ugarte, D., Monot, R., 1997. Size-independent fcc-to-icosahedral structural transition in unsupported silver clusters: An electron diffraction study of clusters produced by inert-gas aggregation. Physical Review B 55, 7868–7881.
Reinhard, D., Hall, B.D., Berthoud, P., Valkealahti, S., Monot, R., 1998. Unsupported nanometer-sized copper clusters studied by electron diffraction and molecular dynamics. Physical Review B 58, 4917–4926.
Ringe, E., 2014. Nanocrystalline materials: Recent advances in crystallographic characterization techniques. IUCrJ 1, 530–539.
Ringe, E., Van Duyne, R.P., Marks, L.D., 2011. Wulff construction for alloy nanoparticles. Nano Letters 11, 3399–3403.
Ringe, E., Van Duyne, R.P., Marks, L.D., 2013. Kinetic and thermodynamic modified wulff constructions for twinned nanoparticles. Journal of Physical Chemistry C 117, 15859–15870.
Rodriguez-Gonzalez, B., Mulvaney, P., Liz-Marzan, L.M., 2007. An electrochemical model for gold colloid formation via citrate reduction. Zeitschrift Fur Physikalische Chemie-International Journal of Research in Physical Chemistry & Chemical Physics 221, 415–426.
Rohrer, G.S., Rohrer, C.L., Mullins, W.W., 2002. Coarsening of faceted crystals. Journal of the American Ceramic Society 85, 675–682.
Romanov, A.E., 2002. Fundamentals of disclination theory: Development of disclination-dislocation structures in deformed materials. Solid State Phenomena 87, 47–56.
Romanov, A.E., 2003. Mechanics and physics of disclinations in solids. European Journal of Mechanics - A/Solids 22, 727–741.
Romanov, A.E., Kolesnikova, A.L., 2009. Application of disclination concept to solid structures. Progress in Materials Science 54, 740–769.
Romanov, A.E., Vikarchuk, A.A., Kolesnikova, A.L., *et al*., 2012. Structural transformations in nano- and microobjects triggered by disclinations. Journal of Materials Research 27, 545–551.
Rosi, N.L., Mirkin, C.A., 2005. Nanostructures in biodiagnostics. Chemical Reviews 105, 1547–1562.
Ross, F.M., Tersoff, J., Tromp, R.M., 1998. Coarsening of self-assembled Ge quantum dots on Si(001). Physical Review Letters 80, 984–987.
Rossi, K., Asara, G.G., Baletto, F., 2020. Structural screening and design of platinum nanosamples for oxygen reduction. ACS Catalysis 10, 3911–3920.
Sakthivel, N.A., Shabaninezhad, M., Sementa, L., *et al*., 2020. The missing link: Au191(SPh-tBu)66 janus nanoparticle with molecular and bulk-metal-like properties. Journal of the American Chemical Society 142, 15799–15814.
Scamarcio, G., Lugara, M., Manno, D., 1992. Size-dependent lattice contraction in CdS1-xSex nanocrystals embedded in glass observed by Raman scattering. Physical Review B Condensed Matter 45, 13792–13795.
Schebarchov, D., Baletto, F., Wales, D.J., 2018. Structure, thermodynamics, and rearrangement mechanisms in gold clusters-insights from the energy landscapes framework. Nanoscale 10, 2004–2016.
Schwoebel, R.L., 1966. Anomalous growth of gold from the vapor phase. Journal of Applied Physics 37, 2515–2516.
Sekerka, R.F., 2005. Equilibrium and growth shapes of crystals: How do they differ and why should we care? Crystal Research and Technology 40, 291–306.
Serpell, C.J., Cookson, J., Ozkaya, D., Beer, P.D., 2011. Core@shell bimetallic nanoparticle synthesis via anion coordination. Nature Chemistry 3, 478–483.
Shah, P., Gavrin, A., 2006. Synthesis of nanoparticles using high-pressure sputtering for magnetic domain imaging. Journal of Magnetism and Magnetic Materials 301, 118–123.
Shao, Y.Q., Tang, D., Xiong, W.H., 2007. In-situ TEM study on microstructural evolution of nanostructured TiO2. Journal of Wuhan University of Technology 22, 209–213.
Shchukin, V.A., Bimberg, D., 1999. Spontaneous ordering of nanostructures on crystal surfaces. Reviews of Modern Physics 71, 1125–1171.
Sheldon, B.W., Rankin, J., 2002. Step-energy barriers and particle shape changes during coarsening. Journal of the American Chemical Society 85, 683–690.
Shreiber, D., Jesser, W.A., 2006. Size dependence of lattice parameter for SixGe1-x nanoparticles. Surface Science 600, 4584–4590.
Silly, F., Castell, M.R., 2005. Self-assembled supported Co nanocrystals: The adhesion energy of face-centered-cubic Co on SrTiO[sub 3](001)-(2 × 2). Applied Physics Letters 87. 053106.
Silly, F., Castell, M.R., 2009. Temperature-dependent stability of supported five-fold twinned copper nanocrystals. ACS Nano 3, 901–906.
Silly, F., Newell, D.T., Castell, M.R., 2006. $SrTiO_3$ (001) reconstructions: The (2 x 2) to c(4 x 4) transition. Surface Science 600, L219–L223.
Sivaramakrishnan, S., Wen, J.G., Scarpelli, M.E., Pierce, B.J., Zuo, J.M., 2010. Equilibrium shapes and triple line energy of epitaxial gold nanocrystals supported on TiO_2(110). Physical Review B 82. 195421.
Smith, D.J., Marks, L.D., 1981. High-resolution studies of small particles of gold and silver .2. Single-crystals, lamellar twins and polyparticles. Journal of Crystal Growth 54, 433–438.
Solliard, C., Flueli, M., 1985. Surface stress and size effect on the lattice-parameter in small particles of gold and platinum. Surface Science 156, 487–494.
Song, M., Wu, Z., Lu, N., Li, D., 2019. Strain relaxation-induced twin interface migration and morphology evolution of silver nanoparticles. Chemistry of Materials 31, 842–850.
Song, Y., Liu, K., Chen, S., 2012. AgAu bimetallic Janus nanoparticles and their electrocatalytic activity for oxygen reduction in alkaline media. Langmuir 28, 17143–17152.
Song, Y.B., Li, Y.W., Li, H., *et al*., 2020. Atomically resolved Au52Cu72(SR)(55) nanoalloy reveals Marks decahedron truncation and Penrose tiling surface. Nature Communications 11, 7.
Soni, V., Sindal, R.S., Mehrotra, R.N., 2007. Kinetics and mechanism of the oxidation of oxalic acid by tetrachloroaurate(III) ion. Inorganica Chimica Acta 360, 3141–3148.
Spencer, B.J., 1999. Asymptotic derivation of the glued-wetting-layer model and contact-angle condition for Stranski-Krastanow islands. Physical Review B 59, 2011–2017.
Spencer, B.J., Tersoff, J., 1997. Equilibrium shapes and properties of epitaxially strained islands. Physical Review Letters 79, 4858–4861.
Spencer, B.J., Voorhees, P.W., Davis, S.H., 1991. Morphological instability in epitaxially strained dislocation-free solid films. Physical Review Letters 67, 3696–3699.
Spencer, B.J., Voorhees, P.W., Davis, S.H., 1993. Morphological instability in epitaxially strained dislocation-free solid films - linear-stability theory. Journal of Applied Physics 73, 4955–4970.
Stappert, S., Rellinghaus, B., Acet, M., Wassermann, E.F., 2003. Gas-phase preparation of L10 ordered FePt nanoparticles. Journal of Crystal Growth 252, 440–450.
Streszewski, B., Jaworski, W., Paclawski, K., *et al*., 2012. Gold nanoparticles formation in the aqueous system of gold(III) chloride complex ions and hydrazine sulfate-Kinetic studies. Colloids and Surfaces a-Physicochemical and Engineering Aspects 397, 63–72.
Suchanek, W.L., Riman, R.E., 2006. Hydrothermal synthesis of advanced ceramic powders. Advances in Science and Technology 45, 184–193.
Sun, Q., Yerino, C.D., Leung, B., Han, J., Coltrin, M.E., 2011. Understanding and controlling heteroepitaxy with the kinetic Wulff plot: A case study with GaN. Journal of Applied Physics 110. 053517.
Sun, Q., Yerino, C.D., Ko, T.S., *et al*., 2008. Understanding nonpolar GaN growth through kinetic Wulff plots. Journal of Applied Physics 104. 093523.
Suntivich, J., Xu, Z., Carlton, C.E., *et al*., 2013. Surface composition tuning of Au-Pt bimetallic nanoparticles for enhanced carbon monoxide and methanol electro-oxidation. Journal of the American Chemical Society 135, 7985–7991.
Takahata, R., Yamazoe, S., Maehara, Y., *et al*., 2020. Electron microscopic observation of an icosahedral Au-13 core in Au-25(SePh)(18) and reversible isomerization between icosahedral and face-centered cubic cores in Au-144(SC2H4Ph)(60). Journal of Physical Chemistry C 124, 6907–6912.
Takeguchi, M., Tanaka, M., Yasuda, H., Furuya, K., 2001. Real-time high-resolution transmission electron microscopy observation of the growth process of (001) surfaces on a nanometer-sized Si multiply twinned particle. Surface Science 493, 414–419.
Tauster, S., 1978. Strong metal-support interactions: Occurrence among the binary oxides of groups IIA?VB. Journal of Catalysis 55, 29–35.
Tauster, S.J., 1987. Strong metal-support interactions. Accounts of Chemical Research 20, 389–394.
Tauster, S.J., Fung, S.C., Garten, R.L., 1978. Strong metal-support interactions - Group-8 noble-metals supported on Tio2. Journal of the American Chemical Society 100, 170–175.
Tauster, S.J., Fung, S.C., Baker, R.T., Horsley, J.A., 1981. Strong interactions in supported-metal catalysts. Science 211, 1121–1125.

Taylor, J.E., 1992. Mean-curvature and weighted mean-curvature .2. Acta Metallurgica Et Materialia 40, 1475–1485.
Taylor, J.E., Cahn, J.W., Handwerker, C.A., 1992. Geometric models of crystal-growth. Acta Metallurgica Et Materialia 40, 1443–1474.
Tersoff, J., Tromp, R.M., 1993. Shape transition in growth of strained islands: Spontaneous formation of quantum wires. Physical Review Letters 70, 2782–2785.
Thanh, N.T., Maclean, N., Mahiddine, S., 2014. Mechanisms of nucleation and growth of nanoparticles in solution. Chemical Reviews 114, 7610–7630.
Theissmann, R., Fendrich, M., Zinetullin, R., *et al.*, 2008. Crystallographic reorientation and nanoparticle coalescence. Physical Review B 78. 205413.
Thurmer, K., Reutt-Robey, J.E., Williams, E.D., 2003. Nucleation limited crystal shape transformations. Surface Science 537, 123–133.
Torabi, S., Lowengrub, J., Voigt, A., Wise, S., 2009. A new phase-field model for strongly anisotropic systems. Proceedings of the Royal Society of London. Series A, Mathematical and Physical Sciences 465, 1337–1359.
Tsagrakis, I., Yasnikov, I.S., Aifantis, E.C., 2018. Gradient elasticity for disclinated micro crystals. Mechanics Research Communications 93, 159–162.
Uehara, T., Sekerka, R.F., 2003. Phase field simulations of faceted growth for strong anisotropy of kinetic coefficient. Journal of Crystal Growth 254, 251–261.
Uppenbrink, J., Wales, D.J., 1992. Structure and energetics of model metal-clusters. Journal of Chemical Physics 96, 8520–8534.
Uppenbrink, J., Wales, D.J., Kirkland, A.I., Jefferson, D.A., Urban, J., 1992. Structure and energetics of model symmetrical and asymmetric decahedra. Philosophical Magazine B-physics of Condensed Matter Statistical Mechanics Electronic Optical and Magnetic Properties 65, 1079–1096.
Volterra, V., 1907. Sur l'equilibre des corps elastiques multiplement connexes.
vandeWaal, B.W., 1996. Cross-twinning model of fcc crystal growth. Journal of Crystal Growth 158, 153–165.
van Deelen, T.W., Hernández Mejía, C., de Jong, K.P., 2019. Control of metal-support interactions in heterogeneous catalysts to enhance activity and selectivity. Nature Catalysis 2, 955–970.
van Huis, M.A., Young, N.P., Pandraud, G., *et al.*, 2009. Atomic imaging of phase transitions and morphology transformations in nanocrystals. Advanced Materials 21, 4992–4995.
Vermaak, J.S., Mays, C.W., Kuhlmann-Wilsdorf, D., 1968. On surface stress and surface tension. Surface Science 12, 128–133.
Vikarchuk, A.A., Gryzunova, N.N., Manokhin, S.S., 2020. Disclination models of transformation of icosaedric copper particles during their growth during electric crystallization. Materials Physics and Mechanics 43, 18–29.
Villain, J., 1991. Nonequilibrium systems - the shape of crystals to come. Nature 350, 273–274.
Volk, A., Thaler, P., Koch, M., *et al.*, 2013. High resolution electron microscopy of Ag-clusters in crystalline and non-crystalline morphologies grown inside superfluid helium nanodroplets. The Journal of Chemical Physics 138. 214312.
Volmer, M., 1939. Kinetics of Phase Transformation. Berlin.
von Laue, M., 1943. Wulff's theorem for the balanced form of crystals. Z Kristallogr 105, 124–133.
Voorhees, P.W., 1985. The theory of ostwald ripening. Journal of Statistical Physics 38, 231–252.
Voorhees, P.W., 1992. Ostwald ripening of 2-phase mixtures. Annual Review of Materials Science 22, 197–215.
Voorhees, P.W., Coriell, S.R., Mcfadden, G.B., Sekerka, R.F., 1984. The effect of anisotropic crystal melt surface-tension on grain-boundary groove morphology. Journal of Crystal Growth 67, 425–440.
Wagner, R.S., 1960. On the growth of germanium dendrites. Acta Metallurgica 8, 57–60.
Wales, D.J., 2015. Perspective: Insight into reaction coordinates and dynamics from the potential energy landscape, The. Journal of Chemical Physics 142. 130901.
Wales, D.J., Doye, J.P.K., Miller, M.A., 2000. Energy landscapes: From clusters to biomolecules. In: Prigogine, I., Walsh, T.R. (Eds.), Advances in Chemical Physics 115.
Walsh, M.J., Barrow, S.J., Tong, W.M., Funston, A.M., Etheridge, J., 2015. Symmetry breaking and silver in gold nanorod growth. Acs Nano 9, 715–724.
Walsh, M.J., Yoshida, K., Kuwabara, A., *et al.*, 2012. On the structural origin of the catalytic properties of inherently strained ultrasmall decahedral gold nanoparticles. Nano Letters 12, 2027–2031.
Wang, D.L., Xin, H.L.L., Hovden, R., *et al.*, 2013. Structurally ordered intermetallic platinum-cobalt core-shell nanoparticles with enhanced activity and stability as oxygen reduction electrocatalysts. Nature Materials 12, 81–87.
Wang, Z.W., Palmer, R.E., 2012. Determination of the ground-state atomic structures of size-selected au nanoclusters by electron-beam-induced transformation. Physical Review Letters 108. 245502.
Warschkow, O., Asta, M., Erdman, N., *et al.*, 2004. TiO2-rich reconstructions of $SrTiO_3$ (001): A theoretical study of structural patterns. Surface Science 573, 446–456.
Wasserma, H.J., Vermaak, J.S., 1970. On determination of a lattice contraction in very small silver particles. Surface Science 22, 164–172.
Wasserman, H.J., Vermaak, J.S., 1972. On the determination of the surface stress of copper and platinum. Surface Science 32, 168–174.
Watari, M., McKendry, R.A., Vogtli, M., *et al.*, 2011. Differential stress induced by thiol adsorption on facetted nanocrystals. Nature Materials 10, 862–866.
Wei, B.Q., Vajtai, R., Jung, Y.J., *et al.*, 2002. Massive icosahedral boron carbide crystals. Journal of Physical Chemistry B 106, 5807–5809.
Wells, D.M., Rossi, G., Ferrando, R., Palmer, R.E., 2015. Metastability of the atomic structures of size-selected gold nanoparticles. Nanoscale 7, 6498–6503.
Wender, H., de Oliveira, L.F., Migowski, P., *et al.*, 2010. Ionic liquid surface composition controls the size of gold nanoparticles prepared by sputtering deposition. Journal of Physical Chemistry C 114, 11764–11768.
Wiley, B.J., Xiong, Y., Li, Z.-Y., Yin, Y., Xia, Y., 2006. Right bipyramids of silver: A new shape derived from single twinned seeds. Nano Letters 6, 765–768.
Winn, D., Doherty, M.F., 2000. Modeling crystal shapes of organic materials grown from solution. Aiche Journal 46, 1348–1367.
Winterbottom, W.L., 1967. Equilibrium shape of a small particle in contact with a foreign substrate. Acta Metallurgica 15, 303–310.
Wise, S., Kim, J., Lowengrub, J., 2007. Solving the regularized, strongly anisotropic Cahn-Hilliard equation by an adaptive nonlinear multigrid method. Journal of Computational Physics 226, 414–446.
Wojnicki, M., Rudnik, E., Luty-Blocho, M., Paclawski, K., Fitzner, K., 2012. Kinetic studies of gold(III) chloride complex reduction and solid phase precipitation in acidic aqueous system using dimethylamine borane as reducing agent. Hydrometallurgy 127, 43–53.
Wu, H., Yu, R., Zhu, J., *et al.*, 2021. Size-dependent strain in fivefold twins of gold. Acta Crystallographica Section B-Structural Science Crystal Engineering and Materials 77, 93–98.
Wuithschick, M., Birnbaum, A., Witte, S., *et al.*, 2015. Turkevich in new robes: Key questions answered for the most common gold nanoparticle synthesis. ACS Nano 9, 7052–7071.
Wuithschick, M., Paul, B., Bienert, R., *et al.*, 2013. Size-controlled synthesis of colloidal silver nanoparticles based on mechanistic understanding. Chemistry of Materials 25, 4679–4689.
Wulff, G., 1901. On the question of speed of growth and dissolution of crystal surfaces. Zeitschrift Fur Krystallographie Und Mineralogie 34, 449–530.
Xia, X., Xie, S., Liu, M., *et al.*, 2013. On the role of surface diffusion in determining the shape or morphology of noble-metal nanocrystals. Proceedings of the National Academy of Sciences of the United States of America 110, 6669–6673.
Xia, Y., Xiong, Y.J., Lim, B., Skrabalak, S.E., 2009. Shape-controlled synthesis of metal nanocrystals: simple chemistry meets complex physics? Angewandte Chemie-International Edition 48, 60–103.
Xu, W.W., Gao, Y., 2015. Unraveling the atomic structures of the Au-68(SR)(34) nanoparticles. Journal of Physical Chemistry C 119, 14224–14229.
Yacaman, M.J., 2012. Private Communication.
Yacaman, M.J., Ascencio, J.A., Liu, H.B., Gardea-Torresdey, J., 2001. Structure shape and stability of nanometric sized particles. Journal of Vacuum Science & Technology B 19, 1091–1103.
Yagi, K., Takayanagi, K., Kobayashi, K., Honjo, G., 1975. Insitu observations of growth processes of multiply twinned particles. Journal of Crystal Growth 28, 117–124.
Yao, T., Sun, Z., Li, Y., *et al.*, 2010. Insights into initial kinetic nucleation of gold nanocrystals. Journal of the American Chemical Society 132, 7696–7701.

Yatsuya, S., Kasukabe, S., Uyeda, R., 1973. Formation of ultrafine metal particles by gas evaporation technique .1. Aluminum in helium. Japanese Journal of Applied Physics 12, 1675–1684.
Yeadon, M., Ghaly, M., Yang, J.C., Averback, R.S., Gibson, J.M., 1998. "Contact epitaxy" observed in supported nanoparticles. Applied Physics Letters 73, 3208–3210.
Yin, Z., Zhang, Y., Chen, K., *et al*., 2014. Monodispersed bimetallic PdAg nanoparticles with twinned structures: Formation and enhancement for the methanol oxidation. Scientific Reports 4, 4288.
Young, N.P., van Huis, M.A., Zandbergen, H.W., Xu, H., Kirkland, A.I., 2010. Transformations of gold nanoparticles investigated using variable temperature high-resolution transmission electron microscopy. Ultramicroscopy 110, 506–516.
Yu, R., Wu, H., Wang, J.D., Zhu, J., 2017. Strain concentration at the boundaries in 5-fold twins of diamond and silicon. ACS Applied Materials & Interfaces 9, 4253–4258.
Yuan, W., Wang, Y., Li, H., *et al*., 2016. Real-time observation of reconstruction dynamics on TiO_2 (001) surface under oxygen via an environmental transmission electron microscope. Nano Letters 16, 132–137.
Yuan, W., Wu, H., Li, H., *et al*., 2017. In Situ STEM determination of the atomic structure and reconstruction mechanism of the TiO_2 (001) (1 $\times$ 4) surface. Chemistry of Materials 29, 3189–3194.
Zeng, C., Li, T., Das, A., Rosi, N.L., Jin, R., 2013. Chiral structure of thiolate-protected 28-gold-atom nanocluster determined by X-ray crystallography. Journal of the American Chemical Society 135, 10011–10013.
Zhang, J., Li, S.Z., Wu, J.S., Schatz, G.C., Mirkin, C.A., 2009. Plasmon-mediated synthesis of silver triangular bipyramids. Angewandte Chemie-International Edition 48, 7787–7791.
Zhang, S., Plessow, P.N., Willis, J.J., *et al*., 2016. Dynamical observation and detailed description of catalysts under strong metal-support interaction. Nano Letters 16, 4528–4534.
Zhang, W., Zheng, W.T., 2015. Transmission electron microscopy finds plenty of room on the surface. Physical Chemistry Chemical Physics 17, 14461–14469.
Zhang, Z., Lagally, M.G., 1997. Atomistic processes in the early stages of thin-film growth. Science 276, 377–383.
Zhu, G.Z., Radtke, G., Botton, G.A., 2012. Bonding and structure of a reconstructed (001) surface of $SrTiO_3$ from TEM. Nature 490, 384–387.
Zhu, X.H., Hang, Q.M., 2013. Microscopical and physical characterization of microwave and microwave-hydrothermal synthesis products. Micron 44, 21–44.
Zia, R.K.P., Avron, J.E., Taylor, J.E., 1988. The summertop construction - crystals in a corner. Journal of Statistical Physics 50, 727–736.
Zinke-Allmang, M., Feldman, L.C., Grabow, M.H., 1992. Clustering on surfaces. Surface Science Reports 16, 377–463.
Zucker, R., Chatain, D., Dahmen, U., Hagège, S., Carter, W.C., 2012. New software tools for the calculation and display of isolated and attached interfacial-energy minimizing particle shapes. Journal of Materials Science 47, 1–13.